

University of Windsor

Scholarship at UWindor

Electronic Theses and Dissertations

Theses, Dissertations, and Major Papers

2013

The Design and Manipulation of Bromate-Based Chemical Oscillators

Jun Li

University of Windsor

Follow this and additional works at: <https://scholar.uwindsor.ca/etd>

Recommended Citation

Li, Jun, "The Design and Manipulation of Bromate-Based Chemical Oscillators" (2013). *Electronic Theses and Dissertations*. 4911.

<https://scholar.uwindsor.ca/etd/4911>

This online database contains the full-text of PhD dissertations and Masters' theses of University of Windsor students from 1954 forward. These documents are made available for personal study and research purposes only, in accordance with the Canadian Copyright Act and the Creative Commons license—CC BY-NC-ND (Attribution, Non-Commercial, No Derivative Works). Under this license, works must always be attributed to the copyright holder (original author), cannot be used for any commercial purposes, and may not be altered. Any other use would require the permission of the copyright holder. Students may inquire about withdrawing their dissertation and/or thesis from this database. For additional inquiries, please contact the repository administrator via email (scholarship@uwindsor.ca) or by telephone at 519-253-3000ext. 3208.

The Design and Manipulation of Bromate-Based Chemical Oscillators

by

Jun Li

A Dissertation
Submitted to the Faculty of Graduate Studies
Through the Department of Chemistry and Biochemistry
in Partial Fulfillment of the Requirements for
the Degree of Doctor of Philosophy at the
University of Windsor

Windsor, Ontario, Canada
2013



Library and Archives
Canada

Published Heritage
Branch

395 Wellington Street
Ottawa ON K1A 0N4
Canada

Bibliothèque et
Archives Canada

Direction du
Patrimoine de l'édition

395, rue Wellington
Ottawa ON K1A 0N4
Canada

Your file Votre référence

ISBN: 978-0-494-98355-3

Our file Notre référence

ISBN: 978-0-494-98355-3

NOTICE:

The author has granted a non-exclusive license allowing Library and Archives Canada to reproduce, publish, archive, preserve, conserve, communicate to the public by telecommunication or on the Internet, loan, distribute and sell theses worldwide, for commercial or non-commercial purposes, in microform, paper, electronic and/or any other formats.

The author retains copyright ownership and moral rights in this thesis. Neither the thesis nor substantial extracts from it may be printed or otherwise reproduced without the author's permission.

In compliance with the Canadian Privacy Act some supporting forms may have been removed from this thesis.

While these forms may be included in the document page count, their removal does not represent any loss of content from the thesis.

AVIS:

L'auteur a accordé une licence non exclusive permettant à la Bibliothèque et Archives Canada de reproduire, publier, archiver, sauvegarder, conserver, transmettre au public par télécommunication ou par l'Internet, prêter, distribuer et vendre des thèses partout dans le monde, à des fins commerciales ou autres, sur support microforme, papier, électronique et/ou autres formats.

L'auteur conserve la propriété du droit d'auteur et des droits moraux qui protègent cette thèse. Ni la thèse ni des extraits substantiels de celle-ci ne doivent être imprimés ou autrement reproduits sans son autorisation.

Conformément à la loi canadienne sur la protection de la vie privée, quelques formulaires secondaires ont été enlevés de cette thèse.

Bien que ces formulaires aient inclus dans la pagination, il n'y aura aucun contenu manquant.

Canada

© 2013 Jun Li

The Design and Manipulation of Bromate-Based Chemical Oscillators

by

Jun Li

APPROVED BY:

O. Steinbock, External Examiner
Florida State University

X. Nie
Mechanical, Automotive and Materials Engineering

R. Schurko
Department of Chemistry and Biochemistry

R. Aroca
Department of Chemistry and Biochemistry

J. Wang, Advisor
Department of Chemistry and Biochemistry

T. Loughead, Chair of Defense
Department of Kinesiology

April 25, 2013

DECLARATION OF CO-AUTHORSHIP/PREVIOUS PUBLICATION

I. Co-Authorship Declaration

I hereby declare that chapter 6 of this thesis incorporates material that is the result of joint research with Xuefeng Hu, who is also under the supervision of Dr. J. Wang, The collaboration is covered in chapter 6 of the thesis.

I am aware of the University of Windsor Senate Policy on Authorship and I certify that I have properly acknowledged the contribution of other researchers to my thesis, and have obtained written permission from each of the co-author(s) to include the above material(s) in my thesis.

I certify that, with the above qualification, this thesis, and the research to which it refers, is the product of my own work.

II. Declaration of Previous Publication

This thesis includes 7 chapters which 5 of them are original papers that have been previously published in peer reviewed journals, as follows:

Thesis Chapter	Publication title / full citation	Publication status
Chapter 2	Complex kinetics and significant influences of bromine removal in ferroin-bromate-metol reaction, J. Li and J. Wang, Phys. Chem. Chem. Phys., 13, 2011, 15539.	Published
Chapter 3	Design of batch minimal bromate oscillator, J. Li and J. Wang, Chem. Phys. Lett., 508, 2011, 320.	Published
Chapter 4	Subtle photochemical behavior in ferroin-bromate-benzoquinone reaction, J. Li and J. Wang, J. Phys. Chem. A, 116, 2012, 386.	Published
Chapter 5	Complex Dynamical Behavior in the Highly Photosensitive Cerium-Bromate-1,4-Benzoquinone Reaction, J. Li and J. Wang, J. Phys. Chem. A, 116, 2012, 8130.	Published
Chapter 6	Structural Transformation of Carbon Electrodes for Simultaneous Determination of Dihydroxybenzene Isomers, X. Hu, J. Li and J. Wang, Electrochem. Commun., 21, 2012, 73.	Published

I certify that I have obtained a written permission from the copyright owner(s) to include the above published material(s) in my thesis. Copies of copyright release are included in Appendix D to G. I certify that the above material describes work completed during my registration as graduate student at the University of Windsor.

I declare that, to the best of my knowledge, my thesis does not infringe upon anyone's copyright nor violate any proprietary rights and that any ideas, techniques, quotations, or any other material from the work of other people included in my thesis, published or otherwise, are fully acknowledged in accordance with the standard referencing practices. Furthermore, to the extent that I have included copyrighted material that surpasses the bounds of fair dealing within the meaning of the Canada Copyright Act, I certify that I have obtained a written permission from the copyright owner(s) to include such material(s) in my thesis.

I declare that this is a true copy of my thesis, including any final revisions, as approved by my thesis committee and the Graduate Studies office, and that this thesis has not been submitted for a higher degree to any other University or Institution.

ABSTRACT

Autocatalytic reactions are a kind of fascinating reactions in nonlinear chemical and biochemical systems because of their unique features. The auto-catalyst can multiply itself leading to the spontaneous generation of order. Coupled autocatalytic reactions, providing a positive/negative feedback to control the multiplication of the auto-catalyst, can give rise to extraordinary complex behavior such as sequential oscillations. A new bromate-based oscillator was successfully designed that employs metol as its organic substrate. Complex reaction behaviors were observed when the system was subjected to bromine removal and oxygen exposure. Transitions from simple to sequential oscillations took place as a function of the age of the metol stock solution, in which an important intermediate is 1,4-hydroquinone and the main final products are 1,4-benzoquinone and bromobenzoquinones. Various analytical techniques were applied such as TOF-MS, GC/MS, NMR, UV, etc.

Since bromobenzoquinones are parts of the major products in metol-bromate-ferroin system, a new type of minimal bromate oscillator is found based on the bromination of 1,4-benzoquinone. The oscillator contains a reagent benzoquinone, which does not react with metal catalyst ferroin/ferriin, but modulates the evolution of bromide ions through the reaction between 1,4-benzoquinone and bromine. It could exhibit spontaneous oscillations in a closed reactor. Due to the role of the organic substrate is only the bromine removal, we define this system as a batch minimal bromate oscillator.

We further investigated the photochemical behavior of the minimal bromate oscillator, in which the reduction of ferriin/Cerium (IV) was dominated by bromide ions rather than by organic substrates as known in most of bromate oscillators. The chemical oscillations

exhibited ultrasensitive response to illumination, and the influence of light evolved from constructive to inhibitory.

In order to determine the dynamic of organic intermediates, such as 1,4-hydroquinone, which is involved in metol-bromate-ferroin and 1,4-cyclohexanedione (CHD)-bromate-metal catalyst systems, a new type of modified carbon electrode was developed to simultaneously determine 1,4-hydroquinone and pyrocatechol with differential pulse voltammetry. By applying it into the test of dynamics of 1,4-hydroquinone in the CHD-bromate uncatalyzed system, we successfully monitored the concentration change of 1,4-hydroquinone during the oscillations.

DEDICATION

This work is dedicated to my wife, who is also my fellow in the same lab, Xuefeng Hu, for her thoughtful kindness, love, pray and encouragement throughout my doctoral life. I could not have achieved my PhD program without you. God bless you.

ACKNOWLEDGEMENTS

To god be all praise and glory, to whom we belong and to whom we shall return. How can we thank God enough for you in return for all the joy we have in the presence of our God because of you?

In academic, first and foremost, I would like to gratefully and sincerely thank Dr. Jichang Wang, my supervisor, for his guidance, support and encouragement during my doctoral studies. He encouraged me to not only grow as an experimentalist but also as an independent thinker. He gave me every opportunity to develop my own individuality for my research and studies and he always helped me to tide over my tough time. For everything you've done for me, I thank you by my heart.

I would also like to thank Dr. Robert Schurko, internal examiner, for his valuable advice during comprehensive exam and proposal exam, and for his careful guidance during the NMR course. Also I am thankful for his valuable comments of my research proposal and thesis.

Particular thanks to Dr. Ricardo Aroca, for his incredibly friendly teaching and supporting in his field of surface spectroscopy and photochemistry, and I am thankful for his great help in my research of testing surface properties.

I am grateful to Dr. Xueyuan, Nie, Mechanical, from the Department of Automotive and Materials Engineering, for his helping enthusiasm during my doctoral journey, and for his careful review of my thesis.

I wish to express my sincere thanks to Dr. James R. Green who taught me how to carry out GC-MS, and NMR analysis. He is a kindness teacher. Whenever I need help from him, he is there.

Lastly, I would like to thank all members in J. Wang's group and in the Department of Chemistry and Biochemistry, who have helped me directly or indirectly during my doctoral program. Especially thanks to Marlene Bezaire, for her constant help during my doctoral life.

TABLE OF CONTENTS

DECLARATION OF CO-AUTHORSHIP/PREVIOUS PUBLICATION	iv
ABSTRACT	vi
DEDICATION	viii
ACKNOWLEDGEMENTS	ix
LIST OF TABLES	xv
LIST OF FIGURES	xvi
LIST OF ABBREVIATIONS	xxi
LIST OF APPENDICES	xxiii
Chapter 1: Introduction	1
1.1 Nonlinear Dynamics in Stirred Systems	1
1.1.1 Requirement of Chemical Oscillations	1
1.1.2 Nonlinear Kinetics in a Closed Reactor	3
1.1.3 Nonlinear Kinetics in an Open Reactor	6
1.2 Nonlinear Behavior in Reaction-Diffusion Media: Pattern Formation	10
1.2.1 Pattern Formation in One-Dimensional Media	12
1.2.2 Waves in Two-Dimensional Media	15
1.2.3 Three-Dimensional Waves	17
1.2.4 Turing Patterns	18
1.3 Recent Developments in the Study of Chemical Oscillators and Their Potential Applications	20
1.3.1 pH Oscillators	20
1.3.2 Oscillations in Protic Ionic Liquids	22

1.3.3 Self-oscillating Gels	23
1.3.4 Controlled-Synthesis of Nano/micro-Materials	25
1.4 Objectives of this Thesis	29
1.5 References	31
Chapter 2: Complex Kinetics and Significant Influences of Bromine Removal in Ferroin-Bromate-Metol Reaction	40
2.1 Introduction	40
2.2 Experimental Procedure	41
2.3 Results and Discussion	43
2.3.1 Significance of Bromine Removal	43
2.3.2 Synergetic Influence of Oxygen and Bromine Remove	45
2.3.3 The Importance of the Age of Metol Stock Solution	47
2.3.4 Dependence of the Oscillations on the Initial Compositions	52
2.3.5 Influences of Stirring Rate	57
2.3.6 Dynamic Perturbation and Characterization	59
2.3.7 Spatiotemporal Behavior	63
2.3.8 Simulation of Pattern Formation	67
2.4 Conclusions	71
2.5 References	72
Chapter 3: Design of a Novel Minimal Bromate Oscillator	76
3.1 Introduction	76
3.2 Experimental Procedure	77
3.3 Results and Discussion	78
3.4 Conclusions	85

3.5 References	87
Chapter 4: Subtle Photochemical Behavior in the Ferroin-Bromate-Benzoquinone Reaction	89
4.1 Introduction	89
4.2 Experimental Procedure	91
4.3 Results and Discussion	92
4.4 Conclusions	104
4.5 References	104
Chapter 5: Complex Behavior in the Highly Photosensitive Cerium-Bromate-1,4-Benzoquinone Reaction	107
5.1 Introduction	107
5.2 Experimental Procedure	108
5.3 Results and Discussion	110
5.3.1 Reaction Behavior in a Dark Room	110
5.3.2 The Influence of Ceiling Light	113
5.3.3 Wavelength and Intensity Dependence	116
5.3.4 Mechanistic Characterization	117
5.3.5 Modeling	120
5.4 Conclusions	123
5.5 References	124
Chapter 6: Electrochemically Modified Carbon Electrodes for Simultaneous Determination of Dihydroxybenzene Isomers	127
6.1 Introduction	127
6.2 Experimental Procedure	128

6.3 Results and Discussion	130
6.4 Conclusions	138
6.5 References	139
Chapter 7: Conclusions and Perspective	142
7.1 Conclusions	142
7.2 Future Work	146
7.3 References	152
APPENDIX	154
VITA AUCTORIS	179

LIST OF TABLES

4.1	Model proposed for the ferroin-bromate-Q oscillator	102
4.2	Rate constants used in the modeling of the ferroin-bromate-Q oscillator	102
5.1	Model proposed for the cerium-bromate-Q oscillator	121
5.2	Rate constants used in the modeling of the cerium-bromate-Q oscillator	122

LIST OF FIGURES

1.1	Attractors conducted in (a) a closed reactor, and (b) an open reactor.	2
1.2	Diagram of the BZ reaction mechanism.	5
1.3	A common CSTR configuration.	7
1.4	Bistability phenomena.	8
1.5	Relationship between active media and spatio-temporal patterns.	13
1.6	Spiral core meandering and local dynamics.	16
2.1	Time series of ferroin-bromate-metol reaction with different configurations of the reactor (a) sealed with parafilm, and (b) flowing nitrogen gas above the solution surface. Initial reaction compositions were [metol] = 0.025 M, [NaBrO ₃] = 0.05 M, [H ₂ SO ₄] = 1.7 M, and [ferroin] = 1.0×10^{-4} M.	44
2.2	Influence of nitrogen flow rate on the oscillatory behavior (a) 40, (b) 60, and (c) 80 ml/min. Other reaction conditions were [metol] = 0.025M, [NaBrO ₃] = 0.05M, [H ₂ SO ₄] = 1.7M, [ferroin] = 1.0×10^{-4} M, and the reaction solution volume was 20 ml.	45
2.3	Time series of ferroin-bromate-metol reaction carried out by flowing (a) 1:1 nitrogen and air mixture, (b) air, and (c) oxygen above the solution surface. Other reaction conditions are the same as those used in Figure 2.1b.	47
2.4	Time series of ferroin-bromate-metol reaction performed with (a) fresh, (b) 1, (c) 4, and (d) 7 days old metol stock solution. Initial reaction compositions were [metol] = 0.025 M, [NaBrO ₃] = 0.05 M, [H ₂ SO ₄] = 1.7 M, and [ferroin] = 1.0×10^{-4} M.	49
2.5	TOF-MS analysis of 3 days old metol solution (a) and 7 days old metol solution (b).	50
2.6	Time series of ferroin-bromate-metol reaction performed with different combination of metol and hydroquinone: (a) [metol] = 0.02 M, [H ₂ Q] = 0.005 M; (b) [metol] = 0.0125 M, [H ₂ Q] = 0.0125 M; and (c) [metol] = 0.01 M, [H ₂ Q] = 0.015 M. Other conditions were the same as in Figure 2.4a.	52
2.7	Phase diagram of ferroin-bromate-metol reaction in the bromate-sulfuric acid concentration plane. All other conditions were the same as those used in Figure 2.4a. The system exhibited spontaneous oscillations only within the marked region: (●) sequential oscillations, (■) damping oscillations (Type II), (▲) oscillations with two distinct frequencies, and (▼) low frequency, large amplitude oscillations (Type I).	54

- 2.8** Time series of ferroin-bromate-metol reaction at different acid concentrations (a) 1.8 M, (b) 1.7 M, (c) 1.3 M, and (d) 0.3 M. Other reaction conditions are [metol] = 0.025 M, [NaBrO₃] = 0.05 M, and [ferroin] = 1.0×10^{-4} M. The reactor was unsealed to allow volatile species diffuse out and allow the air diffuse into the reactor. 55
- 2.9** Time series of ferroin-bromate-metol reaction at different initial concentrations of ferroin: (a) 2.5×10^{-5} M, (b) 5.0×10^{-5} M, (c) 2.0×10^{-4} M, and (d) 4.0×10^{-4} M. Other reaction conditions are [metol] = 0.025 M, [NaBrO₃] = 0.05 M, and [H₂SO₄] = 1.7 M. The reactor was unsealed to allow volatile species diffuse out and air diffuses into the reactor. 56
- 2.10** Time series of ferroin-bromate-metol reaction at different initial concentrations of metol: (a) 0.025 M, (b) 0.02 M. Other reaction conditions are [NaBrO₃] = 0.05 M, [ferroin] = 1.0×10^{-4} M, and [H₂SO₄] = 1.7 M. The reactor was unsealed to allow volatile species diffuse out and air diffuses into the reactor. 57
- 2.11** Influences of stirring rate on the oscillatory behavior: (a) 1200 and (b) 600 rpm, where nitrogen was flow into the reactor at a rate 60 ml/min. Other reaction conditions were [metol] = 0.025M, [NaBrO₃] = 0.05M, [H₂SO₄] = 1.7M, and [ferroin] = 1.0×10^{-4} M. 58
- 2.12** The influence of stirring rate on the oscillatory behavior: (a) 1200, (b) 900, and (c) 600 rpm, where oxygen was flow into the reactor at a rate 60 ml/min. Other reaction conditions were [metol] = 0.025M, [NaBrO₃] = 0.05M, [H₂SO₄] = 1.7M, and [ferroin] = 1.0×10^{-4} M. 59
- 2.13** Effects of bromide ion on bromate-metol catalyzed reaction with [metol] = 0.025 M, [NaBrO₃] = 0.05 M, [ferroin] = 10^{-4} M and [H₂SO₄] = 1.7 M, each perturbation of bromide ion is 0.15 ml [Br⁻] = 10^{-4} M in the mixture. All other conditions were the same as those used in Figure 2.4a. 61
- 2.14** ¹H NMR (500MHz) spectra of the ferroin-bromate-metol reaction at the conditions [metol] = 0.025 M, [NaBrO₃] = 0.05 M, [ferroin] = 1.0×10^{-4} M and [H₂SO₄] = 1.7 M, (a) sealed with parafilm, and (b) flowing nitrogen gas above the solution surface. 62
- 2.15** ¹³C NMR (500MHz) spectra of the ferroin-bromate-metol reaction at the conditions [metol] = 0.025 M, [NaBrO₃] = 0.05 M, [ferroin] = 1.0×10^{-4} M and [H₂SO₄] = 1.7 M, (a) sealed with parafilm, and (b) flowing nitrogen gas above the solution surface. 63
- 2.16** Space-time plot of the ferroin-bromate-metol reaction in a capillary tube. The length of the medium is 50 mm. Time period shown here is between 120 min and 360 min. Reaction compositions are [metol] = 0.025 M, [NaBrO₃] = 0.05 M, [ferroin] = 3×10^{-3} M and [H₂SO₄] = 1.7 M. The inner diameter of the tube is 1.8 mm. (a) two sides of the capillary tube were open to the air, (b) left side of the capillary tube was open to the air, and the right hand side was sealed by water. 65
- 2.17** Typical spiral waves (a) and target patterns (b) formed in the silica gel membrane. The bottom silica gel layer with 1.5 mm thickness was immobilized by 0.03M

ferriin, top solution with 2.5 mm thickness was applied the same configuration as Figure 2.1 except a metal catalyst ferroin. 66

- 2.18** Space-time plots of wave dynamics appearing propagation failure (a), (b) merging and anomalous dispersion, and splitting (c), (d) wave turbulence, x axis represents space, and y axis means time. All diffusion coefficient was $D = 10^{-3}$, (a) $f_1 = 1.0$, (b), (c) and (d) $f_1 = 0.9$. Horizontal axis represents space, and vertical axis means time. 69
- 2.19** Space-time plots of transient breathing pulses in (a) and two dimensional breathing Turing patterns in (b). Parameters applied in (a) were $f_1 = 0.5$, $f_2 = 1.0$, $D_x = D_w = 10^{-4}$, $D_y = D_z = 10^{-3}$, and parameters applied in (a) were $f_1 = f_2 = 1.0$, $D_x = 10^{-6}$, $D_y = D_z = D_w = 10^{-5}$. All other parameters were the same as in Figure 2.18. 70
- 3.1** Time series of ferroin-bromate-benzoquinone reaction at different concentrations of benzoquinone (a) 0.025 M, (b) 0.035 M and (c) 0.035 M. In (c) 3.0×10^{-4} M of 1,10-phenanthroline was added initially. Other reaction conditions were $[\text{NaBrO}_3] = 0.05$ M, $[\text{ferroin}] = 1.0 \times 10^{-4}$ M, and $[\text{H}_2\text{SO}_4] = 0.05$ M. The reaction was carried out in a dark room while the reactor was sealed with parafilm. 80
- 3.2** Time series of ferroin-bromate-benzoquinone reaction carried out at different configurations of the reactor: (a) closed, and (b) flowing nitrogen into the reactor (40 mL/min). Compositions of the reaction solution were $[\text{NaBrO}_3] = 0.05$ M, $[\text{ferroin}] = 1.0 \times 10^{-4}$ M, $[\text{Q}] = 0.035$ M, and $[\text{H}_2\text{SO}_4] = 0.05$ M. 81
- 3.3** Time series of ferroin-bromate-benzoquinone reaction carried out at different configurations of the reactor: (a) closed, and (b) flowing nitrogen into the reactor (40 mL/min). Compositions of the reaction solution were $[\text{NaBrO}_3] = 0.05$ M, $[\text{ferroin}] = 1.0 \times 10^{-4}$ M, $[\text{Q}] = 0.025$ M, and $[\text{H}_2\text{SO}_4] = 0.05$ M. 82
- 3.4** Responses of the oscillation to bromide perturbation. Each time 0.015 mL concentrated bromide was added, resulting 1.0×10^{-5} M bromide after the dilution. Compositions of the reaction solution were $[\text{NaBrO}_3] = 0.05$ M, $[\text{ferroin}] = 1.0 \times 10^{-4}$ M, $[\text{Q}] = 0.03$ M, and $[\text{H}_2\text{SO}_4] = 0.05$ M. To achieve a large number of peaks, nitrogen flow was applied here at a rate of 40 mL/min. 83
- 3.5** (a) Cyclic voltammetry showing the influence of benzoquinone on the redox potential of ferriin/ferroin. The scanning rate is 100 mV/s. The supporting electrolyte is 1 M KNO_3 , $[\text{ferroin}] = 0.0025$ M, $[\text{Q}] = 0.03$ M, and $[\text{H}_2\text{SO}_4] = 0.1$ M. (b) ^1H NMR (500MHz) spectrum from the reaction carried out in Figure 3.2a 2-bromo-1,4-benzoquinone: $\delta = 7.30$ (d, $J = 3.5$ Hz), 6.93 (d, $J = 10.5$ Hz), 6.83 (dd, $J = 10.5, 3.5$ Hz). 85
- 4.1** Time series of ferroin-bromate-benzoquinone reaction carried out (a) in a dark room, and (b) with the room light on ($I = 20 \mu\text{W}/\text{cm}^2$). Other reaction conditions were $[\text{NaBrO}_3] = 0.05$ M, $[\text{ferroin}] = 1.0 \times 10^{-4}$ M, $[\text{H}_2\text{SO}_4] = 0.05$ M, and $[\text{Q}] = 0.035\text{M}$. 93
- 4.2** (a) ^1H NMR spectrum of an illuminated MBO reaction; (b) Time series of ferriin and bromide reaction collected at 510 nm, where the reaction (1) was illuminated with $30 \text{ mW}/\text{cm}^2$ light and reaction (2) was unilluminated. 95

- 4.3** Response of ferroin-bromate-benzoquinone reaction to perturbation of (a) 5 s light pulse of different wavelengths, (b) bromide ions, and (c) 5 s light pulse of $\lambda = 500 \pm 40$ nm and $I = 20$ mW/cm². Other reaction conditions were the same as those used in Figure 4.1b. 98
- 4.4** Time series of ferroin-bromate-benzoquinone reaction illuminated with light of different intensities: (a) 4 μ W/cm², (b) 15 μ W/cm², and (c) 46 μ W/cm². Other reaction conditions were the same as those used in Figure 4.1a. 99
- 4.5** Time series of ferroin-bromate-benzoquinone reaction at different sulfuric acid concentrations: (a1, b1) 0.08 M, (a2, b2) 0.07 M, (a3, b3) 0.05 M, and (a4, b4) 0.03 M. Reactions (a1) to (a4) were illuminated with 500 ± 40 nm light of 15 μ W/cm². Reactions (b1) to (b4) were carried out in a dark room. Other conditions were [NaBrO₃] = 0.05 M, [ferroin] = 1.0×10^{-4} M, and [Q] = 0.035M. 100
- 4.6** (a) Oscillations of the ferroin-bromate-Q reaction in a dark condition. Initial conditions used in the simulation are: [NaBrO₃] = 0.05 M, [ferroin] = 1.0×10^{-4} M, [Q] = 0.035 M, [H⁺] = 0.1 M, [H₂O] = 55 M and [Br⁻] = 1×10^{-8} M, $k_9 = 1.5$ M⁻¹s⁻¹, $k_{11} = 50$ M⁻¹s⁻¹, $k_{12} = 25$ M⁻¹s⁻¹; (b) time series under the influence of light, implemented by resetting $k_9 = 4$ M⁻¹s⁻¹, $k_{11} = 60$ M⁻¹s⁻¹, $k_{12} = 50$ M⁻¹s⁻¹. 103
- 5.1** Time series of the Ce(IV)-bromate-Q reaction carried out at different sulfuric acid concentrations: (a) 0.15 M, (b) 0.2 M and (c) 0.25 M. Other reaction conditions were [NaBrO₃] = 0.05 M, [Ce(IV)] = 1.0×10^{-4} M and [Q] = 0.035M. 110
- 5.2** Time series obtained at the condition that air was flowing above the reaction solution at a rate of 60 ml/min. Other conditions are the same as the corresponding panel in Figure 5.1. 111
- 5.3** Time series of the Ce(IV)-bromate-Q reaction at different concentrations of Ce(IV): (a) 5.0×10^{-5} M, (b) 1.0×10^{-4} M and (c) 2.0×10^{-4} M. Other reaction conditions were the same as those in Figure 5.1b. 113
- 5.4** Time series of the Ce(IV)-bromate-Q reaction under the irradiation of ceiling light (20 μ W/cm²) with different concentrations of sulfuric acid: (a) 0.2M, (b) 0.15M, (c) 0.1M, and (d) 0.05M. Other compositions were the same as those used in Figure 5.1. 114
- 5.5** Time series of the Ce(IV)-bromate-Q reaction under the irradiation of ceiling light (20 μ W/cm²) with different Ce(IV) concentrations: (a) 2.5×10^{-5} M, (b) 5.0×10^{-5} M, (c) 2.0×10^{-4} M, and (d) 4.0×10^{-3} M. Other reaction conditions were the same as those used in Figure 5.3. The inset in (c) shows responses of the system to light pulse perturbation of different wavelengths. 115
- 5.6** Time series of the Ce(IV)-bromate-Q reaction illuminated with 500 ± 40 nm light of different intensities: (a) 2.5 μ W/cm², (b) 5 μ W/cm², (c) 50 μ W/cm², and (d) 500 μ W/cm². Other reaction conditions were the same as Figure 5.1b. 117
- 5.7** Times series carried out with different illumination (150 mW/cm²) time (a) 150s and (b) 600s. Time series were in the initial presence of 2.0 mM QBr (c) and 4.0 mM QBr (d). Other reaction conditions were the same as those in Figure 5.4a, except [Q] = 0.033M in (c) and 0.031M in (d). 118

- 5.8** (a) Absorption spectra of 0.003M of QBr in 0.1M H₂SO₄ solution, (b) Time series of the same QBr solution collected at 350 nm, where the solution was illuminated with 20 mW/cm² light (solid line) or 20μW/cm² ceiling light (dash line). 120
- 5.9** (a) Oscillations of the Ce(IV)-bromate-Q reaction in a dark condition. Initial conditions used in the simulation are: [NaBrO₃] = 0.05 M, [Ce(IV)] = 1.0×10^{-4} M, [Q] = 0.035 M, [H⁺] = 0.4 M, [H₂O] = 55 M, [Br⁻] = 1×10^{-8} M, $k_9 = 19.9 \text{ M}^{-1}\text{s}^{-1}$, $k_{10} = 1 \times 10^4 \text{ M}^{-1}\text{s}^{-1}$, $k_{11} = 50 \text{ M}^{-1}\text{s}^{-1}$; (b) time series under the influence of light, which was implemented by resetting $k_9 = 40 \text{ M}^{-1}\text{s}^{-1}$, $k_{10} = 1 \times 10^4 \text{ M}^{-1}\text{s}^{-1}$, $k_{11} = 60 \text{ M}^{-1}\text{s}^{-1}$; (c) the initial concentration of QBr was set to 1.0×10^{-6} M, while all other parameters are the same as those in (a). 123
- 6.1** SEM images of carbon electrodes: (a) unmodified, (b) modified in H₂SO₄ and (c) modified in H₂SO₄ and NaOH solution. Panel (d) is an EDX spectrum of the electrode shown in (c). Raman spectra of carbon electrodes: (e) unmodified and (f) modified corresponded to a 50% intensity of 514.5 nm exciting laser. 131
- 6.2** (a) CVs at carbon electrodes of unmodified (curve 1), modified in H₂SO₄ (curve 2) and modified in H₂SO₄ and NaOH solution (curve 3) measured in a 0.001 H₂SO₄ solution; (b) CVs of a 0.001 H₂SO₄ solution containing 20.0 μM of H₂Q and CC at carbon electrode (curve 1) and modified carbon electrode (curve 2). 133
- 6.3** DPVs at a modified carbon electrode in (6.3a) 50 μM CC and different concentrations of H₂Q: 0.1, 2.0, 3.0, 5.0, 10.0, 20.0, 30.0, 40.0, 50.0, 60.0, 70.0, 80.0, 90.0, and 100.0 μM (from A to N), and (6.3b) 50 μM H₂Q and different concentrations of CC: 0.1, 5.0, 10.0, 20.0, 30.0, 40.0, 50.0, 60.0, 70.0, 80.0, 90.0 and 100.0 μM (from A to L). The insets show the calibration plots of CC and H₂Q versus peak currents. 135
- 6.4** Oscillation profiles (a) and corresponding DPV situ tests (b), other reaction conditions were [CHD] = 0.1 M, [NaBrO₃] = 0.1 M, [H₂SO₄] = 0.6 M. (c) DPV situ measurements during the induction time of CHD-bromate chemical oscillation, (A) right after prepared solution, (B) 2000 s, (C) 4000 s, (D) 6000 s. Oscillation was occurred at around 6400 s. 137
- 6.5** DPVs at a modified carbon electrode in Figure 6.4a 0.6 M acid and different concentrations of H₂Q: 5.0, 6.0, 7.0, 8.0, 9.0, 10.0 mM (from A to F), and in Figure 6.4b 1.0M acid and different concentrations of H₂Q: 0, 6.0, 7.0, 8.0, 9.0, 10.0, 15.0 mM (from A to G). 138
- 7.1** Time series of CHD-bromate system without or with PdO, [CHD] = 0.1 M, [NaBrO₃] = 0.1 M, [H₂SO₄] = 0.8 M, (a) without adding PdO, (b) adding 20 mg PdO at around 3,800 s. 149
- 7.2** Time series of CHD and H₂Q system with PdO, (a) [CHD] = 0.1 M, [H₂SO₄] = 0.8 M, adding 20 mg PdO at around 3800 s, (b) [H₂Q] = 0.1 M, [H₂SO₄] = 0.8 M, adding 20 mg PdO at around 3800 s. 150
- 7.3** SEM images of CHD-Bromate-PdO system with different aging time. (a) right after oscillation, (b) one day, (c) two days, (d) four days. All other reaction conditions were the same as in Figure 7.1b. 151

LIST OF ABBREVIATIONS

BZ	Belousov-Zhabotinsky
FKN	Field-Korös-Noyes
MA	malonic acid
CIMA	chlorite-iodide-malonic acid
BR	Briggs-Rauscher
CSTR	continuous stirred tank reactor
MBO	minimal bromate oscillator
RD	reaction-diffusion
CHD	1,4-cyclohexanedione
AOT	aerosol OT (sodium bis(2-ethylhexyl) sulfosuccinate)
CFUR	continuously fed unstirred reactors
APILs	aprotic ionic liquids
PILs	protic ionic liquids
NIPAAm	N-isopropylacrylamide
TFP	thermal frontal polymerization
H2Q	1,4-hydroquinone
BQ	1,4-benzoquinone
Metol	p-methylaminophenol
BrQ	2-bromo-1,4-benzoquinone

Br ₂ HQ	2,3-dibromohydroquinone and 2,5-dibromohydroquinone
QOH	2-hydroxy-1,4-benzoquinone
CNT	carbon nanotube
CC	pyrocatechol
CV	cyclic voltammetry
SEM	scanning electron microscopy
SCE	saturated calomel electrode
DPV	differential pulse voltammetry
rpm	round per minute
EDX	energy dispersive X-ray spectroscopy
RSD	relative standard deviation
PdO	palladium oxide hydrate
EPR	electron paramagnetic resonance

LIST OF APPENDICES

A	A Code of the Simulation in Chapter 2	154
B	A Code of the Simulation in Table 4.1	161
C	A Code of the Simulation in Table 5.1	163
D	Copyright Releases Chem. Phys. Lett.	165
E	Copyright Releases J. Phys. Chem. A	171
F	Copyright Releases Phys. Chem. Chem. Phys.	172
G	Copyright Releases Electrochem. Commun.	173

Chapter 1: Introduction

This introductory chapter is an overview of chemical oscillators, including both experimental methods and theoretical analysis employed in related studies.

1.1 Nonlinear Dynamics in Stirred Systems

1.1.1 Requirement of Chemical Oscillations

It is expected that a chemical system that is not at thermodynamic equilibrium will monotonically move toward the equilibrium state [1] due to the second law of thermodynamics, which states “the entropy of an isolated system not in equilibrium will tend to increase over time ($\Delta S > 0$), approaching a maximum value at equilibrium”. At the point of chemical equilibrium, Gibbs energy G is minimum and the thermodynamic requirement of the change in Gibbs free energy ΔG equals 0. If a chemical system is close to the equilibrium, the chemical driving force has a linear relationship with thermodynamic flow. Thus the behavior of this kind of chemical systems will approach their final equilibrium monotonically. Therefore, for a chemical system to display any interesting nonlinear behaviour such as oscillations and chaos, the system is required to stay far from thermodynamic equilibrium [2-4].

When chemical oscillations occur, they never pass through the thermodynamic equilibrium point. How to keep a system far away from equilibrium? It depends on the initial concentrations and the type of reactors [5] as shown in Figure 1.1. Comparing with those oscillating intermediates, in a closed reactor (a) much higher initial concentrations of the reactants are necessary in order to sustain the reaction conditions far-from-equilibrium condition. On the other hand, an open reactor can maintain the far-from-

equilibrium condition indefinitely through continuous inflow of reactants and outflow of products (see the circle loop in (b)).

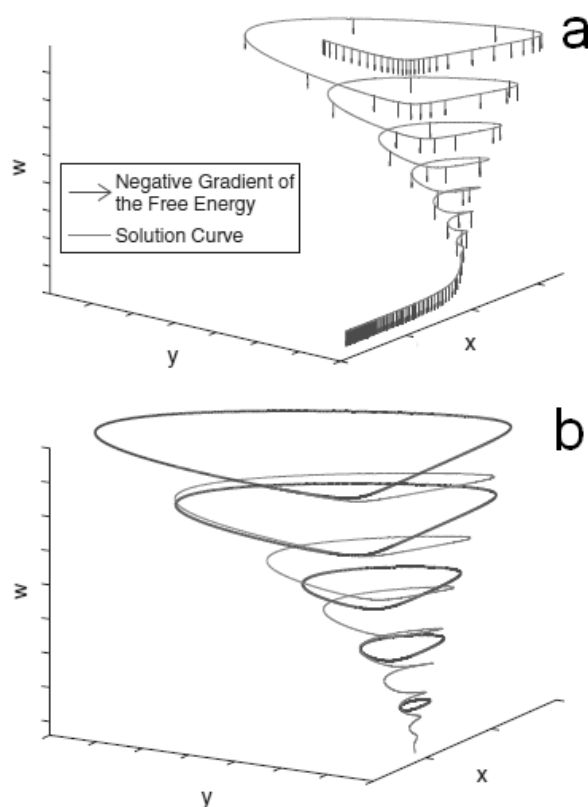


Figure 1.1 Attractors conducted in (a) a closed reactor, and (b) an open reactor.

(quoted from Y. F. Li, H. Qian and Y. F. Yi, J. Chem. Phys., 2008, 129, 154505.)

Another important requirement for a system to exhibit nonlinear phenomena is the presence of nonlinear feedbacks [6]. Such a feedback is defined as either the intermediates or products influencing steps earlier in the reaction mechanism either positively (accelerating the reactions) or negatively (inhibiting the reactions). The most common form in a nonlinear chemical system is autocatalytic reactions, such as the quadratic autocatalysis, $X + Y \rightarrow 2Y + Z$.

1.1.2 Nonlinear Kinetics in a Closed Reactor

The closed reactor plays an important role in investigating the clock reaction [7-9], and represents the simplest configuration in studying macroscopic chemical kinetics. The reaction system is maintained homogeneous by vigorous stirring and thermostatic with a circulating water jacket. No chemicals enter or leave the reactor once the reaction starts. Therefore it is also called a batch reactor.

Relatively few reaction systems can exhibit spontaneous oscillations in a closed reactor. The Bray-Liebhafsky (BL) reaction is the first chemical clock, which is the reaction of iodate, iodine and hydrogen peroxide. Bray [8] in 1921 and Bray and Liebhafsky [9] in 1931 investigated the catalytic role of iodate in the conversion of hydrogen peroxide to oxygen and water. At certain reaction conditions, the evolution of iodine was found like a clock reaction, in which the color of iodine was fading from dark to colorless. After the clock event the system was unable to return to such initial conditions for resetting the clock. Although the chemical clock could repeat at various conditions, chemists thought that the BL reaction was not entirely homogeneous and such a repeated chemical clock was a result of dust or bubbles. Before the development of the Belousov-Zhabotinsky (BZ) oscillator, a number of papers had been published on why true homogeneous oscillation was impossible [10], that is why the BL reaction was treated as a nonhomogeneous reaction [11, 12].

With no doubt, the BZ reaction [13-30] is the first stone knocked at the door of modern nonlinear chemical dynamics. Belousov [10] investigated a batch reaction with potassium bromate, citric acid/malonic acid (MA), sulfuric acid and cerium sulfate, and observed that the solution periodically changed from yellow (Ce^{4+}) to colorless (Ce^{3+}).

Zhabotinsky improved the Belousov recipe by using a new redox indicator, in which ferroin is red in the reduced form and blue in the oxidized state, making the transitions easily visible [15]. As shown the basic BZ reaction mechanism [31-36] in Figure 1.2, M_{red} represents the reduced state of metal catalysts, and M_{ox} denotes the oxidized state. Consumption of bromate by bromide initiates the first autocatalytic cycle to produce HBrO_2 , and such a process results in the oxidation of metal catalyst. On the other hand, the consumption of bromide by HBrO_2 initiates a second reaction cycle for the reduction of the oxidized metal catalyst (dashed line), in which bromide reacts with HBrO_2 to generate HOBr , bromide reacts with HOBr to generate bromine, and bromine reacts with MA to generate brominated MA which is BrMA . The final product of M_{ox} from the first autocatalytic cycle reacts with the final product of BrMA from the second reaction cycle, and then gives rise to the regeneration of bromide. Just like a clock reset, the concentration of bromide eventually falls below some critical level $[\text{Br}^-]_{\text{cr}}$. When the concentration of bromide is above the $[\text{Br}^-]_{\text{cr}}$, bromide consumption reactions dominate. When the concentration of bromide is below the $[\text{Br}^-]_{\text{cr}}$, the bromide regeneration reaction will be the predominant process.

In 1955 Prigogine [10] pointed out that while a closed system must eventually reach equilibrium, transient oscillations might take place as the system approaches to the equilibrium from a far-from-equilibrium condition. In other words, chemical oscillations in closed systems no longer violate the laws of nature. What actually oscillate in the BZ reaction are the concentrations of intermediates such as bromide, bromous acid, etc.

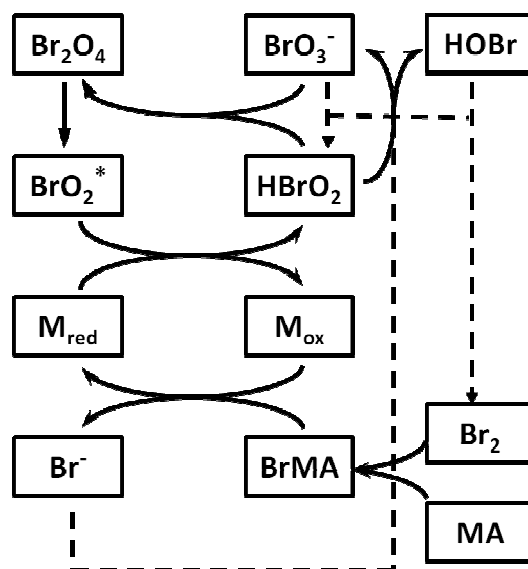
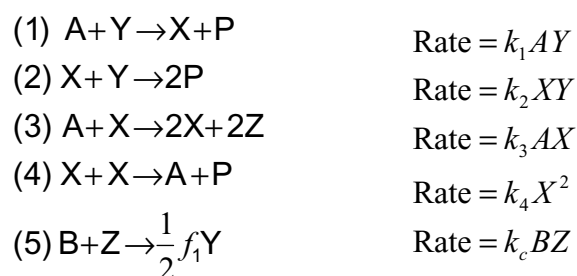


Figure 1.2 Diagram of the BZ reaction mechanism.

In 1972 Richard J. Field, Endre Koros and Richard M. Noyes proposed the first complete mechanism for the BZ reaction [31], which is now commonly known as the FKN mechanism. This full scheme was later simplified to a mathematical model “Oregonator” for qualitatively simulating the BZ oscillations:



The Oregonator consists of five reaction steps, where $\text{X} = \text{HBrO}_2$, $\text{Y} = \text{Br}^-$, $\text{Z} = \text{Ce(IV)}$, $\text{A} = \text{BrO}_3^-$, $\text{B} = \text{CH}_2(\text{COOH})_2$, and $\text{P} = \text{HOBr}$ or $\text{BrCH}(\text{COOH})_2$. Three major processes are involved: (1) Br^- consumption (reactions 1 and 2); (2) HBrO_2 autocatalytic production (reaction 3); and (3) Br^- regeneration (reactions 4 and 5). The study of the FKN mechanism and Oregonator model has led to new insights into nonlinear dynamical

phenomena seen in nature and provided important guidance to experimental exploration of nonlinear kinetics in the laboratory. In the numerical simulations a qualitative change in the nature of the solution to a set of differential equations is known as a bifurcation and bifurcation analysis has been commonly employed to determine the onset of oscillatory behavior [37].

Since the discovery of the BZ reaction, chemists have attempted to use different metal ions or metal complexes as the catalyst as well as employ different organic substrates [38-49] to react with the acidic bromate. Those researches have led to the development of a large number of modified BZ oscillators. In the 1980s, chemists found that some intermediates of the BZ reaction could oscillate in the closed reactor only when bromine was removed by inflowing a stream of nitrogen gas or air through the solution [50, 51]. They defined this configuration as a semi-batch reactor, an alternative to the closed reactor. Later Rabai and Epstein [52] established another kind of semi-batch reactor, in which the beaker was gradually filled up by a pump or with gravity feed as the reaction proceeded. Besides the BZ oscillator, many new oscillators such as the chlorite-iodide-malonic acid (CIMA) [53], Briggs-Rauscher (BR) [54], copper-phosphoric acid system [55], glycolytic reactions [56], etc. have been uncovered in the last three decades.

1.1.3 Nonlinear Kinetics in an Open Reactor

The best way to study chemical oscillations is in an open reactor, for it can capture the oscillation where its amplitude and period are truly constant. It must have a flow of fresh reactants into the system and a flow of products out of it. If a chemical system could generate oscillations in a closed reactor, it generally would also oscillate in an open reactor. For the open reactor, shown in Figure 1.1b, the system can in principle be

maintained at any of the far-from-equilibrium conditions where the oscillation displays on the way to the final equilibrium state in the closed reactor. The major experimental progress for open reactors was the introduction of the continuously flow stirred tank reactor (CSTR) as shown in Figure 1.3, where the pump controls the rate of inflow and outflow. The average time that a molecule spends in the reactor is calculated with volume (mL)/flow rate (mL s^{-1}).

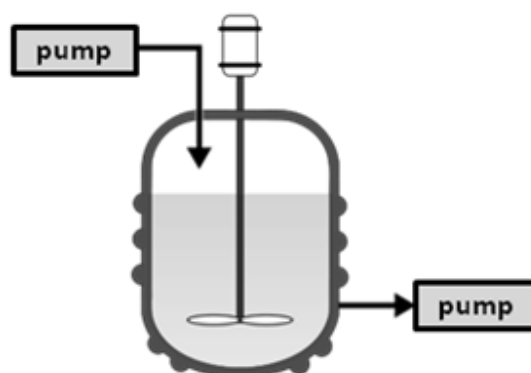


Figure 1.3 A common CSTR configuration.

The simplest nonlinear behavior displayed by a chemical system conducted in an open reactor is bistability. This is the coexistence of two stable steady states over a range of operating parameters, e.g., flow rate. In Figure 1.4 two solid lines indicate the stable branches, while the dashed line is an unstable branch of steady states. At a very high flow rate concentrations of the reactants in a CSTR are similar to their inflow concentrations, this stable branch is known as flow branch. One of the bistable steady states locates on this flow branch. At a low flow rate, the system in a CSTR is close to the thermodynamic equilibrium, such a stable branch is called thermodynamic branch. The other bistable

steady state is located on this thermodynamic branch. Typically a bistable system undergoes transitions from one stable steady state to another when a suitable perturbation is applied or when a control parameter is changed beyond its bistability limit. It is also possible for chemical systems to display multistability, in which there are more than two stable steady states coexist.

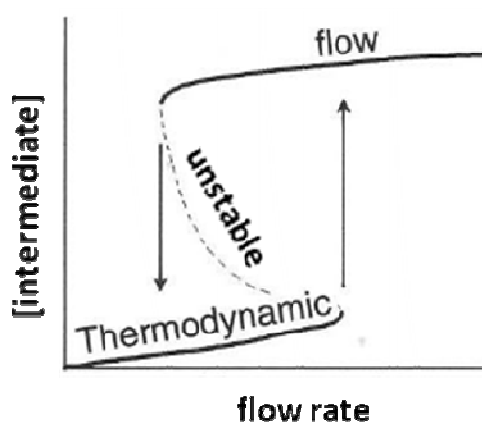


Figure 1.4 Bistability phenomena. (quoted from I. R. Epstein and J. A. Pojman, Oxford University Press, New York, 1998.)

The development of CSTR technique has greatly facilitated the discovery of new chemical oscillators and complex chemical oscillations. For example, Geislar [57] reported that in a CSTR the bromate-bromide-manganese (II) could exhibit sustained oscillations or multiple steady states. Orban and co-workers [58] obtained a narrow oscillatory region in a flow reactor using cerium/manganous ions as the metal catalyst to react with bromate and have referred those systems as the minimal bromate oscillator (MBO). Notably, those classical MBO can only oscillate in a CSTR. A large variety of

complex oscillations have been achieved when the BZ reaction was studied in a CSTR [59-66].

Probably the first example of complex chemical oscillations is bursting phenomenon, which is a form of oscillations usually seen in neurons. Bursting oscillations have a quiescent period before or after each set of oscillations, in which concentrations during the quiescent period changed very little. Sorensen [63] reported bursting oscillations in the BZ reaction in a CSTR, in which the number of oscillations per burst did not change until a bifurcation to the steady state occurred. The second form of complex oscillations observed in the BZ reaction in a CSTR was quasiperiodic oscillations [64]. Such an oscillatory behavior consisted of two distinct frequencies from the analysis of the Fourier spectrum. Quasiperiodicity is commonly observed in a coupled oscillator or a single oscillator with an external periodical forcing. Zhabotinsky [65] was the first to report multi-peaked periodic states in the BZ-CSTR system, Maselko and Swinney [66] observed and defined such basic patterns as mixed-mode oscillations, denoted with L^S , consisting of L as large amplitude oscillation and S as small amplitude oscillation.

Other complex oscillations such as period doubling and chaos had also been observed in BZ-CSTR systems. Chaos is one of the unwelcome discoveries in science, where duplicated experiments can lead to very different results because of tiny, unavoidable differences in the initial conditions. In other words, the chaotic systems can have outcomes that are entirely unpredictable. The man who forced the science community to confront chaos was Edward Lorenz. In the early 1960s [67], he tried to find mathematical equations that could help to predict the weather, like all his contemporaries. He believed that in principle, the weather system was no different than our solar system, which could

be described as a mechanical system and be predicted by mathematics. However, he was wrong, when Lorenz wrote down what looked like perfectly simple mathematic equations to describe the movement of air currents, they did not behave accordingly. Initial differences, however small, ultimately grow to different macroscopic behaviors. This phenomenon is very famous today, referred as the “butterfly effect” [68]. If the weather is indeed governed by true equations with chaotic solutions, regardless of if weather sensors had been distributed all over the world to feed weather information in real time into the equations’ programming, differences in initial wind velocities resulting from a butterfly flapping its wings may result in a hurricane instead of a beautiful day in Category.

Chaos in a CSTR has been found not only in the BZ reaction, but also in the chlorite-thiosulfate [69], bromate-chlorite-iodide [70] and chlorite-thiourea [71] reactions. Chemical chaos can be generated through three routes, period-doubling, periodic-chaotic sequences and intermittency [10]. The unpredictable and unrepeatable chaotic systems have allured scientists to develop various algorithms to control them, in which the basic idea is to introduce a carefully chosen, time-dependent perturbation into the chaotic system to drive the chaos back to normal oscillations.

1.2 Nonlinear Behavior in Reaction-Diffusion Media: Pattern Formation

Formation of ordered structures in nature is ubiquitous. From skin patterns on animals to the galaxy, the phenomenon of self-organization is encountered in diverse contexts in physical, chemical and biochemical systems. Well known cases in chemical processes are target patterns, spiral waves and Turing patterns. In biochemical processes spatiotemporal self-organized behavior has been studied in the context of pulsations of the heart, calcium waves and enzyme autocatalytic networks.

Those beautiful structures, whether it is in a chemical or biochemical system, can be united through a set of partial differential equations. When the chemical system is unstirred, it will be governed by reaction and diffusion, which is referred to as a reaction-diffusion (RD) system shown in the following:

$$\frac{du}{dt} = f(u, v) + D_u \nabla^2 u \quad (1.1)$$

$$\frac{dv}{dt} = g(u, v) + D_v \nabla^2 v \quad (1.2)$$

Where the kinetic terms contain nonlinear feedbacks. D denotes the diffusion coefficient for each chemical species, ∇^2 is a gradient operator in two or more dimensions (i.e., Laplace operator). In general, pattern formation can be understood as the cooperative behavior of a large number of individual local oscillators. They are governed by the reaction terms and are coupled through diffusion terms in the equation (1.1) and (1.2). Experimentally the RD system has been investigated in one-, two- or three-dimensional media, such as capillary tubes, petri dishes or beakers. The confinement of RD systems to different dimensions can give rise to various spatiotemporal structures like travelling pulses, target patterns, spiral waves and scroll waves.

Travelling waves of excitation are the common phenomena in a variety of systems far from thermodynamic equilibrium [72]. Of particular interest are so called excitable systems that reveal a great variety of spatiotemporal patterns that have fascinated scientists for several decades, such as electrical propagation in the brain, in nerves and in cardiac tissue. Constant amplitude and no interference behavior of such excitation waves arise from the spatial coupling of local nonlinear processes [73]. Of particular importance are wave patterns in excitable systems in which a local perturbation must exceed a certain

threshold value in order to trigger the propagating waves. According to the type of behavior affecting finite wave packets, the list of diverse types of propagating wave structures in reaction-diffusion systems [74] is long and includes propagation failure in the oxidation of CO on platinum surfaces [75], wave merging, stacking, breathing and backfiring in cyclohexanedione BZ (CHD-BZ) reaction [76], splitting autowaves by exposing BZ media to short light pulses [77] and electrical fields [78].

1.2.1 Pattern Formation in One-Dimensional Media

Spatiotemporal patterns developed in a capillary tube are often treated as one dimensional activity. Due to the small diameter of the capillary tube, the diffusion terms are only effective in the direction parallel to the capillary tube, and the concentration in each cross section is assumed to be identical. It is essential that at least a clock reaction is happening in order to generate front waves in one dimensional media. The wave “front” consists of a single point or a very narrow interval where concentrations jump from one nearly constant level to another. The wave profile in space resembles the concentration versus time profile for the homogeneous reaction. In some way, the type of spatiotemporal patterns is determined by the type of active media. Such as “front” propagation in a bistable medium, traveling waves in excitable media, and wave trains in oscillatory media [79] (see Figure 1.5).

Ignoring the diffusion term and then setting equations 1.1 and 1.2 equal to zero, two null lines are obtained in Figure 1.5 (a-c). A large perturbation from the left fixed point to point B in (a) may leads to a final state at the other fixed point. In such a case, once the reaction front reaches the right fixed point in one dimensional capillary tube, it will stay at the final state and never go back to the left fixed point. Phenomenonologically, before

the reaction front propagates, it keeps dark. After the front “burns” this place, it turns white and never changes back to dark color. There are two separate regions in the space-temporal plot in (d), and the behavior is called front propagation.

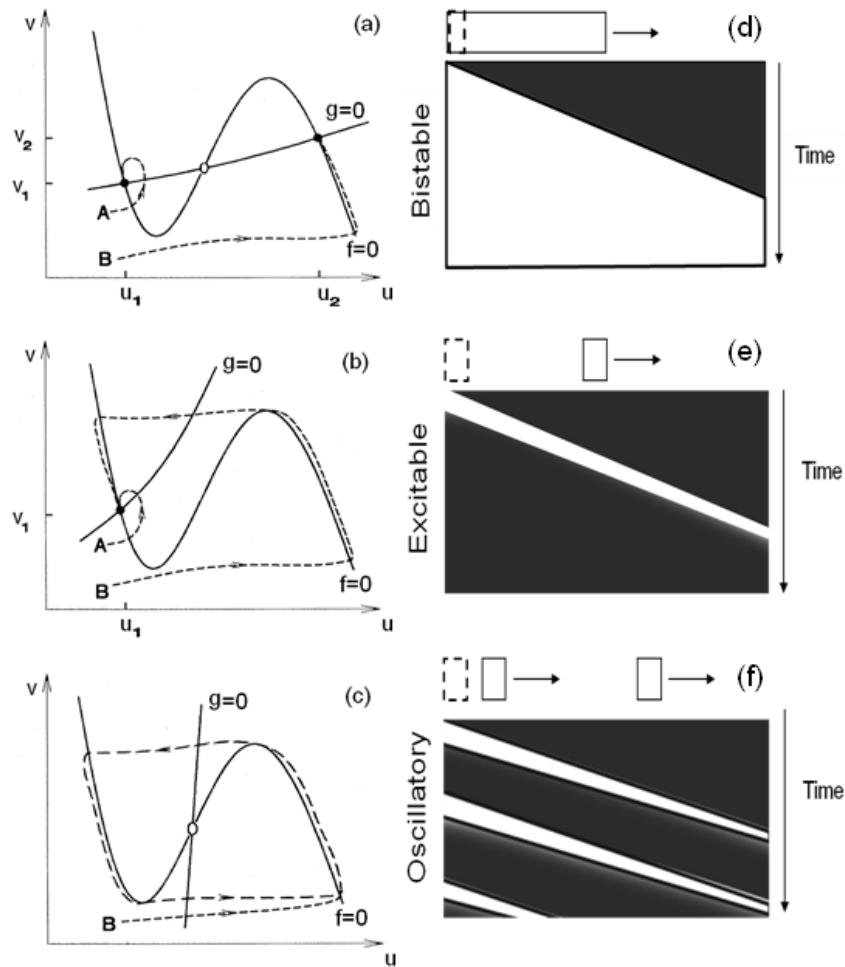


Figure 1.5 Relationship between active media and spatio-temporal patterns.

(quoted from M. C. Cross and P. C. Hohenberg, Rev. Mod. Phys., 1993, 65, 854.)

In an excited system (see Figure 1.5(b)), there is just one stable fixed point. Small perturbations (e.g. to point A) lead to responses confined to the neighborhood of the fixed

point, whereas large perturbations (e.g. to point B) lead to large excursions along the dashed line before the concentrations ultimately relax back to the fixed point. When large local perturbations are applied to the reaction system in the capillary tube, after the front passes one region, such region will relax back to the fixed point, which has the same color as the region before the front comes. As a result, one white region will travel from left of the tube to right. This behavior is called travelling pulses (see Figure 1.5(e)). Figure 1.5c shows null clines of an oscillatory case, consisting of large amplitude relaxation oscillations together with an unstable fixed point. Here, after one wave passes through, the clock reaction will reset and generate another wave because no stable fixed points exist in the oscillatory case. Eventually, a wave train as shown in Figure 1.5(e) is developed in the capillary tube.

As demonstrated in Figure 1.5, a chemical wave can be generated by applying a sufficiently large local perturbation. Where the initial perturbation comes from is a question that still needs to be addressed. One possibility is to manipulate the local reaction kinetics by electrical stimulation, light illumination or other chemical means. Sometimes, the chemical waves can arise spontaneously without an external perturbation. A more interesting question comes, how has this occurred? Two main possibilities were found after a great deal of effort into trying to establish the routes by which waves arise in the BZ reaction. First, a spontaneous concentration fluctuation at a particular point in the medium may cause the initial perturbation. Second, inhomogeneous, mechanism involves the presence of a pacemaker or catalytic site, such as a dust particle. Some researchers have attempted to study whether heterogeneous pacemakers are necessary for the initiation of waves in the BZ reaction. After carefully microfiltrating the solution and

using the remaining dust free conditions, it is possible to greatly increase the average time required for spontaneous generation of waves in BZ solution. They suggest the dust particles do serve as pacemakers [80].

1.2.2 Waves in Two-Dimensional Media

Pattern formation in two dimensional media is arguably the one that occurs frequently in biochemical and physical systems, and is the one that has been studied predominately in the laboratory and in simulations. A thin layer of two-dimensional reaction medium such as the BZ reaction can be spontaneously oscillating or excitable. To achieve the pattern formation in excitable media, one needs to initiate local oscillations at a point in the medium. After the wave front has been initiated, there will be a new feature arising in the two dimensional space, which is absent in one dimensional reaction-diffusion configuration. The new feature is that the wave front may be curved due to two-dimensional diffusion transportation. The radius R that best fits the wave front in the neighborhood of point is defined as curvature, K (equal to $1/R$). Zykov, Tyson and Foerster [81-83] have shown both theoretically and experimentally that the velocity of a curved wave front depends on the curvature in Equation 1.3:

$$N = c + DK \quad (1.3)$$

Where N is the normal velocity of the wave front, c is the velocity of a plane wave, and D is the diffusion coefficient of propagating species u .

In a homogeneous two-dimensional medium, a wavefront initiated from a point produces a circular front, travelling at the same speed in all direction. When such a wavefront is generated periodically by a localized pacemaker, the front then moves outward repeatedly as expanding concentric circles, which form a target pattern. If a

target pattern or wave front is broken by a physical disruption such as hitting the boundary of the medium or placing an obstacle in the medium, free ends will be created, which lead to the formation of spiral waves. Spiral waves have been observed in a wide range of chemical and biochemical systems, such as BZ reaction in a Petri dish [84], carbon monoxide oxidation on platinum surface [85], developing frog eggs [86], cardiac muscle [87], etc. One particular feature of spiral waves is the center or core from which the waves emanate. If one watches a spiral wave carefully for a long time, the core of the spiral may be seen moving around certain trajectory. The motion of the spiral core was discovered in both numerical studies of the Oregonator model [88] and in a ferroin-catalyzed BZ medium [89].

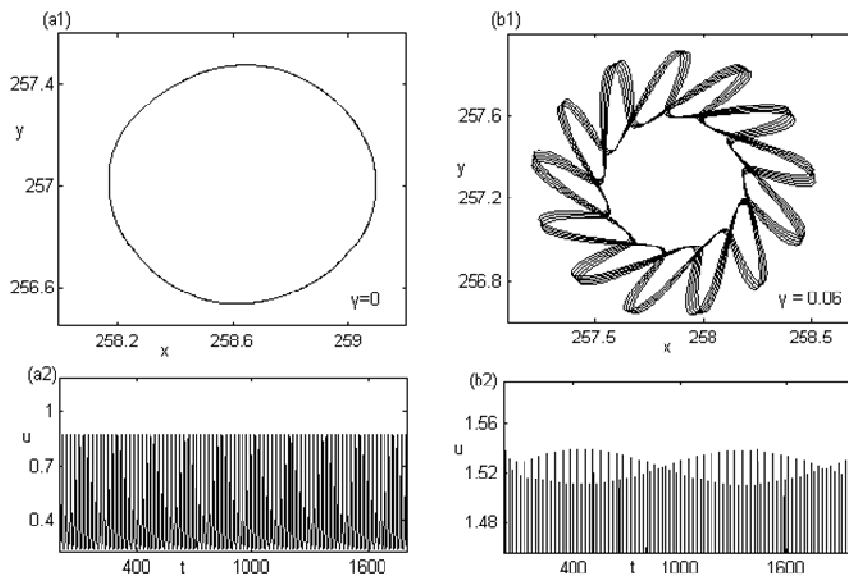


Figure 1.6 Spiral core meandering and local dynamics. (quoted from Q.

Y. Gao, J. Li, K. L. Zhang and I. R. Epstein, *Chaos*, 2009, 19, 033134)

One focus of the present study on spiral waves is their dynamical response toward periodic forcing. For example, the effect of external forcing on spiral waves in two-

dimensional light sensitive BZ media has been experimentally examined [90], in which transitions from spiral waves to spatiotemporal chaos have been found. Theoretically there are many numerical models for the study of spiral instabilities toward periodic forcing, such as Oregonator, CGLE, Barkley and Brusselator model, et al. A wide variety of spiral instabilities have been observed based on different forcing amplitudes and frequencies, such as near-core spiral break up, far-field spiral break up, and complex phenomena which include back firing, spiral synchronization, spiral regeneration, and amplitude modulation from line defects [91]. In each case, the spiral core meandering becomes more and more complex and irregular as the forcing amplitude increases as shown in Figure 1.6. With no periodic forcing the meandering pattern of spiral core is a regular circle in (a1) which corresponds to local dynamics of simple oscillation in (a2). After applying the periodic forcing into the Brusselator model, the meandering patterns of spiral core becomes more complex and the local dynamics exhibit quasiperiodic oscillations. The investigation of spiral waves and their stabilities in chemical RD media with complex dynamics offers promise for understanding similar pattern behavior in biological development and natural evolution such as pine cones, cauliflower, nautilus shells and galaxies, to name a few.

1.2.3 Three-Dimensional Waves

RD systems in three dimensions are particularly attractive by virtue of their versatility and their relevance to biochemical pattern formation. Although their experimental accessibility is much difficult, researchers are fascinated to study such systems not only for the importance of these phenomena in nature, but also the intellectual challenge of explaining their origin. As opposed to circular and spiral waves in two dimensional media,

spherical waves and scroll waves are seen in three-dimensional systems. The line connecting all spiral cores is called the filament, which is supposed to be straight. When filament starts to grow in extension, it will lose its original straight shape and lead to elaborate patterns and even chaos in three dimensions. The instability of scroll waves has been reported in the CHD-BZ system, where scroll rings and pairs underwent different types of collisions due to shrinking or expanding of the filaments [92]. Several other phenomena such as standing waves and packet waves have also been observed [93] in the three-dimensional BZ-AOT system, i.e., the BZ reaction in water-in-oil reverse microemulsion that was stabilized by the surfactant sodium bis(2-ethylhexyl) sulfosuccinate (AOT).

1.2.4 Turing Patterns

Different from the propagating waves discussed above, there is another unique class of wave activity, which is independent of time. Such a spatial structure is named Turing patterns in memory of its discovery by Alan Turing [94], who is widely considered to be the father of computer science and artificial intelligence. Turing's purpose was to propose a mechanism on how the genes could determine the structures of developing organisms. As catalysts, genes regulated production of organism components. There was no physical law which could account for the complex physiochemical processes. Therefore, chemical reactions and diffusion governed such processes. Turing suggested there is a chemical state, staying stable against perturbations in the absence of diffusion, but becoming unstable against perturbations in the presence of diffusion. Such diffusion-driven instability may result in spatial variations and induce chemical patterns.

Scientists have realized that the emergence of Turing patterns had two requirements [10]. Firstly, the system must maintain the state far from thermodynamic equilibrium, such as by using continuously fed unstirred reactors (CFUR). Secondly, the diffusion coefficients of the activator and inhibitory processes are unequal. In common, Turing instability occurs when the inhibitory diffusion rate is significantly faster than that of the activator. However, since most of the RD systems were carried out in the aqueous solutions, in which the diffusion coefficients of all species are on the same order, the experimental observation of Turing pattern in a RD system was not achieved until 1990. Patrick De Kepper and his group [95] observed a stationary spotty pattern in the CIMA system using starch as an indicator. In the experiment a slab of hydrogel was employed to decrease the diffusion rate of activator species (iodide ions).

Another chemical system that was recently found to support Turing patterns is the BZ-AOT system, in which the microheterogeneous microemulsion results in different chemical species diffusing at very different rates. In such a system, various types of Turing patterns were developed based on different control parameters. For example [96], stationary Turing patterns have been found in the $\text{Ru}(\text{bpy})_3$ -catalyzed BZ-AOT system at high temperature, while a new type of oscillatory Turing patterns were observed at low temperature. Turing patterns generally occur in one of the three forms: hexagonal spots, stripes, and honeycombs. Coexistence of the two can also be found at specific parameters.

1.3 Recent Developments in the Study of Chemical Oscillators and Their Potential Applications

1.3.1 pH Oscillators

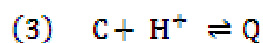
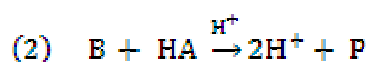
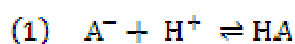
pH oscillators are defined as systems in which H^+ plays the most important kinetic role in the oscillatory behavior. In such systems, the variation in pH can be as large as four pH units. Loosely speaking, almost all chemical oscillators have periodic changes in H^+ concentration, even in the BZ reaction that requires strongly acidic media. They don't belong to pH oscillators not simply because the pH range is negligible, but also due to the different driving force of the oscillations. In pH oscillators [97-99], the driving force is the reaction producing H^+ in an autocatalytic fashion, and another major composite reaction is consuming H^+ in a slow process.

Along with the 200 variants of chemical oscillators known already, pH oscillators represent the group that provides the greatest opportunity for practical applications, such as inducing the conformation change in pH-responsive gels [100-102], pH-sensitive conformational switching of DNA used to realize autonomous molecular computers [103, 104]. pH oscillators have been reported to produce a spontaneous drug delivery rhythm [105, 106]. In the last case, the periodic changes in pH-responsive hydrogel which undergo periodic swelling and deswelling could act as a micro "motor" enabling the chemical energy to be transformed into mechanical work.

Among the 20 pH oscillators [107] reported to date, an oxidant like IO_3^- , IO_4^- , H_2O_2 , BrO_2^- , BrO_3^- and one or two other initial reactants like S^{2-} , SO_3^{2-} , $S_2O_3^{2-}$, HCO_3^- , NH_2OH , Mn^{2+} , $CaCO_3$, $CaSO_3$, $Fe(CN)_6^{4-}$, thiourea, phenol are used. Almost all of them could function only in a CSTR or in a semi-batch reactor. In a CSTR, all reagents are supplied

continuously and thus sustained pH oscillations can be observed. In the case of a semibatch reactor, the mixture of oxidants is introduced continuously, and long lasting but only transient pH oscillations appear. Recently, pH oscillations were also generated in a closed reactor [97] via replacing the inflow of chemicals with a layer of silica gel impregnated with the key reactants. Such a technique has been successfully applied to the $\text{BrO}_3^- - \text{Mn}^{2+} - \text{SO}_3^{2-}$, $\text{IO}_3^- - \text{Fe}(\text{CN})_6^{4-} - \text{SO}_3^{2-}$, and $\text{BrO}_3^- - \text{Fe}(\text{CN})_6^{4-} - \text{SO}_3^{2-}$ systems, in which the key reactant sulfite ion was replenished via the dissolution from the gel layer. Another long lasting pH oscillatory system in a closed reactor [99] is $\text{CaSO}_3 - \text{H}_2\text{O}_2 - \text{HCO}_3^-$, utilizing the slow dissolution of solid CaSO_3 (i.e., it serves as a continuous supply of the key intermediate HSO_3^-). An advantage of batch pH oscillators is that it is likely to be of considerable applications in biochemical systems involving expensive materials such as DNA, enzymes, etc.

pH oscillations have been simulated with a relatively simple mechanism. For instance, the following simple skeleton mechanism which consists of three reaction steps has been developed by Rabai [108]:



Where B denotes the oxidant, A^- and C stand for the two initial reactants, P and Q are products. Reaction (2) represents an autocatalytic step for producing hydrogen ion, reactions (1) and (3) consume H^+ in a slow process.

1.3.2 Oscillations in Protic Ionic Liquids

Except the BZ-AOT system [93, 96], almost all the chemical oscillators have been studied in aqueous solution, which limits the application of oscillations in organic phase. This is due to no protons as well as difficulties in dissolving inorganic salts such as bromate in organic solvent. Such problems can be solved by applying ionic liquids, which are room-temperature molten salts consisting entirely of ions. There are two different classes of ionic liquids: aprotic ionic liquids (APILs) and protic ionic liquids (PILs). PILs are generally prepared by a neutralization reaction from an organic base like an amine and an acid. If both are strong enough, proton transfer from the acid to the base occurs. PILs include active protons while APILs do not include active protons. Certain kinds of PILs have high proton activity compared to acidic water. Therefore PILs are assumed to be a promising class of preservation medium for supporting BZ oscillations.

Yoshida and his co-workers for the first time applied PILs to study BZ reaction [109]. They recently reported the BZ oscillations that used PILs as a proton source instead of a conventional acid such as sulfuric acid or nitric acid. In their research the cations were selected from quaternized aliphatic ammonium ions with different saturated or unsaturated alkyl groups. The anions were common oxo- or amide acids. After neutralization, the pH of PILs strongly depended on the structures of anions. [dema- H^+][HSO_4^-], [DBN- H^+][HSO_4^-], and [dmea- H^+][CH_3SO_3^-], were found to release protons when mixed with water, which led to the initiation of the BZ reaction. These long lasting BZ oscillations in the PILs media with a short oscillatory period can be explained by the rapid chemical reactions in bromide regeneration processes, where protons produced in such processes can be eliminated quickly by a free neutral proton acceptor such as neutral

amine [dema] which exists in the reaction system when [dema-H⁺][HSO₄⁻] is mixed with water.

1.3.3 Self-oscillating Gels

Gels are interesting objects which have both liquid-like and solid-like properties. The solid-like property is due to the cross-linking of the polymers in the form of network. It is not a new discovery that gels can change their volume more than a thousand fold between the swelling state and deswelling state in responding to changes in temperature, pH, or the applied electric field, etc. yet they do provide a great opportunity for applications in areas such as mass transfer and drug delivery. For the first time, Yoshida and coworkers in 1996 developed self-oscillating polymer gels which autonomously swell and deswell periodically in a closed homogeneous BZ solution without any external stimuli [110]. The mechanical oscillation is achieved by applying BZ reactions within the swollen polymer network. The polymer gel consists of N-isopropylacrylamide (NIPAAm) in which ruthenium (II) tris- (2,2'-bipyridine) (Ru(bpy)₃²⁺), a catalyst for the BZ reaction, is covalently bonded to the polymer chain. The poly(NIPAAm-co-Ru(bpy)₃²⁺) copolymer gel has a phase transition temperature because of the thermo-sensitive constituent NIPAAm. The oxidation of the Ru(bpy)₃²⁺ moiety results in not only swelling of the gel, but also a rise in the transition temperature. These characteristics may be interpreted by considering an increase in hydrophilicity of the polymer chains due to the oxidation of Ru(II) to Ru(III) in the Ru(bpy)₃ moiety. Therefore, it is expected that the gel would undergo a cyclic swelling-deswelling alteration when the Ru(bpy)₃ moiety is periodically oxidized and reduced. When the gel is immersed in the BZ solution that does not contain the ruthenium catalyst, the reaction solution penetrates into the polymer network and the

BZ reaction occurs in the gel. Consequently, periodical $\text{Ru}(\text{bpy})_3$ redox changes induced by the BZ reaction produce periodical swelling-deswelling changes of the gel.

The behavior of a self-oscillating BZ gel can be controlled by several factors. The first factor is heat, where since the NIPAAm gel is a thermoresponsive material, it will go to the swelling state at a low temperature and change to the deswelling state when being heated. The thermal sensitivity of the gels depends on the chemical structure of the polymer as well as the crosslink density of the network. A second factor is light, resulting from the well-known photosensitivity of the ruthenium-BZ reaction. Illumination of the BZ reaction may accelerate the oscillation frequency, which induces the fast swelling-deswelling switch of the BZ gels. Yoshida and coworkers have indeed developed the photo controlled peristaltic motion of a porous membrane made of BZ gels [111]. A third factor is the concentration of BZ reactants such as MA, bromate, acid and metal catalysts.

Epstein and coworkers designed and synthesized new polymerizable ruthenium complexes for self-oscillating BZ gels [112]. They produced six new copolymers that acted as matrices of BZ gels. Their research found that the distance modified between the ruthenium catalysts and polymer backbone has a significant impact on the oscillatory behavior of the BZ gels. Increasing the distance causes a shorter initiation time for oscillations. Intermediate distance performs the best while further extension of the distance slows the oscillations of the gels. Yashin and Balazs found that the visible oscillation within non-oscillating, droplet BZ gels could be resuscitated [113]. That is, chemical oscillations in BZ gels can be restored by mechanically compressing the BZ gels beyond a critical stress, which is an important implication for restoring functionalities in extending the lifetime of devices.

Yoshida and coworkers proposed that by utilizing the peristaltic motion of the BZ gels, the functionalized surface can exhibit autonomous mass transfer of cargo [114]. Thus, BZ gels are ideal media for transforming chemical energy to mechanical work. Overall, self-oscillating BZ gels [110-118] open up great opportunities for designing nano-/micro-scale, bio-functional devices that operate in an autonomous manner such as microactuators, mass transfer surfaces, pulsatile drug delivery, etc.

1.3.4 Controlled-Synthesis of Nano/micro-Materials

Nano/micro-materials [119-126] are of great importance in many areas such as in batteries, catalysis, chemical/biochemical sensing, cosmetics, drug, gene delivery, hydrogen production and storage, etc. In many cases, the nano/micro-materials exhibit varied functionalities in terms of their size and shape. Thus, a technique allowing fabrication of large quantities of uniform particles would be a great asset to many advanced applications. Conventional synthetic approaches can be divided into several categories: hard templating synthesis, soft templating synthesis and template free methods. Researchers working in the field of nonlinear chemical dynamics are quite familiar with the control of kinetics, which is certainly an important factor in materials fabrication. Two nonlinear research groups are actively involved in utilizing reaction-diffusion systems to synthesize new types of nano/micro-materials, i.e., silica gardens in Oliver Steinbock's group [127-129] and frontal polymerization in John A. Pojman's group [130-132].

Silica gardens have been studied since the 1940s [133]. The experiments were normally performed by adding solid metal salts such as copper sulfate to an aqueous solution of sodium silicate from the top. The growth of plant like micro-scaled hollow

tubular structures is controlled by chemical reactions and physical diffusion. The silica gardens help one to understand the nature of that growth process. Small size and large scale production make these hollow tubes interesting materials for various applications. Steinbock and coworkers reported a novel method for constructing silica microstructures [127]. They produced agarose beads as a microvessel, then loaded diffusively with copper sulfate solution and finally exposed to a large volume of sodium silicate solution. Air bubble-guided hollow microtubes formed quickly and linearly, and the tube radius was found closely related to the bubble size. In the absence of the attached bubble on the surface of the beads, hollow microtubes evolved slowly and less linearly. To maintain microtubes growth over longer distances, Steinbock's group [128] carried out experiments by injecting copper sulfate or zinc sulfate solutions directly into silicate solution from the bottom, where the gas injection from a needle created a bubble which could pin to the top of growing tube. It was found that the wall thickness increases in an inward direction which suggests a travelling reaction-diffusion front occurred and controlled the wall growth in the radial direction. They also demonstrated the construction of multi-layered microtubes.

Recently, Steinbock et al. [129] demonstrated nonequilibrium synthesis of iron oxide-silica magnetite tubes, in which the magnetite particles followed first-order nucleation-growth kinetics. Similar techniques were employed in the growth of iron oxide-silica magnetite tubes as the above techniques of copper or zinc-based microtubes synthesis, except they applied an air-filled glass rod moving upward with a computer-controlled speed to guide the growth of iron oxide-silica magnetite tubes. These iron oxide-silica tubes lacked mechanical stability and could be improved by increasing the sodium

silicate concentration. It was found that the rod and air bubble moved vertically up forming a nearly straight iron oxide-silica microtube which exhibited superparamagnetic behavior.

In Pojman's group research was focused on studies of frontal polymerization. Conventional polymerization occurs in the homogeneous environment while frontal polymerization is a process in which the polymerization reaction propagates directionally through the reaction vessel, like a front propagation in Figure 1.5d. There are mainly four types of frontal polymerization reported [134]: thermal frontal polymerization (TFP), which uses external energy sources to initiate the polymerization reaction; photofrontal polymerization, which is driven by an external UV irradiation continuously; isothermal frontal polymerization, which relies on a polymer seed to initiate a front; cryogenic polymerization, a fascinating mode of frontal polymerization due to the requirement of low temperature (4-77K), however, it requires gamma radiation for the front initiation. Frontal polymerization, first discovered by Chechilo's group [135], has many potential applications, such as curing large composites, and new types of materials cannot be achieved by conventional polymerization methods.

The biggest concern in frontal polymerization is with very high temperature (250 °C), especially in TFP process. At such high temperature, polymerization will produce smoke and release volatile compounds resulting from the exceeding polymerization and unreacted initiator such as peroxide, thereby limiting their applications. Pojman et al. in 2011 [131] reported the first electron paramagnetic resonance study of free radicals in front polymerizing and bulk polymerized acrylates. They pointed out the absolute radical concentrations in both regions, where the radical concentrations are significantly higher

near the point of frontal region than in the bulk region. Moreover, the radical concentrations are nearly constant for weeks and even months in the absence of oxygen. According to this paper, methods to reduce the radical concentrations to the appropriate level which can sustain the frontal polymerization and methods to get rid of unreacted initiator become significant for reducing the polymerization temperature. In the same year, the same group [130] proposed that addition of thiols can lower the front polymerization temperature and increase the flexibility of a polymer because thiols can undergo copolymerization with acrylates, with a lower enthalpy (60 kJ/mol) than for acrylates homopolymerization (80 kJ/mol). Moreover, the heat release of thiols-acrylates reaction per mass is less than acrylates homopolymerization, thus lowering the front temperature and the amount of smoke produced. Addition of thiols can also eliminate the unreacted peroxide due to thiols and peroxide having been shown to react together at room temperature.

In recent years various new methods [123-126] have been developed for the controlled-synthesis of nano/micro-materials. One of the desired properties is the facet of the as-prepared nanocrystals. The formation of different facets is determined by their growth conditions [136, 137]. For example, in the presence of KI, iodide ions preferentially adsorb on the {100} palladium facet, which subsequently allow the palladium crystal to grow along other facets. The final outcome is the as-prepared palladium crystals will be enclosed with the {100} facet. So far, in existing research on this topic, a fixed amount of KI was added initially. Using the iodide oscillator to grow palladium crystals, for example, would create exciting opportunities to achieve facet control and novel microstructures. Notably, bromide ions have similar adsorption

properties [138] as iodide and therefore bromate oscillators can be employed to achieve the controlled synthesis of nanocrystals.

1.4 Objectives of this Thesis

Despite that a large number of chemical oscillators have been developed in the last three decades, bromate-based chemical oscillators [93, 96, 110-118] remain to be the most popular model systems for the understanding of complex nonlinear behaviours encountered in nature. This is partially because bromate oscillators often exhibit long lasting and rich nonlinear phenomena and its core reaction mechanisms are well understood. To further advance our understanding of bromate-based chemical oscillators and explore novel nonlinear chemical behaviors, which are no doubt important to the study of nonlinear dynamics as a whole, this research choose metol and 1,4-benzoquinone as the organic substrates to develop new bromate oscillators. Notably, in those proposed new systems the consumption of bromine is slower than that in the classic BZ reaction. Such a kinetic property causes the buildup of bromine in the reaction solution, which subsequently allows us to test different ways to manipulate bromine concentration. We would like to note that the recycling of bromine/bromide represents important steps in all bromate-based chemical oscillators, therefore being able to manipulate bromine concentration does not only permit one to gain new significant insights into the underlying reaction mechanisms, but also offers a great opportunity to uncover new phenomena.

The proposed research activities are carried out in the following order:

- a) Reaction behavior and mechanisms of the ferroin-bromate-metol oscillator were studied first in a batch reactor, in which the effect of gas flow on the

ferroin-bromate-metol oscillations was characterized. Nonlinear spatiotemporal behavior in the ferroin-bromate-metol system was explored in one- and two-dimensional media.

- b) A new type of minimal bromate oscillator was developed, which utilized 1,4-benzoquinone to modulate the concentration of bromine/bromide in the reaction solution. The new reaction could exhibit spontaneous oscillations in a closed system. Mechanistic studies were carried out to determine the intermediate and final products.
- c) Interactions of the new minimal bromate oscillator and external forcing were investigated. The external forcing was conveniently implemented with light. Effects of varying the intensity and wavelength of the applied light were carried out in both ferroin- and cerium- catalyzed minimal bromate oscillators. Possible photoreaction mechanisms were proposed and numerical simulations were performed accordingly.
- d) A new kind of modified carbon electrode was developed for the in-situ determination of 1,4-hydroquinone in the proposed bromate oscillators. A good relationship between the concentration of 1,4-hydroquinone and oscillatory potential profile has been found.
- e) Preliminary exploration of using bromate oscillators to achieve facet-controlled synthesis of palladium nanoparticles was carried out in a batch reactor.

1.5 References

- 1 1 K. S. Pitzer, Thermodynamics, McGraw-Hill Series In Advanced Chemistry, 3rd Edition, 1995.
- 2 S. R. de Groot and P. Mazur, Nonequilibrium Thermodynamics, Dover, New York, 1984.
- 3 G. Nicolis and I. Prigogine, Self-Organization in Nonequilibrium systems, Wiley, New York, 1977.
- 4 4. G. Nicolis and I. Prigogine, Exploring Complexity, W. H. Freeman, New York, 1989.
- 5 Y. F. Li, H. Qian and Y. F. Yi, J. Chem. Phys., 2008, 129, 154505.
- 6 S. K. Scott, Oscillations, Waves and Chaos in Chemical Kinetics, Oxford University Press Inc, New York, 1994.
- 7 H. Landolt, Ber. Dtsch. Chem. Ges., 1886, 19, 1317.
- 8 W. C. Bray, J. Am. Chem. Soc., 1921, 43, 1262.
- 9 W. C. Bray and H. A. Liebhafsky, J. Am. Chem. Soc., 1931, 53, 38.
- 10 I. R. Epstein and J. A. Pojman, An Introduction to Nonlinear Chemical Dynamics. Oscillations: Waves, Patterns and Chaos, Oxford University Press, New York, 1998.
- 11 F. O. Rice and O. M. Reiff, J. Phys. Chem., 1927, 31, 1352.
- 12 M. G. Peard and C. F. Cullis, Trans. Faraday Soc., 1951, 47, 616.
- 13 A. M. Zhabotinsky, Biofizika, 1964, 9, 306.
- 14 A. M. Zhabotinsky, Chaos, 1991, 1, 379.
- 15 A. N. Zaikin and A. M. Zhabotinsky, Nature, 1970, 225, 535.

- 16 P. G. Bowers, K. E. Caidwell and D. F. Prendeigast, *J. Phys. Chem.*, 1972, 76, 2185.
- 17 M. T. Beck and Z. B. Varadi, *React. Kinet. Catal. Lett.*, 1977, 6, 275.
- 18 R. P. Rastogi, K. D. S. Yadav and P. Rastogi, *Indian. J. Chem.*, 1977, 15a, 338.
- 19 V. J. Farage. P. Stroot and D. Janjic. *Helv. Chim. Acta*, 1977, 60, 231.
- 20 E. Koros and M. Orban, *Nature*, 1978, 273, 371.
- 21 E. J. Heilweil, M. J. Henchman and I. R. Epstein, *J. Am. Chem. Soc.*, 1979, 101, 3698.
- 22 L. F. Salter and J. G. Sheppard, *Int. J. Chem. Kinet.*, 1982, 14, 815.
- 23 P. K. Srivastava, Y. Mori and I. Hanazaki, *J. Phys. Chem.*, 1991, 95, 1636.
- 24 Y. Gao, H D. Foérsterling, Z. Noszticzius and B. Meyer, *J. Phys. Chem.*, 1994, 98, 8377.
- 25 R. R. Aliev and V. N. Biktashev, *J. Phys. Chem.*, 1994, 98, 9676.
- 26 A. Sirimungkala and H. D. Fo1rsterling, *J. Phys. Chem.*, 1996, 100, 3051.
- 27 L. Adamčíková, Z. Farbulová and P. Ševčík, *New J. Chem.*, 2001, 25, 487.
- 28 I. R. Epstein, *Faraday Discuss.*, 2001, 120, 421.
- 29 S. G. Sobel, H. M. Hastings and R. J. Field, *J. Phys. Chem. A*, 2006, 110, 5.
- 30 H. Onuma, A. Okubo, M. Yokokawa, M. Endo, A. Kurihashi and H. Sawahata, *J. Phys. Chem. A*, 2011, 115, 14137.
- 31 R. J. Field, E. Körös and R. M. Noyes, *J. Am. Chem. Soc.*, 1972, 94, 8649.
- 32 R. J. Field and R. M. Noyes, *J. Chem. Phys.*, 1974, 60, 1877.
- 33 H. D. Försterling, and M. Varga, *J. Phys. Chem.*, 1993, 97, 7932.
- 34 I. Szalai, J. Oslonovitch and H. D. Försterling, *J. Phys. Chem.*, 2000, 104, 1495.

- 35 R. J. Field and H. D. Försterling, *J. phys. Chem.*, 1986, 90, 5400.
- 36 Y. Gao and H. D. Försterling, *J. Phys. Chem.*, 1995, 99, 8638.
- 37 P. Gray and S. K. Scott, *Chemical Oscillations and Instabilities, Nonlinear Chemical Kinetics*, Clarendon, Oxford, 1990.
- 38 K. Showalter, R. M. Noyes and K. Bar-Eli, *J. Chem. Phys.*, 1978, 69, 2514.
- 39 M. Harati and J. Wang, *J. Phys. Chem. A*, 2008, 112, 4241.
- 40 Z. Noszticzius, P. Stirling and M. Wittmann, *J. Phys. Chem.*, 1985, 89, 4914.
- 41 M. T. Beck and Z. B. Varadi, *React. Kinet. Catal. Lett.*, 1977, 6, 275.
- 42 K. Kurin-Csörgei, I. Szalai and E. Körös, *React. Kinet. Catal. Lett.* 1995, 54, 217.
- 43 D. S. Huh, Y. J. Kim, H. S. Kim, J. K. Kang and J. Wang, *Phys. Chem. Chem. Phys.* 2003, 5, 3188.
- 44 L. Treindl and V. Zvac, *React. Kinet. Catal. Lett.*, 1983, 22, 451.
- 45 R. P. Rastogi, P. Chand, M. K. Pandey and M. Das, *J. Phys. Chem. A*, 2005, 109, 4562.
- 46 N. Li, J. Zhao, and J. Wang, *J. Chem. Phys.* 2008, 128, 244509.
- 47 J. A. Pojman, D. C. Leard and W. West, *J. Am. Chem. Soc.*, 1992, 114, 8298.
- 48 L. Treindl, T. Matsumura-Inoue and P. Ruoff, *J. Phys. Chem. A*, 2002, 106, 5271.
- 49 H. D. Försterling, S. Murányi and Z. Noszticzius, *J. Phys. Chem.*, 1990, 94, 2915.
- 50 P. Sevcik and L. Adamčíková, *Collect. Czech. Chem. Commun.*, 1982, 47, 891.
- 51 Z. Noszticzius, P. Stirling and M. Wittmann, *J. Phys. Chem.*, 1985, 89, 4914.
- 52 G. Rabai and I. R. Epstein, *J. Am. Chem. Soc.*, 1992, 114, 1529.
- 53 P. De Kepper, I. R. Epstein, K. Kustin, and M. Orban, *J. Phys. Chem.*, 1982, 86, 170.

- 54 T. S. Briggs and W. C. Rauscher, *J. Chem. Educ.*, 1973, 50, 496.
- 55 S. H. Glarum and J. H. Marshall, *J. Electrochem. Soc.*, 1985, 132, 2872.
- 56 K. Nielsen, P.G. Sørensen, F. Hynne and H. G. Busse, *Biophys. Chem.*, 1998, 72, 49.
- 57 W. Geiseler, *J. Phys. Chem.*, 1982, 86, 4394.
- 58 M. Orban, P. De Kepper and I. R. Epstein, *J. Am. Chem. Soc.*, 1982, 104, 2657.
- 59 K. Bar-Eli, *J. Phys. Chem.*, 1985, 89, 2855.
- 60 A. K. Dutt and M. Menzinger, *J. Phys. Chem.*, 1991, 95, 3429.
- 61 A. K. Dutt and M. Menzinger, *J. Chem. Phys.*, 1999, 110, 7591.
- 62 L. Gyorgyi and R. J. Field, *J. Phys. Chem.*, 1992, 96, 1220.
- 63 P. G. Sorensen, *Faraday Symp. Chem. Soc.*, 1974, 9, 88.
- 64 P. Richetti, J. C. Roux, F. Argoul and A. Arneodo, *J. Chem. Phys.*, 1987, 86, 3339.
- 65 A. M. Zhabotinsky, *Dokl. Akad. Nauk SSSR*, 1964, 157, 392.
- 66 J. Maselko and H. L. Swinney, *J. Chem. Phys.*, 1986, 85, 6430.
- 67 E. N. Lorenz, *Tellus*, 1964, 16, 1.
- 68 E. N. Lorenz, *J. Atmos. Sci.*, 1973, 20, 130.
- 69 M. Orban, P. De Kepper and I. R. Epstein, *J. Phys. Chem.*, 1982, 86, 431.
- 70 J. Maselko, M. Alamgir and I. R. Epstein, *Phys. D*, 1986, 19, 153.
- 71 M. Alamgir and I. R. Epstein, *Int. J. Chem. Kinet.*, 1985, 17, 429.
- 72 A. G. Merzhanov, and E. N. Rumanov, *Rev. Mod. Phys.*, 1999, 71, 1173.
- 73 J. Ross, S. C. Müller and C. Vidal, *Science*, 1988, 240, 460.
- 74 S. K. Scott, *Chem. Eng. Sci.*, 2000, 55, 209.
- 75 H. H. Rotermund, *J. Elec. Spec. Rel. Phen.*, 1999, 99, 41.

- 76 N. Manz and O. Steinbock, *Chaos*, 2006, 16, 037112.
- 77 A. P. Muñuzuri, V. Pérez-Villar and M. Markus, *Phys. Rev. Lett.*, 1997, 79, 1941.
- 78 H. Ševčíková, J. Kosek and M. Marek, *J. Phys. Chem.*, 1996, 100, 1666.
- 79 M. C. Cross and P. C. Hohenberg, *Rev. Mod. Phys.*, 1993, 65, 854.
- 80 A. Pagola and C. Vidal, *J. Phys. Chem.*, 1987, 91, 501.
- 81 V. S. Zykov, *Biophysics*, 1980, 25, 906.
- 82 J. P. Keener and J. J. Tyson, *Phys. D*, 1986, 21, 307.
- 83 P. Foerster, S. C. Müller and B. Hess, *Science*, 1988, 241, 685.
- 84 T. Yamaguchi, L. Kuhnert, Z. Nagy-Ungvarai, S. C. Müller and B. Hess, *J. Phys. Chem.*, 1991, 95, 5831.
- 85 S. Jakubith, H. H. Rotermund, W. Engel, A. von Oertzen and G. Ertl, *Phys. Rev. Lett.*, 1990, 65, 3013.
- 86 P. Camacho and J. D. Lechleiter, *Science*, 1993, 260, 226.
- 87 J. M. Davidenko, A. V. Pertsov, R. Salomonsz, W. Baxter and J. Jalife, *Nature*, 1992, 355, 349.
- 88 A. Winfree, *Science*, 1972, 175, 634.
- 89 T. Plesser, S. C. Müller and B. Hess, *J. Phys. Chem.*, 1990, 94, 7501.
- 90 V. Petrov, Q. Ouyang and H. L. Swinney, *Nature*, 1997, 388, 655.
- 91 Q. Y. Gao, J. Li, K. L. Zhang and I. R. Epstein, *Chaos*, 2009, 19, 033134.
- 92 T. Bánsági Jr. and O. Steinbock, *Chaos*, 2008, 18, 026102.
- 93 T. Bánsági Jr., V. K. Vanag and I. R. Epstein, *Phys. Rev. E*, 2012, 86, 045202(R).
- 94 A. M. Turing, *Philos. Trans. Roy. Soc. London, Ser. B*, 1952, 237, 37.

- 95 V. Castets, E. Dulos, J. Boissonade and P. De Kepper, *Phys. Rev. Lett.*, 1990, 64, 2953.
- 96 V. K. Vanag and I. R. Epstein, *Chaos*, 2008, 18, 026107.
- 97 E. Poros, V. Horvath, K. Kurin-Csorgei, I. R. Epstein and M. Orban, *J. Am. Chem. Soc.*, 2011, 133, 7174.
- 98 L. Ji, H. Y. Wang and X. T. Hou, *J. Phys. Chem. A*, 2012, 116, 7462.
- 99 G. Rabai, *Phys. Chem. Chem. Phys.*, 2011, 13, 13604.
- 100 R. Yoshida, H. Ichijo, T. Hakuta and T. Yamaguchi, *Macromol. Rapid Commun.*, 1995, 16, 305.
- 101 V. Labrot, P. De Kepper, J. Boissonade, I. Szalai and F. Gauffre, *J. Phys. Chem. B*, 2005, 109, 21476.
- 102 C. J. Crook, A. Smith, R. A. L. Jones and A. Ryan, *J. Phys. Chem. Chem. Phys.*, 2002, 4, 1367.
- 103 T. Liedl, M. Olapinski and F. C. Simmel, *Angew. Chem. Int. Ed.*, 2006, 45, 5007.
- 104 Y. Benenson, T. Paz-Elizur, R. Adar, E. Keinan, Z. Livneh and E. Shapiro, *Nature*, 2001, 414, 430.
- 105 I. Varga, I. Szalai, R. Meszaros and T. Gilanyi, *J. Phys. Chem. B*, 2006, 110, 20297.
- 106 V. Balamuralidhara, T. M. Pramodkumar, N. Srujana, M. P. Venkatesh, N. V. Gupta, K. L. Krishna and H. V. Gangadharappa, *Am. J. Drug. Discov. Dev.*, 2011, 1, 24.
- 107 I. Szalai, K. Kurin-Csorgei and M. Orban, *Reac. Kinet. Mech. Cat.*, 2012, 106, 257.

- 108 G. Rabai, *ACH Models Chem.*, 1998, 135, 381.
- 109 T. Ueki, M. Watanabe and R. Yoshida, *Angew. Chem. Int. Ed.*, 2012, 51, 11991.
- 110 R. Yoshida, T. Takahashi, T. Yamaguchi and H. Ichijo, *J. Am. Chem. Soc.*, 1996, 118, 5134.
- 111 Y. Takeoka, M. Watanabe and R. Yoshida, *J. Am. Chem. Soc.*, 2003, 125, 13320.
- 112 Y. Zhang, N. Li, J. Delgado, N. Zhou, R. Yoshida, S. Fraden, I. R. Epstein and B. Xu, *Soft Matter*, 2012, 8, 7056.
- 113 I. C. Chen, O. Kuksenok, V. V. Yashin, A. C. Balazs and K. J. Van Vliet, *Adv. Funct. Mater.*, 2012, 22, 2535.
- 114 R. Yoshida and Y. Murase, *Coll. Surf. B: Biointerfaces*, 2012, 99, 60.
- 115 P. Dayal, O. Kuksenok and A. C. Balazs, *PANS*, 2013, 110, 431.
- 116 V. V. Yashin and A. C. Balazs, *Science*, 2006, 314, 798.
- 117 R. Yoshida, *Sensors*, 2010, 10, 1810.
- 118 V. V. Yashin, O. Kuksenok, P. Dayal and A. C. Balazs, *Rep. Prog. Phys.*, 2012, 75, 066601.
- 119 D. K. Hwang, D. Dendukuri and P. S. Doyle, *Lab Chip*, 2008, 8, 1640.
- 120 J. H. Jung, T. J. Park, S. Y. Lee and T. S. Seo, *Angew. Chem. Int. Ed.*, 2012, 51, 5634.
- 121 F. S. Majedi, M. M. Hasani-Sadrabadi, S. H. Emami, M. Taghipoor, E. Dashtimoghadam, A. Bertsch, H. Moaddelc and P. Renaud, *Chem. Commun.*, 2012, 48, 7744.
- 122 A. B. Moshe and G. Markovich, *Chem. Mater.*, 2011, 23, 1239.

- 123 T. Torimoto, J. P. Reyes, K. Iwasaki, B. Pal, T. Shibayama, K. Sugawara, H. Takahashi and B. Ohtani, *J. Am. Chem. Soc.*, 2003, 125, 316.
- 124 H. Z. Zhang, B. Gilbert, F. Huang and J. F. Banfield, *Nature*, 2003, 424, 1025.
- 125 A. Heredia, I. Bdikin, S. Kopyl, E. Mishina, S. Semin, A. Sigov, K. German, V. Bystrov, J. Gracio and A. L. Kholkin, *J. Phys. D: Appl. Phys.*, 2010, 43, 462001.
- 126 X. X. Zou, G. D. Li, J. Zhao, P. P. Wang, Y. N. Wang, L. J. Zhou, J. Su, L. Li and J. S. Chen, *Inorg. Chem.*, 2011, 50, 9106.
- 127 R. Makki, M. Al-Humiari, S. Dutta and O. Steinbock, *Angew. Chem. Int. Ed.*, 2009, 48, 8752.
- 128 L. Roszol and O. Steinbock, *Phys. Chem. Chem. Phys.*, 2011, 13, 20100.
- 129 R. Makki and O. Steinbock, *J. Am. Chem. Soc.*, 2012, 134, 15519.
- 130 V. Viner and J. A. Pojman, *J. Polym. Sci. Part A: Polym Chem.*, 2011, 49, 4556.
- 131 A. Thoma, A. Dahal, A. Regmi, A. Valencia, V. Viner, R. Cueto, B. Baker, P. Bunton and J. A. Pojman, *J. Polym. Sci. Part A: Polym Chem.*, 2011, 49, 4261.
- 132 C. A. Parrinello, C. O. Bounds, M. L. T. Liveri, J. A. Pojman, *J. Polym. Sci. Part A: Polym Chem.*, 2012, 50, 2337.
- 133 J. H. E. Cartwright, J. M. Garcia-Ruiz, M. L. Novella and F. Otalora, *J. Coll. Int. Sci.*, 2002, 256, 351.
- 134 J. A. Pojman, Frontal Polymerization. In: Matyjaszewski K and Möller M (eds.) *Polymer Science: A Comprehensive Reference*, Amsterdam: Elsevier, 2012.
- 135 N. M. Chechilo, R. J. Khvilivitskii and N. S. Enikolopyan, *Dokl. Akad. Nauk SSSR*, 1972, 204, 1180.

- 136 B. T. Sneed, C. H. Kuo, C. N. Brodsky and C. K. Tsung, *J. Am. Chem. Soc.*, 2012, 134, 18417.
- 137 W. X. Niu, L. Zhang and G. B. Xu, *ACS Nano*, 2010, 4, 1987.
- 138 W. Zhang, Q. Wang, F. Qin, H. Zhou, Z. Lu and R. Chen, *J. Nanosci. Nanotechnol.*, 2011, 9, 7794.

Chapter 2: Complex Kinetics and Significant Influences of Bromine Removal in Ferroin-Bromate-Metol Reaction

2.1 Introduction

Since the discovery of the Belousov-Zhabotinsky (BZ) reaction [1-3], a large family of bromate-based chemical oscillators has been uncovered in the past three decades, including both catalyzed and uncatalyzed systems [4-18]. The majority of those bromate oscillators are the replacement of malonic acid of the BZ reaction by different organic substrates [7-18]. When malonic acid is replaced, the consumption rate of bromine molecules and the production paths of bromide ions, that modulate the autocatalytic feedback cycles, are alternated [19]. As a result, those modified BZ systems may exhibit very different reaction behaviour. For example, Heilweil et al. observed sequential oscillations in a closed BZ system using malonic acid, acetylacetone and ethyl acetoacetate as the substrates [20]. Salter and Sheppard reported dual-frequency (i.e., birhythmic) oscillations when ethyl acetoacetate was employed as the substrate [21]. Dual-frequency oscillations were also reported respectively by Srivastava et al. and by Adamčíková and co-workers with acetylphenols and phenol as the substrates [22, 23].

In the following, we investigated nonlinear kinetics of the ferroin-bromate-metol reaction and, more importantly, explored the influences of manipulating bromine concentration on the observed nonlinear behavior. Similar to many of the organic substrates used in the modified BZ reactions, metol does not react with bromine fast enough to keep bromine concentration as low as seen in the malonic acid-bromate system.

Considering that bromine is an important precursor of bromide ions, the loss of bromine in those modified BZ systems might have significant impacts on the nonlinear behavior. So far, the importance of such a kinetic factor has been largely ignored. A study by Noszticzius and co-workers on the oxalic acid-BZ reaction did, however, show that spontaneous oscillations could be induced when a stream of inert gas was bubbled through the reaction solution [24, 25].

For the economic reasons, if the insert gas is replaced by air to bubble the solution, oxygen would be introduced in the process. The influence of oxygen on the BZ oscillations has been reported earlier, and the influence was attributed to interactions of oxygen with malonyl radicals [26-33], implying that the oxygen effect might depend on the organic substrates used. In this chapter, the synergistic influences of oxygen and bromine removal were also investigated, which was implemented via flowing air instead of nitrogen gas into the space above the ferroin-bromate-metol reaction mixture. As shown in the following, the coupling of oxygen and bromine removal resulted in complex oscillations in this new bromate-based oscillator, even under the conditions where the unperturbed system did not produce spontaneous oscillations. Characterization of the outflow gas with AgNO_3 solution showed the production of yellow AgBr precipitates.

2.2 Experimental Procedure

Reactions were run in a thermal-jacketed 50 mL glass reactor with the temperature maintained constant at $25.0 \pm 0.1^\circ\text{C}$ by a circulation water bath (ThermoNesLab RTE 7). The solution was stirred by a magnetic stirrer (Fisher Isotemp) at around 600 round per minute (rpm), except when stirring was characterized as a variable. A Teflon cap was placed on top of the cylindrical reactor to hold electrodes and nitrogen/oxygen inflow

tube. Volume of the reaction solution was fixed at 30.0 ml unless otherwise stated. Oscillatory profiles were monitored with a platinum electrode coupled with a $\text{Hg} \mid \text{Hg}_2\text{SO}_4 \mid \text{K}_2\text{SO}_4$ reference electrode (Radiometer Analytical, XR200 and M231Pt-9). All measurements were recorded with a personal computer connected to a pH/potential meter (Radiometer PHM220) through a PowerLab/4SP data logger. The evolution of the spatially extended medium was monitored with a CCD camera equipped with a zoom lens. The CCD camera was connected to a personal computer running a frame grabber program (Matrox Imaging Library).

Reaction mixtures were prepared from aqueous stock solutions of analytical grade sodium bromate (NaBrO_3 , Aldrich, 99%), 1.0 M, and sulfuric acid (H_2SO_4 , Aldrich, 95-98%), 6.0 M. Ferroin stock solution (0.01 M) was prepared from a calculated amount of $\text{FeSO}_4 \cdot 7\text{H}_2\text{O}$ (Aldrich, 99+%) and 1,10-phenanthroline (Aldrich, 99+%). Metol (4-methylaminophenol hemisulfate salt, Aldrich, 99%) and 1,4-hydroquinone (Aldrich, 99+%) were directly dissolved in the reaction mixture, except that when the age of metol solution was studied as a variable, where 0.05 M stock solution was prepared with doubly distilled water and stored in a brown bottle. Mass spectrometric measurements were carried out with Electrospray Ionization Time-of-Flight Mass Spectrometer and a 1200 L single quadrupole MS (Varian) through a direct insertion probe. All ^1H -NMR and ^{13}C -NMR studies were performed on a Bruker Avance 500MHz spectrometer and with the same sample that was used for mass spectrometry studies, but dissolved in deuterated chloroform (Cambridge Isotope Laboratories, 99.8%).

2. 3 Results and Discussion

2.3.1 Significance of Bromine Removal

Figure 2.1 presents the ferroin-bromate-metol reaction carried out under different configurations of the reactor: (a) sealed with parafilm, and (b) flowing nitrogen into the space above the reaction solution. Compositions of the reaction solution were $[\text{NaBrO}_3] = 0.05 \text{ M}$, $[\text{metol}] = 0.025 \text{ M}$, $[\text{ferroin}] = 1.0 \times 10^{-4} \text{ M}$ and $[\text{H}_2\text{SO}_4] = 1.7 \text{ M}$. In (a), volatile substances, mainly bromine molecules, were prevented from migrating out of the reactor, no spontaneous oscillations took place. Although in experiment (a) there was about 1 cm space above the reaction solution, the natural diffusion of volatile species out of the solution seemed to be negligible because the same result was achieved when the reaction solution was increased to fill up the reactor (i.e., no free space above the solution level). In experiment (b) nitrogen gas was flow into the space above the reaction solution at a rate of 60 ml/min. When the outflow nitrogen gas passed through a AgNO_3 solution, pale yellow precipitates formed, suggesting that volatile reagent bromine has been brought out of the reactor by the gas stream. Significantly, spontaneous oscillations took place after about 20,000 seconds in (b). This result suggests that bromine concentration in the unperturbed metol system was too high to support spontaneous chemical oscillations. More importantly, the removal of bromine has dramatic influence on the nonlinear kinetics of the ferroin-bromate-metol reaction.

Further experiments showed that even when the reactor was not sealed with parafilm, where bromine could migrate diffusively out of the reactor through loose contacts between the cap and glass reactor, the flow of nitrogen gas was still required for the system to exhibit spontaneous oscillations. This highlights the importance of enhanced

bromine removal in the metol system and possibly in other bromate-based chemical oscillators in which organic substrates do not consume bromine rapidly. As the bromine removal rate was increased by increasing the nitrogen flow rate, in Figure 2.2 the induction time was greatly shortened, suggesting that chemical oscillations were favored by the enhanced bromine removal process. However, the number of oscillations decreased as the flow rate of nitrogen was increased.

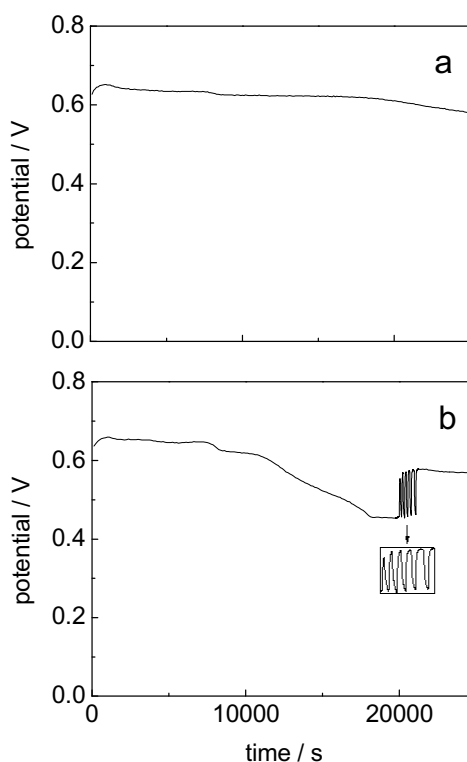


Figure 2.1 Time series of the ferroin-bromate-metol reaction with different configurations of the reactor: (a) sealed with parafilm, and (b) flowing nitrogen gas above the solution surface. Initial reaction compositions are $[\text{metol}] = 0.025 \text{ M}$, $[\text{NaBrO}_3] = 0.05 \text{ M}$, $[\text{H}_2\text{SO}_4] = 1.7 \text{ M}$, and $[\text{ferroin}] = 1.0 \times 10^{-4} \text{ M}$.

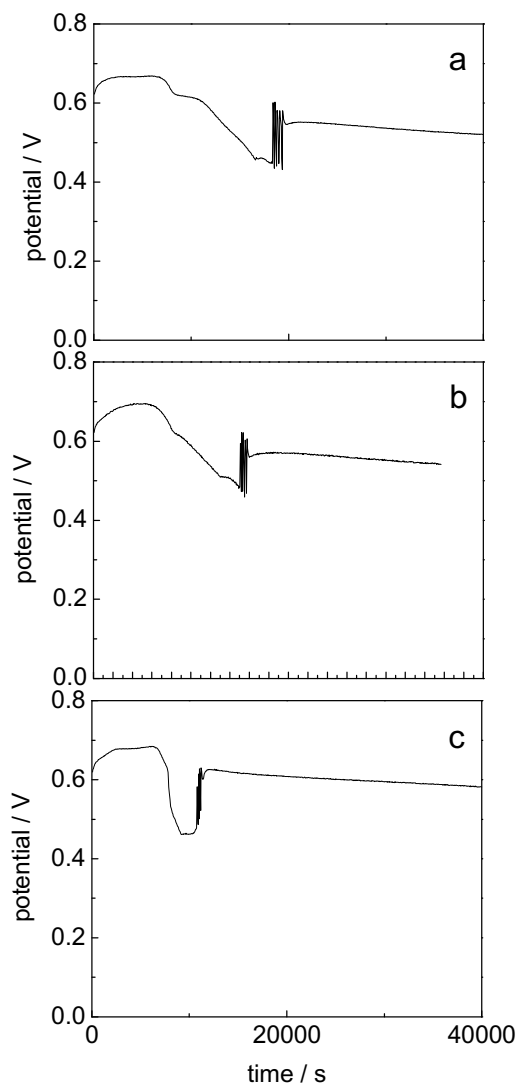


Figure 2.2 Influence of nitrogen flow rate on the oscillatory behavior (a) 40, (b) 60, and (c) 80 ml/min. Other reaction conditions were $[\text{metol}] = 0.025\text{M}$, $[\text{NaBrO}_3] = 0.05\text{M}$, $[\text{H}_2\text{SO}_4] = 1.7\text{M}$, $[\text{ferriin}] = 1.0 \times 10^{-4}\text{M}$, and the reaction solution volume was 20 ml.

2.3.2 Synergetic Influence of Oxygen and Bromine Removal

In Figure 2.3 nitrogen stream was replaced by (a) 1:1 nitrogen and air mixture, (b) air, and (c) pure oxygen, while the flow rate was kept constant at 60 ml/min. Upon replacing

nitrogen with the mixture of nitrogen and air, a new group of spontaneous oscillations developed at about 60,000 s and there was a long non-oscillatory evolution period between the two oscillation windows, a characteristic of sequential oscillations [20]. As the oxygen concentration was increased, the total number of peaks within the second oscillation window was greatly increased. Another noticeable change in (b) is that within the second group of oscillations there are two distinct oscillation frequencies. The abrupt transition from one frequency to another is in contrast to the gradual consumption of reagents, leading us to speculate that the system might support birhythmic oscillations if studied in an open system where reaction conditions can be maintained stable. In (c), where pure oxygen was employed, the number of peaks within the first window increased, while the quiescent window was further shortened. The phenomenon of oscillations with two distinct oscillation frequencies can still be seen in (c). Unlike seen in the classic BZ reaction [29], our measurement with oxygen electrode showed that oxygen concentration decreased exponentially within the first 2500 seconds and then stayed at the low concentration throughout the process and no oscillations was detected.

The results in Figure 2.3 illustrate that oxygen does not only have the same role as nitrogen stream in removing bromine molecules for the occurrence of spontaneous oscillations, but also has important effects on inducing the second oscillatory window. More specifically, as the concentration of oxygen was increased from (a) to (c), the induction time of the first oscillatory window was delayed while the second oscillatory window appeared earlier.

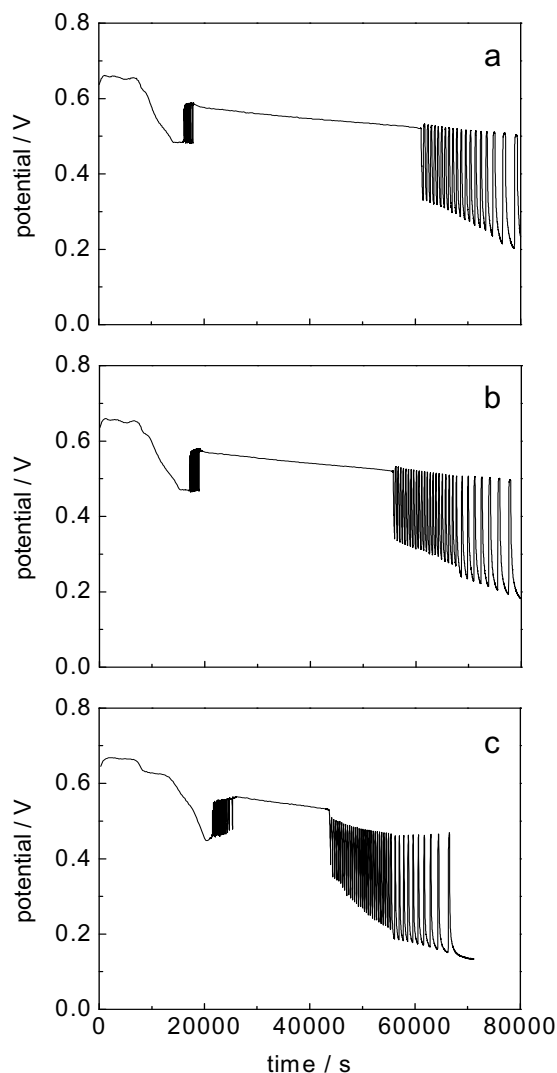


Figure 2.3 Time series of ferriin-bromate-metol reaction carried out by flowing (a) 1:1 nitrogen and air mixture, (b) air, and (c) oxygen above the solution surface. Other reaction conditions are the same as those used in Figure 2.1b.

2.3.3 The Importance of the Age of Metol Stock Solution

To shed light on how oxygen gets involved in the above reaction, particularly its interactions with the substrate metol, in Figure 2.4 we characterized how the reaction

behaviour was affected by the age of metol stock solution: (a) fresh, (b) 1, (c) 4, and (d) 7 days old. Other reaction conditions were $[\text{metol}] = 0.025 \text{ M}$, $[\text{NaBrO}_3] = 0.05 \text{ M}$, $[\text{H}_2\text{SO}_4] = 1.7 \text{ M}$, and $[\text{ferroin}] = 1.0 \times 10^{-4} \text{ M}$. Here, the reactor was configured in such a way that volatile reagents and air were allowed to freely diffuse through a 2 mm hole (in diameter) in the Teflon cap. No nitrogen gas was flow into it. As shown in (a), a large number of oscillations with two distinct frequencies were observed. The induction time is significantly longer than that achieved under the flow of nitrogen or air (see Figure 2.3), suggesting that high bromine concentration in the solution is an important factor in the observed long induction time. We would like to note that when bromine was added initially to the system to brominate metol, there was no significant change in the induction time, which was different from what was seen in the BZ system in which the presence of bromomalonic acid would reduce or eliminate the induction time. Figure 2.4(b) shows that the reaction with one day old metol solution exhibited one oscillatory window with a gradual decrease of oscillation frequency. Four day old metol solution led to oscillations with two distinct frequencies in Figure 2.4(c). Seven day old metol solution, on the other hand, produced sequential oscillations in Figure 2.4(d), where a few small amplitude oscillations developed during the quiescent period.

TOF-MS analysis in Figure 2.5a shows that for the moderately old metol solution (<3 days) the largest peak remains at 345 m/e, which corresponds to the original metol sulphate salt (M). The second largest peak sits at 243 m/e, corresponding to benzoquinone dimmers [34]. There is another small peak at 364 m/e, which corresponds to 1,4-hydroquinone-p-methylaminophenol complex ($\text{H}_2\text{Q-M}$). After seven days the spectrum in Figure 2.5(b) shows that the peak at 243m/e becomes higher than the one at

345 m/e, indicating a greater degree of metol decay. More importantly, the peak at 364 m/e becomes ten times higher than that seen within 3 days old metol solution. The above mass spectrometry analysis suggests that the decay of metol in air undergoes from metol to hydroquinone and then to benzoquinone species.

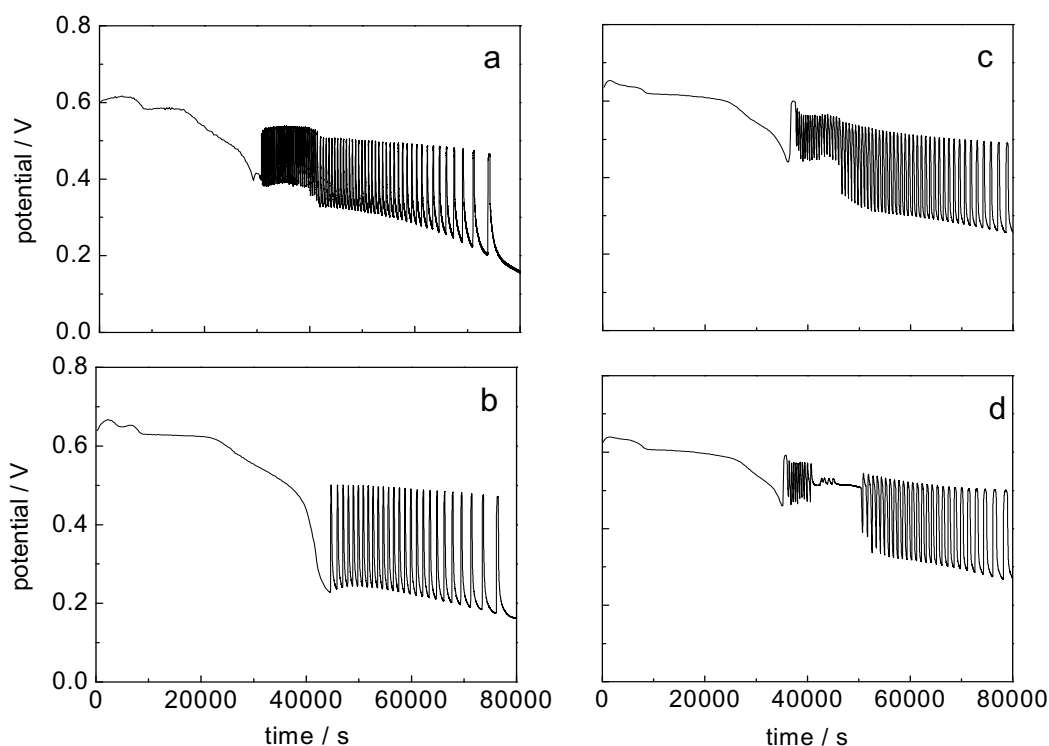
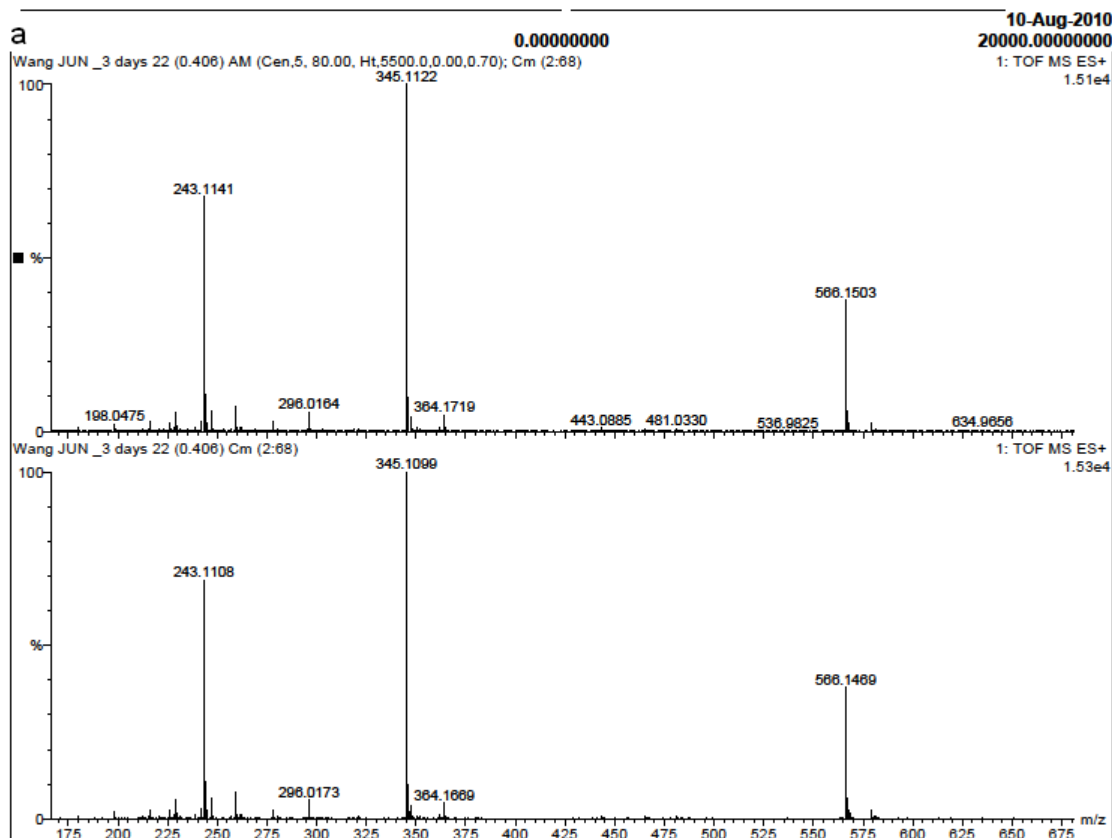


Figure 2.4 Time series of ferroin-bromate-metol reaction performed with (a) fresh, (b) 1, (c) 4, and (d) 7 days old metol stock solution. Initial reaction compositions were $[\text{metol}] = 0.025 \text{ M}$, $[\text{NaBrO}_3] = 0.05 \text{ M}$, $[\text{H}_2\text{SO}_4] = 1.7 \text{ M}$, and $[\text{ferroin}] = 1.0 \times 10^{-4} \text{ M}$.

The difference in the reaction behaviour when fresh or one day old metol solution was used is qualitatively the same as that observed when the initial concentration of metol was decreased. Such an observation suggests that influences of a moderately old metol solution on the reaction phenomenon are mainly due to the decay of metol. However, as the decay of metol continued, decay products such as hydroquinone would insert stronger

influences, leading to more complicated oscillatory behavior. The influences might take place through the reaction of hydroquinone with bromine, bromine dioxide radicals etc.



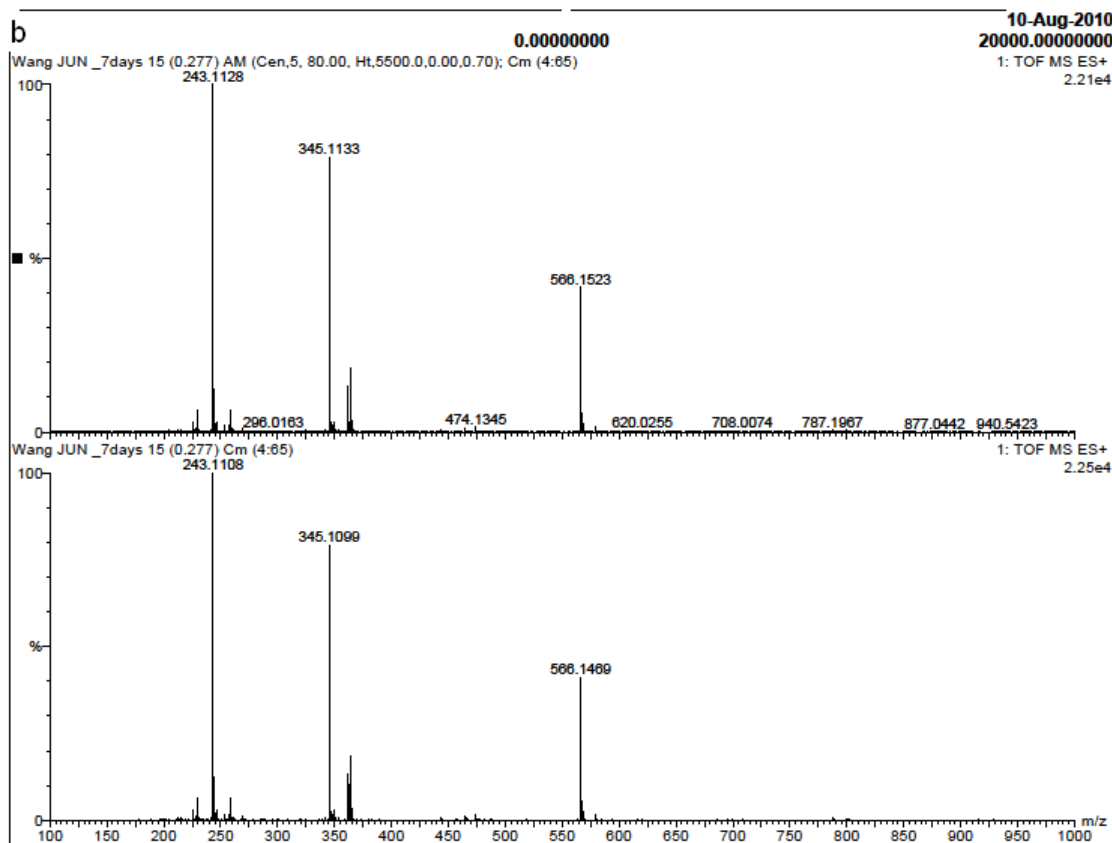


Figure 2.5 TOF-MS analysis of 3 days old metol solution (a) and 7 days old metol solution (b).

To test the above hypothesis, Figure 2.6 presents time series obtained at different combinations of hydroquinone and metol, while the total amount of substrate was kept constant: (a) $[\text{metol}] = 0.02 \text{ M}$ and $[\text{H}_2\text{Q}] = 0.005 \text{ M}$, (b) $[\text{metol}] = 0.0125 \text{ M}$ and $[\text{H}_2\text{Q}] = 0.0125 \text{ M}$, and (c) $[\text{metol}] = 0.01 \text{ M}$ and $[\text{H}_2\text{Q}] = 0.015 \text{ M}$. Other reaction conditions are the same as those used in Figure 2.4. In (a), similar to what was achieved in Figure 2.4b, only one oscillation window was achieved. One group of oscillations with two distinct frequencies was seen in Figure 2.6(b) as a result of increasing H_2Q and decreasing metol concentration. Sequential oscillations were observed in Figure 2.6(c). The trend of the variation is the same as that seen in Figure 2.4. Together with the mass spectroscopic

study, the above kinetic experiments lend strong support that the influence of oxygen on the ferroin-bromate-metol oscillations may take place through the substrate metol, causing the formation of hydroquinone.

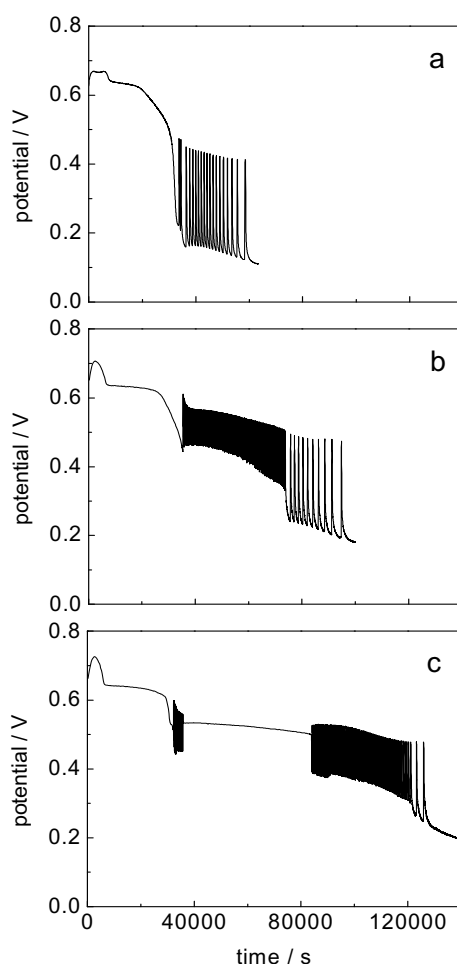


Figure 2.6 Time series of ferroin-bromate-metol reaction performed with different combination of metol and hydroquinone: (a) $[\text{metol}] = 0.02 \text{ M}$, $[\text{H}_2\text{Q}] = 0.005 \text{ M}$; (b) $[\text{metol}] = 0.0125 \text{ M}$, $[\text{H}_2\text{Q}] = 0.0125 \text{ M}$; and (c) $[\text{metol}] = 0.01 \text{ M}$, $[\text{H}_2\text{Q}] = 0.015 \text{ M}$. Other conditions were the same as in Figure 2.4a.

2.3.4 Dependence of the Oscillations on the Initial Compositions

In the following we systematically characterized the influence of the concentration of each reagent on the oscillatory behavior. Figure 2.7 is a phase diagram in the bromate-

sulfuric acid concentration phase plane, where squares, circles, upper and lower triangles denote the conditions where the system exhibits different forms of spontaneous oscillations. The unmarked region is the conditions where no spontaneous oscillations were observed. The configuration of the reactor was the same as that used in Figures 2.4a and concentrations of metol and ferroin were fixed respectively at 0.025 M and 1.0×10^{-4} M. Simple oscillations with a large amplitude and low frequency are defined as simple type I, whereas simple damping oscillations as shown in Figure 2.8d are defined as simple type-II.

First glance of this phase diagram indicates that oscillatory phenomena exist over broad concentrations of bromate and sulfuric acid, where sequential oscillations are the dominant behavior. No oscillation was observed for bromate above 0.1 M or below 0.02 M. Within such a range, decreasing bromate concentration from 0.1 M first resulted in oscillations with two distinct frequencies that were similar to the phenomenon seen in Figure 2.4a. Further decrease of bromate concentration led to sequential oscillations like those presented in Figure 2.4d. Effects of bromate on the reaction behavior are qualitatively the same as sulfuric acid. In the absence of bromine removal and oxygen effects, however, spontaneous oscillations exist within a smaller parameter window and sequential oscillations are replaced by simple transient oscillations. For example, at the condition $[\text{NaBrO}_3] = 0.05$ M and $[\text{H}_2\text{SO}_4] = 1.7$ M, the system could not oscillate in the absence of bromine removal and oxygen effects.

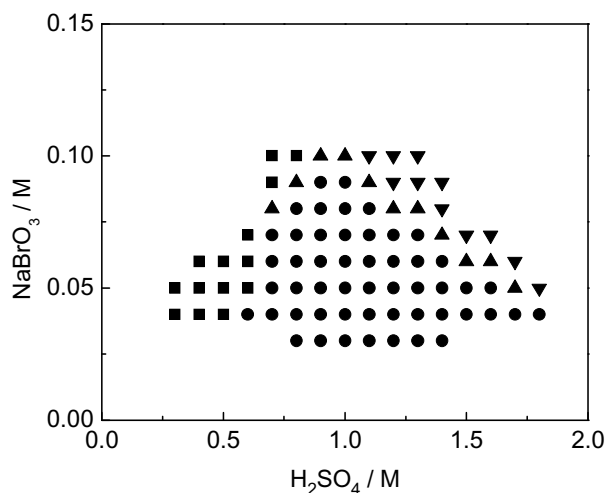


Figure 2.7 Phase diagram of the ferriin-bromate-metol reaction in bromate-sulfuric acid concentration plane. All other conditions were the same as those used in Figure 2.4a. The system exhibited spontaneous oscillations only within the marked region: (●) sequential oscillations, (■) damping oscillations (Type II), (▲) oscillations with two distinct frequencies, and (▼) low frequency, large amplitude oscillations (Type I).

Representative series about the influence of each reagent on the reaction behavior can be seen in Figures 2.8 to 2.10, where Figure 2.8 shows that as the acid concentration was decreased just below the top threshold, a few oscillations with large amplitude and low frequency took place in (a). When the acid concentration was too high (> 1.9 M) or too low (< 0.2 M), the system did not exhibit any oscillatory phenomenon. When the acid concentration was decreased further, the system exhibited one group of oscillations with two distinct frequencies in (b). The oscillations were separated in (c) as the acid concentration was lowered still, forming the phenomenon of sequential oscillations. Eventually, only one group of damping oscillations were generated by decreasing the acid concentration to even lower value 0.3M in (d), with a very long induction time.

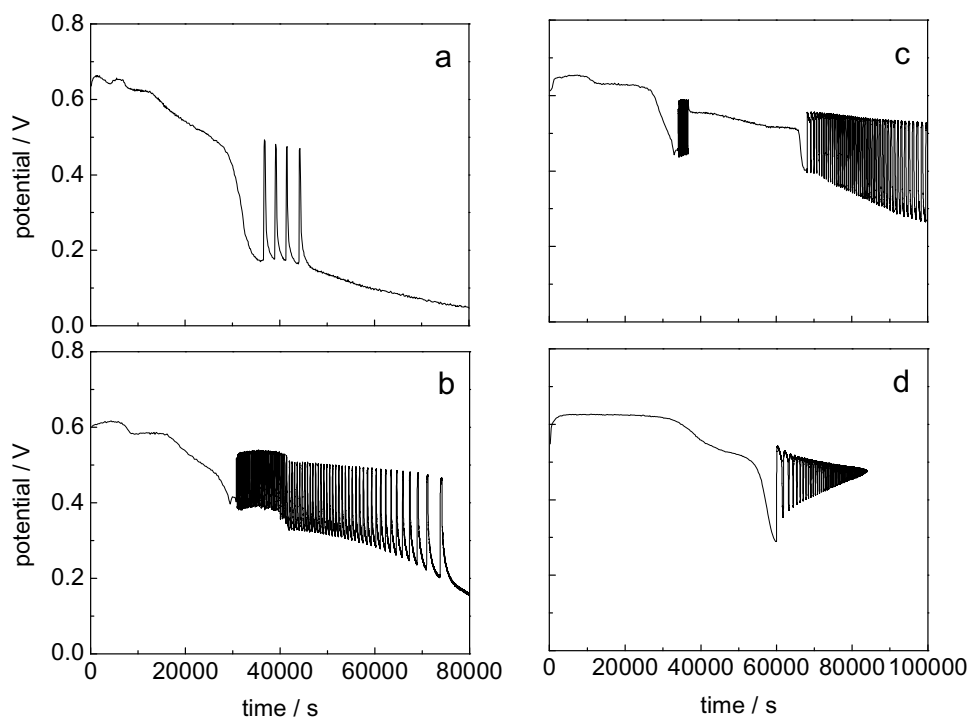


Figure 2.8 Time series of ferroin-bromate-metol reaction at different acid concentrations (a) 1.8 M, (b) 1.7 M, (c) 1.3 M, and (d) 0.3 M. Other reaction conditions are $[\text{metol}] = 0.025 \text{ M}$, $[\text{NaBrO}_3] = 0.05 \text{ M}$, and $[\text{ferroin}] = 1.0 \times 10^{-4} \text{ M}$. The reactor was unsealed to allow volatile species diffuse out and allow the air diffuse into the reactor.

Results in Figure 2.9 show that as ferroin concentration was above a threshold value, a large number of oscillations appeared. Notably, in Figure 2.9(c) the frequency of oscillation increased initially, despite the continuous consumption of reactants in time. As the reaction approached to end, the oscillation frequency decreased as seen normally in a closed oscillatory system. The adjustment of ferroin concentration has so far failed to transform these oscillations into sequential oscillations.

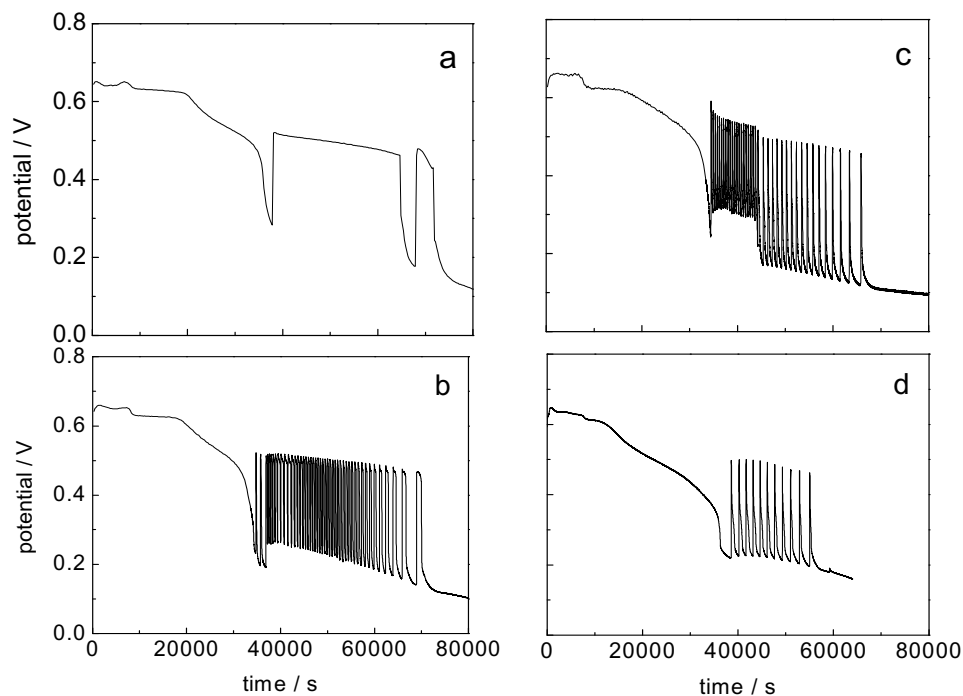


Figure 2.9 Time series of ferriin-bromate-metol reaction at different initial concentrations of ferriin: (a) 2.5×10^{-5} M, (b) 5.0×10^{-5} M, (c) 2.0×10^{-4} M, and (d) 4.0×10^{-4} M. Other reaction conditions are $[\text{metol}] = 0.025$ M, $[\text{NaBrO}_3] = 0.05$ M, and $[\text{H}_2\text{SO}_4] = 1.7$ M. The reactor was unsealed to allow volatile species diffuse out and air diffuses into the reactor.

Figure 2.10 shows that as the concentration of metol was decreased from (a) 0.025M to (b) 0.02M, the induction time became longer. Meanwhile, the oscillation pattern also became simpler. Such a trend is qualitatively the same as that seen in Figure 2.4 (a) and (b), in which the age of metol solution was characterized as the only parameter.

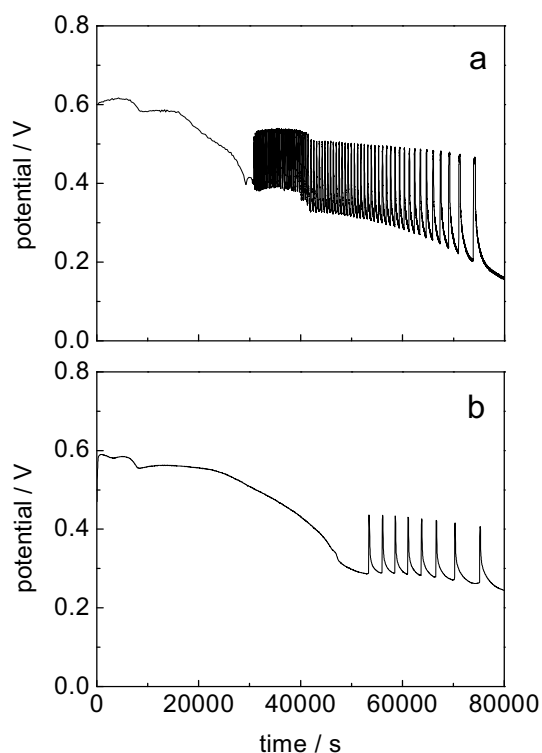


Figure 2.10 Time series of ferriin-bromate-metol reaction at different initial concentrations of metol: (a) 0.025 M, (b) 0.02 M. Other reaction conditions are $[\text{NaBrO}_3] = 0.05 \text{ M}$, $[\text{ferriin}] = 1.0 \times 10^{-4} \text{ M}$, and $[\text{H}_2\text{SO}_4] = 1.7 \text{ M}$. The reactor was unsealed to allow volatile species diffuse out and allow air diffuse into the reactor.

2.3.5 Influences of Stirring Rate

Figures 2.11 and 2.12 investigated influences of stirring on the reaction behavior. Unlike observed in the classic BZ reaction, in which stirring rate does not affect the chemical dynamics much, in Figure 2.11 the induction time was greatly shortened when the stirring rate was increased. Such an effect is similar to that of increasing nitrogen flow (see Figure 2.2). It is understandable since both increasing the mixing rate and the nitrogen gas flow will cause the accelerated loss of bromine.

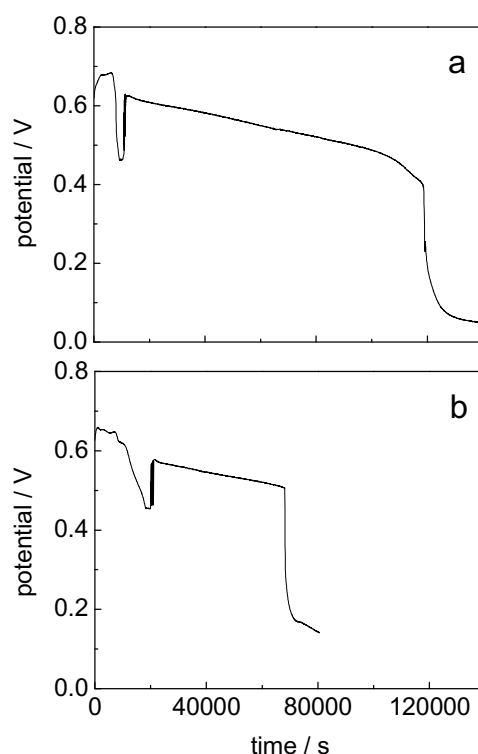


Figure 2.11 Influences of stirring rate on the oscillatory behavior: (a) 1200 and (b) 600 rpm, where nitrogen was flow into the reactor at a rate 60 ml/min. Other reaction conditions were [metol] = 0.025M, [NaBrO₃] = 0.05M, [H₂SO₄] = 1.7M, and [ferriin] = 1.0×10^{-4} M.

Figure 2.12 shows the influence of stirring on the oscillatory behavior when pure oxygen instead of nitrogen was flow into the reactor at a rate 60 ml/min. Here, the stirring does not only affect the bromine removal, but also influence the oxygen dissolution. The combination of the above two factors induced a new oscillatory window in which oscillations have two distinct frequencies (see (c)).

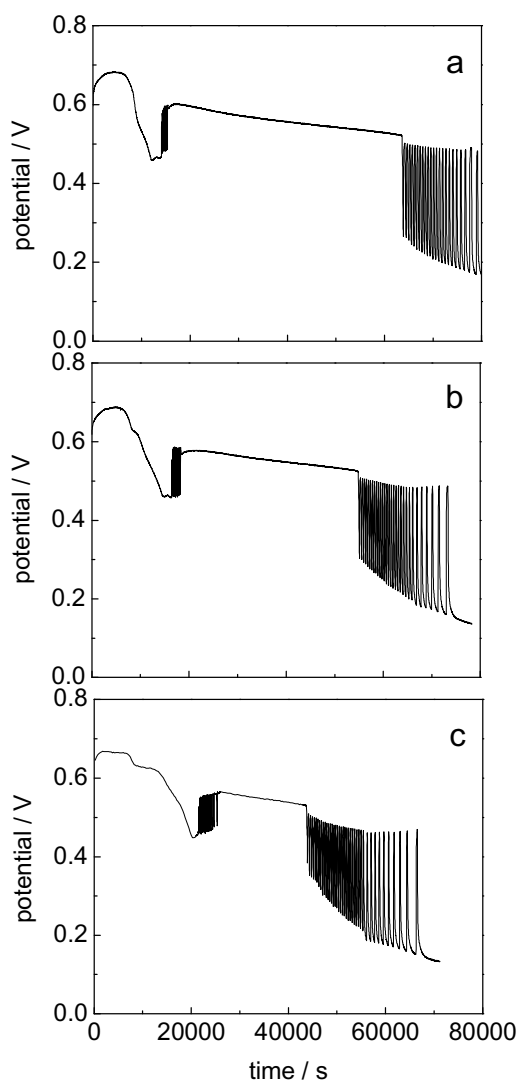


Figure 2.12 The influence of stirring rate on the oscillatory behavior: (a) 1200, (b) 900, and (c) 600 rpm, where oxygen was flow into the reactor at a rate 60 ml/min. Other reaction conditions were $[\text{metol}] = 0.025\text{M}$, $[\text{NaBrO}_3] = 0.05\text{M}$, $[\text{H}_2\text{SO}_4] = 1.7\text{M}$, and $[\text{ferroin}] = 1.0 \times 10^{-4}\text{M}$.

2.3.6 Dynamic Perturbation and Characterization

Perturbation with bromide ions has been frequently employed to decipher the mechanism of bromate-based chemical oscillations [35, 36]. Here we found that these

spontaneous oscillations could be temporally quenched by adding 1.0×10^{-4} M bromide ions and the effect of bromide depended on the oscillation phase, similar to the quenching phenomena reported in the BZ reaction. Another consequence of Br^- perturbation is that it prolonged the quiescent window of the sequential oscillations, presumably due to the production of brominated substrates. When bromide perturbation was applied specifically to the quiescent window of the sequential oscillations, large amplitude transient oscillations were induced. For example, adding 1.0×10^{-4} M bromide induced three oscillations with the first peak having a long recovery period (i.e. low frequency). This observation indicates that the system is at an excitable, but not far from the oscillatory state during the non-oscillatory evolution. Such a steady state is likely a result of competition between two sub-oscillators, similar to the earlier report on CHD-BZ system [37]. Here, the second sub-oscillator is due to hydroquinone-bromate reaction.

Figure 2.13 shows the bromide ion perturbation during the oscillation, (a) perturbing high frequency oscillations, (b) perturbing low frequency oscillations. In both cases, four phases were examined and they behaved the same in (a) and (b). After injecting 0.15 ml of 10^{-4} M Br^- solution to the reaction mixture, the system responded to the disturbance with a larger amplitude excursion and then gradually relaxed back to the normal oscillatory mode, suggesting such a perturbation was small enough to lead the dynamics confined to the neighborhood of the limit cycle. Specifically, when the bromide perturbation was applied at the phase where the redox potential increased to middle of the amplitude (second perturbation in (a) and (b)), potential abruptly decreased to the bottom, which required a long time to recover. This rapid response is because bromide quickly consumed the autocatalyst HBrO_2 .

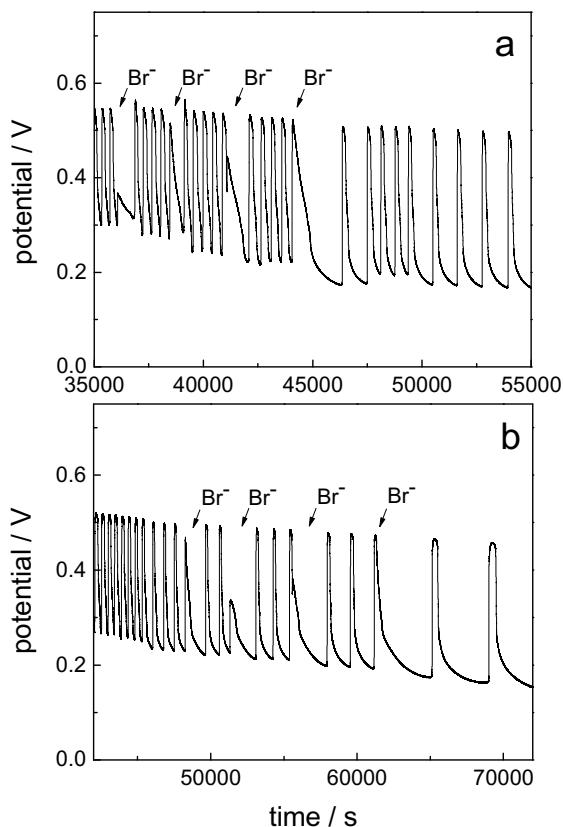


Figure 2.13 Effects of bromide ion on bromate-metal catalyzed reaction with $[\text{metol}] = 0.025 \text{ M}$, $[\text{NaBrO}_3] = 0.05 \text{ M}$, $[\text{ferroin}] = 10^{-4} \text{ M}$ and $[\text{H}_2\text{SO}_4] = 1.7 \text{ M}$, each perturbation of bromide ion is $0.15 \text{ ml } [\text{Br}^-] = 10^{-4} \text{ M}$ in the mixture. All other conditions were the same as those used in Figure 2.4a.

Fig. 2.14 presents ^1H -NMR spectra obtained from the reaction solution of (a) in Figure 2.1a and (b) in Figure 2.1b, respectively. The solution was extracted after 60000s with diethylether. A ^1H NMR resonance at $\delta = 6.79$ is attributable to 1,4-benzoquinone (BQ), this was further supported by the ^{13}C NMR spectral resonances at 136.6 and 187.4 ppm (see Figure 2.15). The ^1H NMR spectral resonance appearing at $\delta = 7.31$ (d, $J = 2.3 \text{ Hz}$); 6.95 (d, $J = 10.1 \text{ Hz}$); 6.84 (dd, $J = 10.1, 2.3 \text{ Hz}$) correspond to the product 2-bromo-1,4-

benzoquinone (BrQ). The two spectra are almost identical, except that the magnitude of those major peaks, suggesting that bromine removal and oxygen exposure did not alter the compositions of the final products. However, nitrogen flow clearly reduced the amount of BrQ produced.

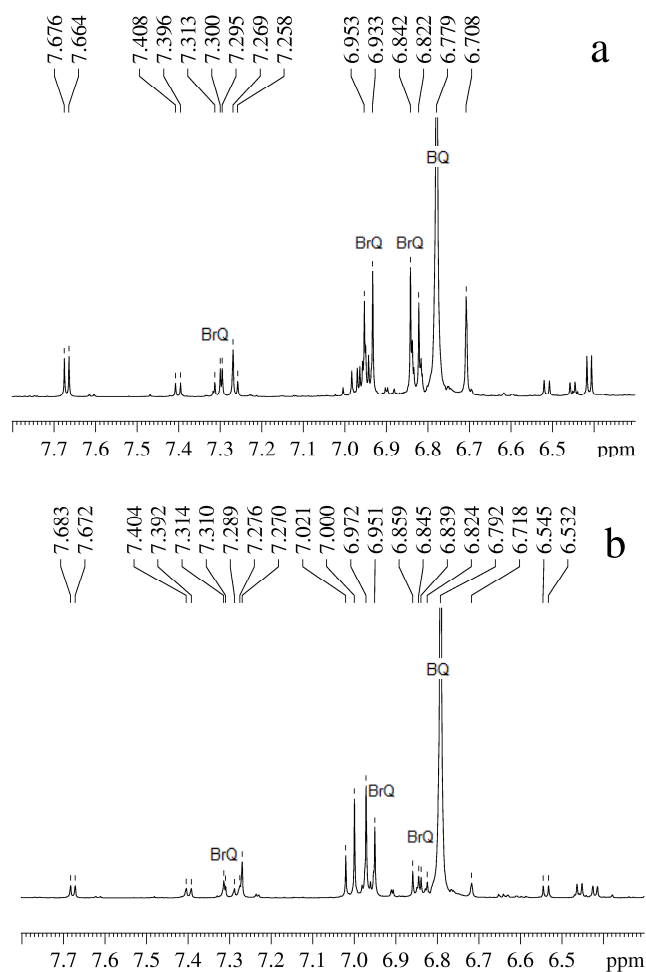


Figure 2.14 ^1H NMR (500MHz) spectra of the ferroin-bromate-metol reaction at the conditions $[\text{metol}] = 0.025 \text{ M}$, $[\text{NaBrO}_3] = 0.05 \text{ M}$, $[\text{ferroin}] = 1.0 \times 10^{-4} \text{ M}$ and $[\text{H}_2\text{SO}_4] = 1.7 \text{ M}$, (a) sealed with parafilm, and (b) flowing nitrogen gas above the solution surface.

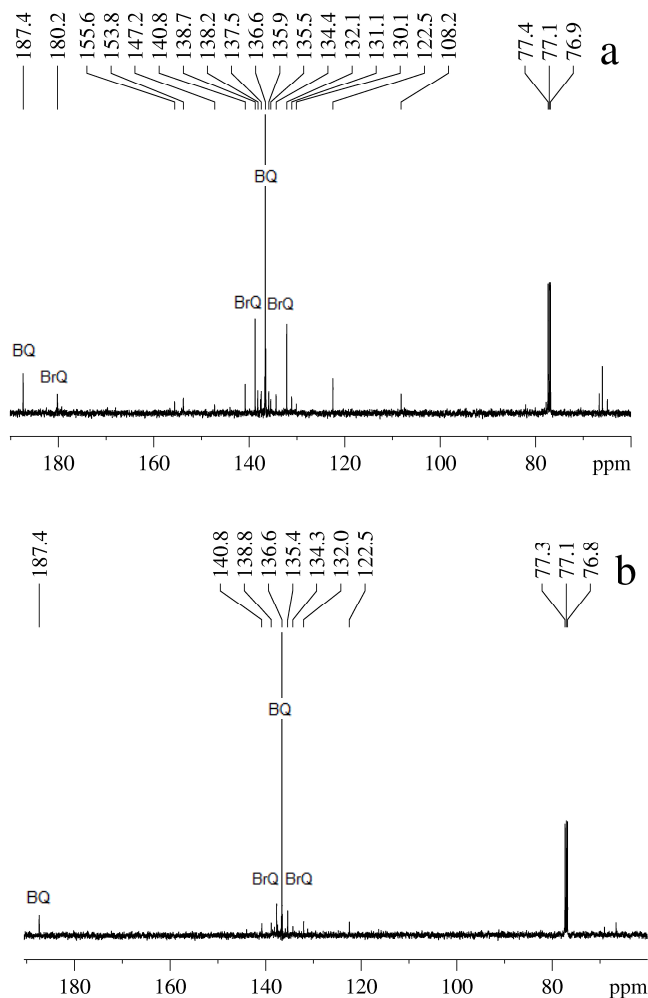


Figure 2.15 ^{13}C NMR (500MHz) spectra of the ferroin-bromate-metol reaction at the conditions $[\text{metol}] = 0.025 \text{ M}$, $[\text{NaBrO}_3] = 0.05 \text{ M}$, $[\text{ferroin}] = 1.0 \times 10^{-4} \text{ M}$ and $[\text{H}_2\text{SO}_4] = 1.7 \text{ M}$, (a) sealed with parafilm, and (b) flowing nitrogen gas above the solution surface.

2.3.7 Spatiotemporal Behavior

Preliminary exploration of spatiotemporal behaviour in the ferroin-bromate-metol system was carried out in a capillary tube. The space-time plot presented in Fig. 2.16 was

generated by taking one horizontal cut through the center of the snapshot of the capillary tube and sequentially piling up these one-dimensional images. The horizontal and vertical axes are, respectively, the space and time. The time evolves in an upward direction. Bright and dark colors correspond respectively to ferriin and ferroin. Under the conditions in (a), reduction (dark) fronts were first developed at both free ends. They propagated toward, but failed to reach the center of the medium. Later, consecutive reduction pulses developed at locations near the boundary, forming directional wave train. Near the end of the reaction process, two reduction (dark) fronts were propagating toward each other and emerged to form a uniform medium. In order to investigate the effect of air flow on the wave behavior, the left end of the capillary tube in (b) was not sealed (i.e., exposed to air). Notably, these propagating pulses could only develop at the left half of the medium. Phenomenon similar to pulses merging behavior reported in ferroin-bromate-CHD system was seen in the above process. The above primitive study indicates that this ferroin-bromate-metol oscillator has a great potential to exhibit novel nonlinear spatiotemporal dynamics and more systematic exploration is deserved. Importantly, results in Fig. 2.16b highlight that bromine removal and oxygen have significant impacts on the pattern formation too.

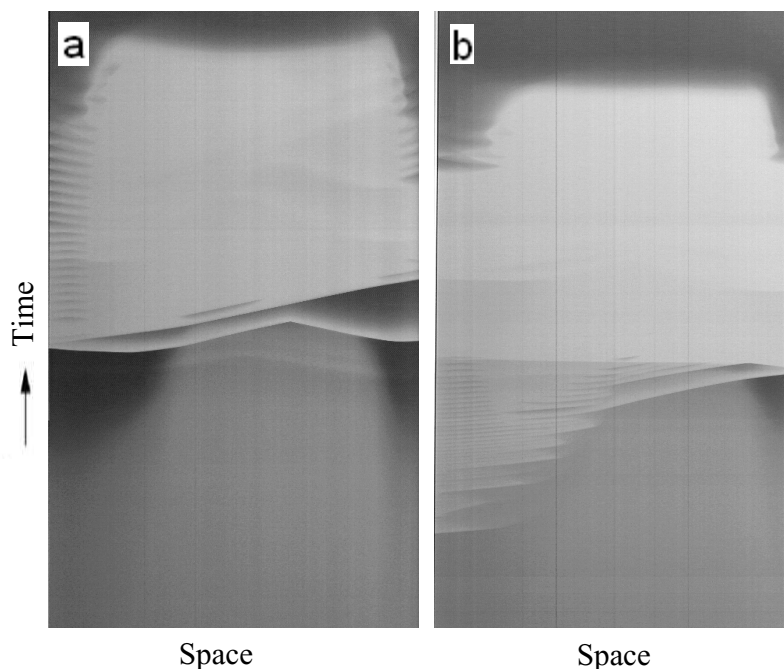


Figure 2.16 Space-time plot of the ferroin-bromate-metol reaction in a capillary tube. The length of the medium is 50 mm. Time period shown here is between 120 min and 360 min. Reaction compositions are $[\text{metol}] = 0.025 \text{ M}$, $[\text{NaBrO}_3] = 0.05 \text{ M}$, $[\text{ferroin}] = 3 \times 10^{-3} \text{ M}$ and $[\text{H}_2\text{SO}_4] = 1.7 \text{ M}$. The inner diameter of the tube is 1.8 mm. (a) two sides of the capillary tube were open to the air, (b) left side of the capillary tube was open to the air, and the right hand side was sealed by water.

The spatiotemporal behaviour was also investigated in a thin layer of silica gel, which was prepared by mixing 10 mL of 30% (w/w) sodium silicate solution with 1.5 mL of 0.03 M ferroin solution and 1.9 mL of 6 M H_2SO_4 . The gelation took place after pouring the above silicate mixture into a petri dish. The thin layer of silica gel formed has a thickness of 1.5 mm. To study the pattern formation, 20 mL of reaction solution consisting of $[\text{metol}] = 0.025 \text{ M}$, $[\text{NaBrO}_3] = 0.05 \text{ M}$ and $[\text{H}_2\text{SO}_4] = 1.7 \text{ M}$ was poured on top of the silica gel. The solution layer was around 2.5 mm. After the system has evolved for 20 hours, reduction (dark) fronts were developed first at the boundary and then

propagated toward the center of the petri dish. The free ends of these wave segments led to the formation of spiral waves after around 28 hours in (a). As the reaction progressed, the spiral rotation slowed down and eventually transformed into target patterns as see in (b) after 31 hours.

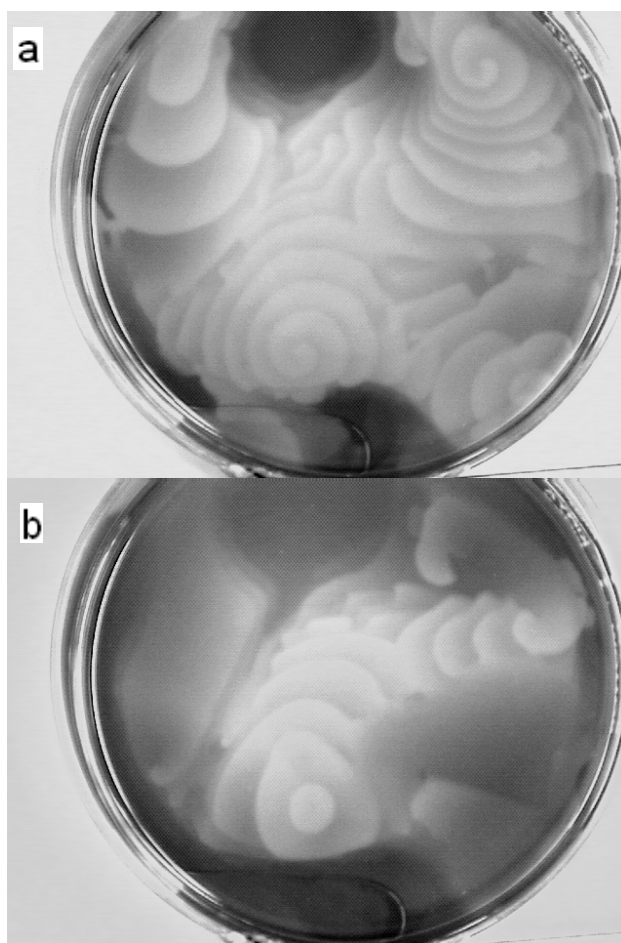
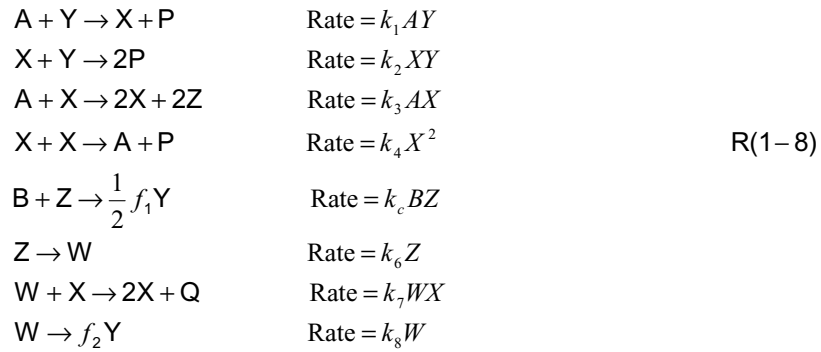


Figure 2.17 Typical spiral waves (a) and target patterns (b) formed in the silica gel membrane. The bottom silica gel layer with 1.5 mm thickness was immobilized by 0.03M ferrion, top solution with 2.5 mm thickness was applied the same configuration as Figure 2.1 except a metal catalyst ferriox.

2.3.8 Simulation of Pattern Formation

While the detailed mechanisms of ferriin-bromate-metol reaction remain to be understood, preliminary mechanistic study has suggested the presence of hydroquinone as an intermediate reagent, benzoquinone as one of the products under the conditions investigated here. Since hydroquinone reacts with bromine dioxide radicals to form an autocatalytic nonlinear feedback, the ferriin-bromate-metol system may consist of two sub-oscillators, similar to the ferriin-bromate-CHD system. Notably, in the ferriin-bromate-CHD medium pulses undergoing complex sequences of propagation failures, backfiring and breathing have been reported. To shed light on the importance of coupled autocatalytic cycles in the emergence of complex propagating wave behavior like seen in Fig. 2.16, in the following we modified the Oregonator model through incorporating a second autocatalytic cycle (R5 to R8).



Where X = concentration of $HBrO_2$, Y = concentration of Br^- , Z = concentration of Ce^{4+} , W = concentration of H_2Q , A = concentration of BrO_3^- , B = concentration of MA, P = final products. The R5 can be understood as a reaction between the ferriin and CHD (or metol) to produce hydroquinone, which reacts with bromine dioxide to produce $HBrO_2$.

The bromination of hydroquinone may be accompanied by the formation of bromide ions and such a process is denoted by R8. By assuming that concentrations of bromate, malonic acid, CHD (or metol) are constant, the above modified Oregonator model can be described with the following 4 differential equations with the dimensionless variables x , y , z , w and τ and by using the dimensionless constants q , r , s , ε_1 , ε_2 , ε_3 , f_1 , f_2 .

$$\varepsilon_1 \frac{dx}{d\tau} = qy - xy + x - x^2 + wx \quad (\text{L1})$$

$$\varepsilon_2 \frac{dy}{d\tau} = -qy - xy + f_1 z - f_2 rw \quad (\text{L2})$$

$$\frac{dz}{d\tau} = x - z - sz \quad (\text{L3})$$

$$\varepsilon_3 \frac{dw}{d\tau} = 2sz - wx - rw \quad (\text{L4})$$

$$\begin{aligned} X &= \frac{k_3 A}{2k_4} x, \quad Y = \frac{k_3 A}{k_2} y, \quad Z = \frac{(k_3 A)^2}{k_4 k_c B}, \quad t = \frac{1}{k_c B} \tau \\ \varepsilon_1 &= \frac{k_c B}{k_3 A}, \quad \varepsilon_2 = \frac{2k_4 k_c B}{k_2 k_3 A}, \quad \varepsilon_3 = \frac{2k_4 k_c B}{k_7 k_3 A} \\ q &= \frac{2k_1 k_4}{k_2 k_3}, \quad r = \frac{2k_4 k_8}{k_7 k_3 A}, \quad s = \frac{k_6}{k_c B} \end{aligned}$$

Where parameter values in Figure 2.19 were adopted from the normal experimental conditions with $A = 0.06\text{M}$, $B = 0.02\text{M}$, $[\text{H}^+] = 0.8\text{M}$, $k_1 = 1.28$, $k_2 = 8 \times 10^5$, $k_3 = 8$, $k_4 = 2 \times 10^3$, $k_c = 1$, $k_6 = 0.017$, $k_7 = 1600$, $k_8 = 0.08$, $f_1 = 0 - 1.0$, $f_2 = 1.0$.

In both 1D and 2D calculations, we used a time step $\Delta t = 0.0001$ (its critic value is 0.001) and a grid $\Delta x = \Delta y = 0.001$. The diffusion coefficient D and control parameter f_1 were adjusted each time. The differential equations (L1) to (L4) were integrated with an explicit Euler method, where the Laplace operator was approximated with three or five

nearest neighbor sites. Zero-flux boundary conditions were employed. The same results were obtained when the space and time steps were reduced. As shown in Figure 2.19, propagation failure can be observed in (a) at the conditions where the system exhibited spontaneous oscillations. Panels (b) to (c) show other interesting propagating pulse behavior, which are similar to anomalous dispersion, merging waves and intermittent pulses seen experimentally.

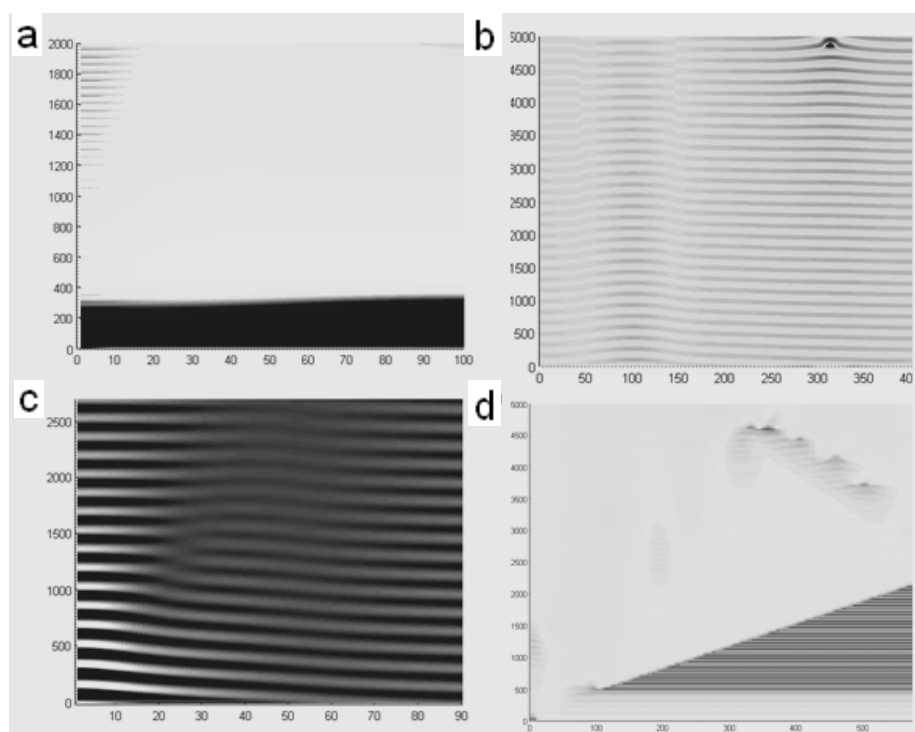


Figure 2.18 Space-time plots of wave dynamics appearing propagation failure (a), (b) merging and anomalous dispersion, and splitting (c), (d) wave turbulence, x axis represents space, and y axis means time. All diffusion coefficient was $D = 10^{-3}$, (a) $f_1 = 1.0$, (b), (c) and (d) $f_1 = 0.9$. Horizontal axis represents space, and vertical axis means time.

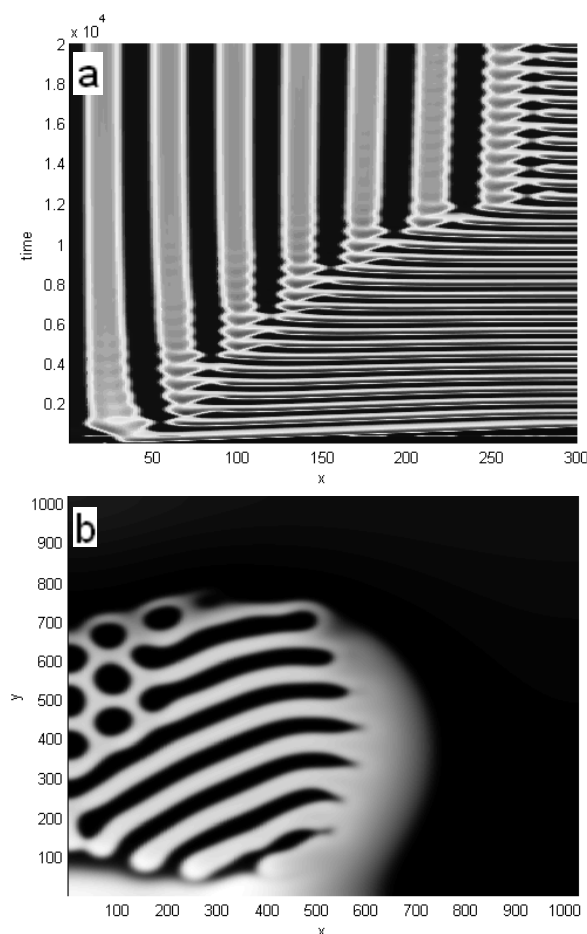


Figure 2.19 Space-time plots of transient breathing pulses in (a) and two dimensional breathing Turing patterns in (b). Parameters applied in (a) were $f1 = 0.5, f2 = 1.0, D_x = D_w = 10^{-4}, D_y = D_z = 10^{-3}$, and parameters applied in (a) were $f1 = f2 = 1.0, D_x = 10^{-6}, D_y = D_z = D_w = 10^{-5}$. All other parameters were the same as in Figure 2.19.

By further changing the coupling strength and diffusion coefficients of the four variables, the above proposed model could generate more complicated spatiotemporal phenomena. Various instabilities such as space-time plots of transient breathing pulses in Fig. 2.20(a) and two dimensional breathing Turing patterns in Fig. 2.20(b) have been observed. The results confirm the significance of competing nonlinear feedback processes. Since systems with coupled autocatalytic processes provide not only the potential of achieving complex dynamics, but also additional paths of manipulating the

relative diffusivity of the chemical reagents, they offer a promising playground for searching for novel nonlinear spatiotemporal behavior.

2.4 Conclusions

This study investigated the behavior of ferroin-bromate-metol reaction in a batch reactor and found that bromine removal had a significant impact on the underlying nonlinear kinetics. Both simple and complex oscillations were achieved via manifesting bromine removal. Similar dramatic impact of bromine removal is expected to exist in other modified BZ oscillators, in which organic substrates do not react with bromine rapidly and thus allow the build up of bromine in the system. Despite their significant influence on the kinetics, GC/MS spectrometry and NMR measurements illustrate that bromine removal and oxygen did not change the major products, which are 1,4-benzoquinone and bromobenzoquinones, similar to the products detected in the ferroin-bromate-CHD reaction [38, 39]. Using different nitrogen flow rates, experiments illustrate that bromine concentration has strong influence on the long induction, where bromine removal shortens the induction time. The presence of brominated metol substances, on the other hand, does not affect the induction time.

Spectroscopy measurement suggests that oxygen causes the decay of metol to produce hydroquinone species and then benzoquinones. This conclusion is strongly supported by the kinetic study, in which the influence of the age of metol solution was qualitatively reproduced by adding different amounts of hydroquinone into the system. As known from CHD systems [10, 38, 39], hydroquinone reacts with bromine dioxide radicals to form an autocatalytic feedback. The presence of coupled autocatalytic cycles may consequently result in sequential oscillations, in a way similar to that discussed in the

CHD modified malonic acid-BZ reaction [37]. The above argument is consistent with the experimental observation that increasing the amount of hydroquinone added causes the transition from simple to sequential oscillations, and increasing oxygen concentration (i.e. enhancing hydroquinone production) also resulted in sequential oscillations. Since metol reacts with ferriin and bromine, despite slowly, the core mechanism of this ferriin-bromate-metol shall be very similar to the BZ reaction, where metol replaces malonic acid. However, it is important to point out that metol and bromate in acid solution alone exhibited a clock reaction behavior, where our spectroscopy measurements showed the production of benzoquinone. Such a clock reaction process may consist of the formation of hydroquinone from metol and bromate and, then the autocatalytic oxidation of hydroquinone by bromine dioxide radicals, similar to the CHD and bromate reaction [10]. The hydroquinone formation from bromate and metol interaction also accounts for the emergence of sequential oscillations in the absence of oxygen.

In summary, this study presents a new bromate-based oscillator that exhibits complex temporal reaction behavior and interesting spatiotemporal dynamics. Results presented above also provide concrete evidences that bromine removal can be an effective and feasible means of manipulating the behavior of bromate-based chemical oscillations.

2.5 References

- 1 A. M. Zhabotinsky, *Biofizika*, 1964, 9, 306.
- 2 R. J. Field and M. Burger, Eds. *Oscillations and Traveling Waves in Chemical Systems*; Wiley-Interscience: New York, 1985.
- 3 S. K. Scott, *Oscillations, Waves and Chaos in Chemical Kinetics*, Oxford University Press Inc, New York, 1994.

- 4 V. J. Farage and D. Janjic, Chem. Phys. Lett., 1982, 88, 301.
- 5 M. Orbán and E. Körös, J. Phys. Chem., 1978, 82, 1672.
- 6 B. Zhao and J. Wang, Chem. Phys. Lett., 2006, 430, 41.
- 7 K. Showalter, R. M. Noyes and K. Bar-Eli, J. Chem. Phys., 1978, 69, 2514.
- 8 M. Harati and J. Wang, J. Phys. Chem. A, 2008, 112, 4241.
- 9 Z. Noszticzius, P. Stirling and M. Wittmann, J. Phys. Chem., 1985, 89, 4914.
- 10 M. T. Beck and Z. B. Varadi, React. Kinet. Catal. Lett., 1977, 6, 275.
- 11 K. Kurin-Csörgei, I. Szalai and E. Körös, React. Kinet. Catal. Lett., 1995, 54, 217.
- 12 D. S. Huh, Y. J. Kim, H. S. Kim, J. K. Kang and J. Wang, Phys. Chem. Chem. Phys., 2003, 5, 3188.
- 13 L. Treindl and V. Zvac, React. Kinet. Catal. Lett., 1983, 22, 451.
- 14 R. P. Rastogi, P. Chand, M. K. Pandey and M. Das, J. Phys. Chem. A, 2005, 109, 4562.
- 15 N. Li, J. Zhao, and J. Wang, J. Chem. Phys., 2008, 128, 244509.
- 16 J. A. Pojman, D. C. Leard and W. West, J. Am. Chem. Soc., 1992, 114, 8298.
- 17 L. Treindl, T. Matsumura-Inoue and P. Ruoff, J. Phys. Chem. A, 2002, 106, 5271.
- 18 H.-D. Försterling, S. Murányi and Z. Noszticzius, J. Phys. Chem., 1990, 94, 2915.
- 19 R. J. Field, E. Körös and R. M. Noyes, J. Am. Chem. Soc., 1972, 94, 8649.
- 20 E. J. Heilweil, M. J. Henchman and I. R. Epstein, J. Am. Chem. Soc., 1979, 101, 3698.
- 21 L. F. Salter and J. G. Sheppard, Int. J. Chem. Kinet., 1982, 14, 815.
- 22 P. K. Srivastava, Y. Mori and I. Hanazaki, J. Phys. Chem., 1991, 95, 1636.
- 23 L. Adamčíková, Z. Farbulová and P. Ševčík, New J. Chem., 2001, 25, 487.

- 24 K. Pelle, M. Wittmann, K. Lovrics, Z. Noszticzius, M. L. Turco Liveri and R. Lombardo, J. Phys. Chem. A, 2004, 108, 5377.
- 25 K. Pelle, M. Wittmann, K. Lovrics and Z. Noszticzius, J. Phys. Chem. A, 2004, 108, 7554.
- 26 S. Barkin, M. Bixon, R. M. Noyes and K. Bar-Eli, Int. J. Chem. Kinet., 1978, 10, 619.
- 27 K. Bar-Eli and S. Haddad, J. Phys. Chem., 1979, 83, 2952.
- 28 B. Neumann, S. C. Müller, M. J. B. Hauser, O. Steinbock, R. H. Simoyi and N. S. Dalal, J. Am. Chem. Soc., 1995, 117, 6372.
- 29 J. Wang, F. Hynne, P. G. Sørensen and K. Nielsen, J. Phys. Chem., 1996, 100, 17593.
- 30 P. Ruoff and R. M. Noyes, J. Phys. Chem., 1989, 93, 7394.
- 31 L. Treindl, P. Ruoff and P. O. Kvernberg, J. Phys. Chem. A, 1997, 101, 4606.
- 32 O. Steinbock, C. T. Hamik and B. Steinbock, J. Phys. Chem. A, 2000, 104, 6411.
- 33 A. F. Taylor, V. Gaspar, B. R. Johnson and S. K. Scott, Phys. Chem. Chem. Phys., 1999, 1, 4595.
- 34 M. Aceituno, C. Stalikas, L. Lunar, S. Rubio and D. Pérez-Bendito, Water Research, 2002, 36, 3582.
- 35 P. Ruoff, J. Phys. Chem., 1984, 88, 2851.
- 36 F. Hynne, P. G. Sorensen and H. Neergaard, J. Phys. Chem., 1991, 95, 1315.
- 37 Y. Chen and J. Wang, J. Phys. Chem., 2005, 109, 3950.
- 38 I. Szalai, K. Kurin-Csörgei and M. Orbán, Phys. Chem. Chem. Phys., 2002, 4, 1271.

- 39 I. Szalai, K. Kurin-Csörgei, I. R. Epstein and M. Orbán, J. Phys. Chem. A, 2003, 107, 10074.
- 40 N. Manz, C. T. Hamik, and O. Steinbock, Phys. Rev. Lett., 2004, 92, 248301.
- 41 N. Manz, B. T. Ginn, and O. Steinbock, Phys. Rev. E, 2006, 73, 066218.
- 42 N. Manz and O. Steinbock, J. Phys. Chem. A, 2004, 108, 5295.
- 43 C. T. Hamik, N. Manz, and O. Steinbock, J. Phys. Chem. A, 2001, 05, 6144.

Chapter 3: Design of a Novel Minimal Bromate Oscillator

3.1 Introduction

A large family of bromate-based chemical oscillators has been developed in the past three decades [1-15]. The vast majority of those bromate oscillators are constructed by replacing malonic acid of the BZ reaction with other organic substrates [3-15]. When malonic acid is replaced, the consumption of bromine molecules as well as the reduction of oxidized metal catalysts such as ferriin and Ce^{4+} is alternated. As a result, those modified systems may exhibit reaction behaviours that are very different from those seen in the classic BZ reaction [16-19]. Mechanistic study has illustrated that the BZ reaction and related bromate oscillators consist of a large number of intermediates and reaction steps [20, 21]. Earlier, researchers had attempted to develop a simplified bromate-oscillator, known as minimal bromate oscillators, by excluding organic substrates [22-26].

No spontaneous oscillations have been reported when those minimal bromate oscillators were investigated in a closed system [22-26]. Beck and co-workers did achieve spontaneous oscillations in the ferroin-bromate reaction carried out in a batch system, however the presence of gas stream was determined to be necessary to bring out bromine molecules, making their system a semi-open system, strictly speaking [22]. The usage of extremely high concentrations also resulted in the formation of red precipitates, which appeared to have an important role there. Small amplitude oscillations were reported in the bromate, bromide, and cerous or manganous ions systems operated in a CSTR, in which the inflow of reduced metal catalysts sustained the autocatalytic process and inflow of bromide ions would quench the autocatalytic cycle [23,24]. According to

the work by Beck and co-workers [22,25,26], ferriin could be reduced by bromide ions in the ferroin-bromate reaction. Therefore, the autocatalytic cycle can be sustained. A key of making the ferroin-bromate minimal oscillator oscillate in a closed system lies in the implementation of processes that can modulate bromide ions. In chapter 2, we have learned that 1,4-benzoquinone could be brominated, while it did not react with the metal catalyst ferriin [27,28]. Such a result inspires us to develop a new type of minimal bromate oscillator that can oscillate in a batch system.

In this chapter we investigated the nonlinear kinetics of ferroin-bromate-benzoquinone reaction in a closed system. As shown in the following, transient spontaneous oscillations were indeed observed when the concentration of benzoquinone was above a critical level. The increase of 1,4-benzoquinone concentration resulted in more oscillation peaks, while reducing the induction time. When this new minimal bromate oscillator was coupled to the bromine removal by nitrogen stream, the total number of peaks was increased further.

3.2 Experimental Procedure

All reactions were run in a thermal-jacketed 50mL glass reactor with the temperature maintained constant at $25.0 \pm 0.1^\circ\text{C}$ by a circulation water bath (ThermoNesLab RTE 7). The reaction was stirred by a magnetic stirrer (Fisher Isotemp) at around 600 rpm for all experiments. A Teflon cap was placed on top of the cylindrical reactor to hold electrodes. Volume of the reaction solution was fixed at 30.0 ml. Oscillatory profiles were monitored with a platinum electrode coupled with a $\text{Hg}|\text{Hg}_2\text{SO}_4|\text{K}_2\text{SO}_4$ reference electrode (Radiometer Analytical, XR200 and M231Pt-9). All measurements were recorded with a personal computer connected to the pH/potential meter (Radiometer PHM220) through a

PowerLab/4SP data logger. Because of the photosensitivity of benzoquinone, all reactions were run in a dark room.

Reaction mixtures were prepared from aqueous stock solutions of analytical-grade sodium bromate (NaBrO_3 , Aldrich, 99%), 1.0 M, and sulfuric acid (H_2SO_4 , Aldrich, 95-98%), 6.0 M. Ferroin stock solution (0.01 M) was prepared from a calculated amount of $\text{FeSO}_4 \cdot 7\text{H}_2\text{O}$ (Aldrich, 99+%) and 1,10-phenanthroline (Aldrich, 99+%). 1,4-Benzoquinone (Sigma-Aldrich, 98%) was directly dissolved in the reaction mixture. Mass spectrometric measurements were performed on a Varian CP-3800/Varian 1200L system, using a 15 m Varian CP-Sil 5CB column. All ^1H -NMR and ^{13}C -NMR studies were performed by Bruker Avance 500MHz spectrometer and with the same sample that was used for mass spectrometry studies, but dissolved in deuterated chloroform (Cambridge Isotope Laboratories, 99.8%). Cyclic voltammetry spectra were measured with VoltaLab 100 from Radiometer Analytical, in which a three-electrode cell was used.

3.3 Results and Discussion

Figure 3.1 presents two time series of the ferroin-bromate-benzoquinone reaction at different concentrations of benzoquinone: (a) 0.025 M, and (b) 0.035 M. Other reagents were $[\text{NaBrO}_3] = 0.05 \text{ M}$, $[\text{ferroin}] = 1.0 \times 10^{-4} \text{ M}$, and $[\text{H}_2\text{SO}_4] = 0.05 \text{ M}$. The reactor was tightly sealed with parafilm to prevent the loss of volatile species such as bromine. In the absence of benzoquinone this ferroin-bromate system did not exhibit any oscillatory behavior in the batch system, where only the autocatalytic oxidation of ferroin was observed after a long induction time. As shown in (a), however, the presence of benzoquinone led to the development of spontaneous oscillations in this closed system. NMR and Mass spectrometry measurements showed the formation of brominated

benzoquinone, suggesting that benzoquinone indeed interacted with bromine/HOBr to modulate bromide concentration. This chemical approach is similar to the physical means required in the Beck report, in which for ferroin to react with bromate alone in an oscillatory manner the continuous and partial removal of bromine and high concentrations of both reactants were necessary [22]. Under the conditions investigated here, no precipitate is formed.

Figure 3.1b indicates that when benzoquinone concentration was increased further, the number of oscillations also increased. Meanwhile, the induction time became slightly shorter. This observation implicates that the rate of bromine removal via its reaction with benzoquinone does not only have great impact on the number of peaks, but may also be responsible for the long induction time here. To examine whether the formation of brominated benzoquinone is responsible for the above observed long induction time, we have initially added some bromide into the reaction mixture to produce bromine and subsequently brominated benzoquinones, but no obviously change in the induction time was observed. Limited by the low solubility of benzoquinone, no higher benzoquinone concentration was tested in Figure 3.1. To shed light on the possible influence of 1,10-phenanthroline from ferroin complex, 3×10^{-4} M of 1,10-phenanthroline was added at the beginning of the reaction. As seen in time series (c), there is no change in the oscillatory behavior, suggesting that the substrate from metal catalyst is not responsible for the spontaneous oscillations.

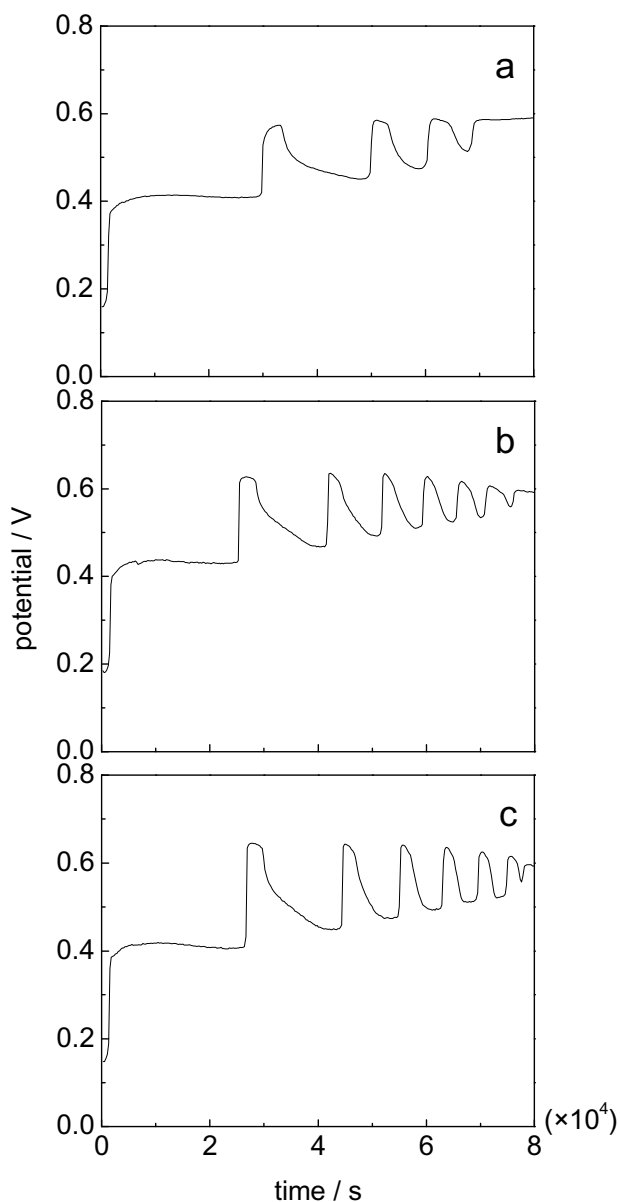


Figure 3.1 Time series of ferroin-bromate-benzoquinone reaction at different concentrations of benzoquinone (a) 0.025 M, (b) 0.035 M and (c) 0.035 M. In (c) 3.0×10^{-4} M of 1,10-phenanthroline was added initially. Other reaction conditions were $[\text{NaBrO}_3] = 0.05$ M, $[\text{ferroin}] = 1.0 \times 10^{-4}$ M, and $[\text{H}_2\text{SO}_4] = 0.05$ M. The reaction was carried out in a dark room while the reactor was sealed with parafilm.

To further examine the importance of bromine removal in this new minimal bromate oscillator, in Figure 3.2 nonlinear behaviour of the ferroin-bromate-benzoquinone reaction was investigated under different configurations of the reactor. In experiment (a),

volatile substances such as bromine molecules were prevented from migrating out of the reactor by sealing it with parafilm. There was about 1 cm space above the reaction solution, but the same result was achieved when the reaction solution volume was increased to fill up the reactor (i.e., no free space above the solution level). In experiment (b), nitrogen gas was flowed into the space above the reaction solution at a rate of 40 ml/min to bring out volatile species such as bromine with it. As a result, the number of spontaneous oscillations increased from 6 to 12. The induction time is nearly the same in both cases. Reactions conditions in Figure 3.2 are $[\text{NaBrO}_3] = 0.05 \text{ M}$, $[\text{ferroin}] = 1.0 \times 10^{-4} \text{ M}$, $[\text{Q}] = 0.035 \text{ M}$, and $[\text{H}_2\text{SO}_4] = 0.05 \text{ M}$.

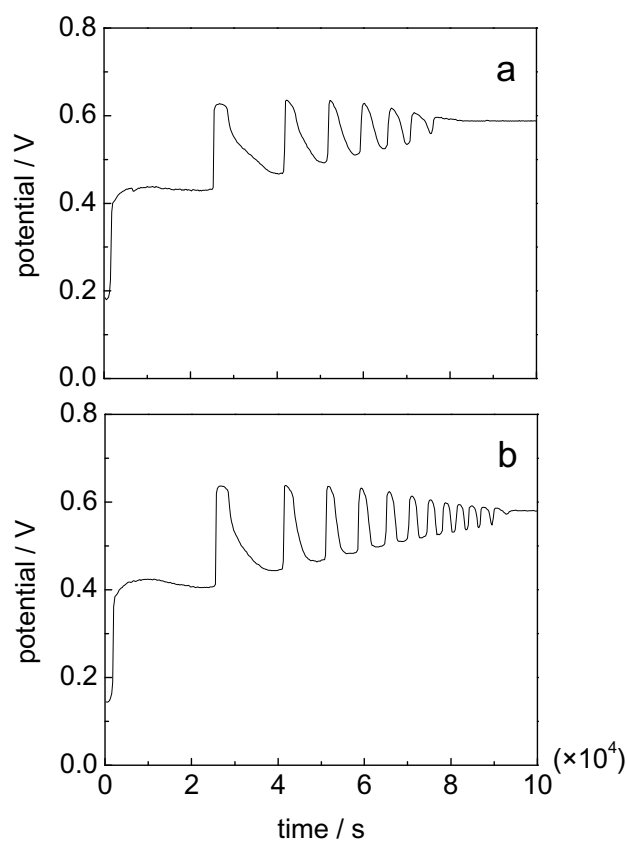


Figure 3.2 Time series of ferroin-bromate-benzoquinone reaction carried out at different configurations of the reactor: (a) closed, and (b) flowing nitrogen gas into the reactor (40 mL/min). Compositions of the reaction solution were $[\text{NaBrO}_3] = 0.05 \text{ M}$, $[\text{ferroin}] = 1.0 \times 10^{-4} \text{ M}$, $[\text{Q}] = 0.035 \text{ M}$, and $[\text{H}_2\text{SO}_4] = 0.05 \text{ M}$.

Additional experiments in Figure 3.3 indicate that the above observed influence of bromine removal by nitrogen stream depends on the concentration of benzoquinone. For example, when the same operation protocol was applied to the reaction containing 0.025 M benzoquinone, the number of oscillation peak remained at 3, but the induction time was decreased from 29,843 to 22,719 s.

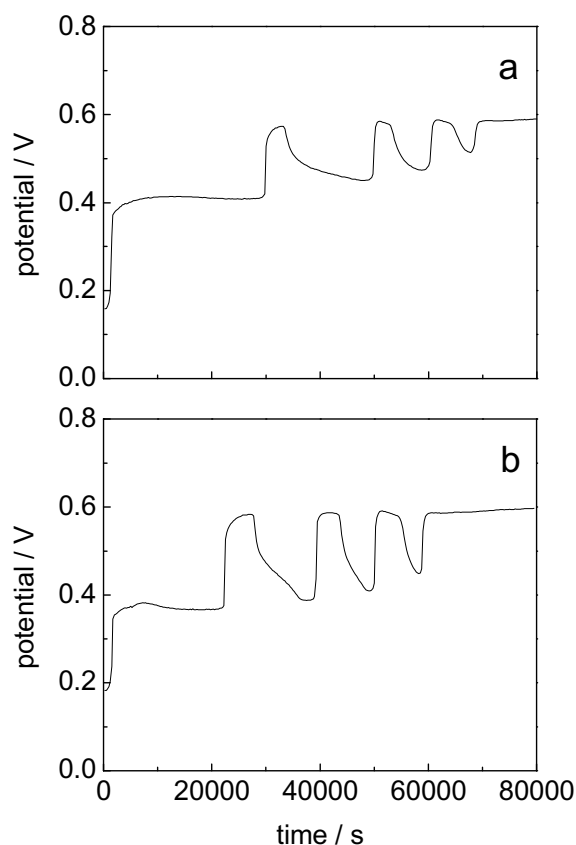


Figure 3.3 Time series of ferriin-bromate-benzoquinone reaction carried out at different configurations of the reactor: (a) closed, and (b) flowing nitrogen into the reactor (40 mL/min). Compositions of the reaction solution were $[\text{NaBrO}_3] = 0.05 \text{ M}$, $[\text{ferriin}] = 1.0 \times 10^{-4} \text{ M}$, $[\text{Q}] = 0.025 \text{ M}$, and $[\text{H}_2\text{SO}_4] = 0.05 \text{ M}$.

Figure 3.4 shows how the above observed chemical oscillations respond to bromide perturbation, in which the high Pt potential corresponds to the low bromide concentration. Upon the addition of $1.0 \times 10^{-4} \text{ M}$ bromide, the Pt potential shifted immediately to a low

value and stayed there for several hours. The “permanent” quenching suggests that the amount of bromide added is excess and the corresponding product bromine cannot be consumed fast enough to allow oscillation revival. In Figure 3.4, adding 1.0×10^{-5} M bromide at the top of the peak shifted the system to a low potential, but the regular oscillation restored after a small amplitude, low frequency oscillation. When the same magnitude bromide perturbation was applied at the opposite phase, there was no obvious decrease in the Pt potential as bromide concentration was already high at such a phase. After the perturbation, the system evolved gradually through a low frequency oscillation, followed by regular transient oscillations. This result demonstrates that this ferroin-bromate-benzoquinone system is still bromide-controlled. The bromide concentration of the unstable focus is on the order of 10^{-5} M.

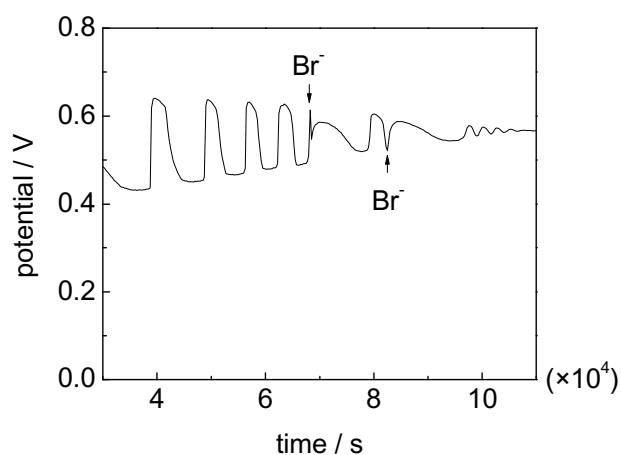


Figure 3.4 Responses of the oscillation to bromide perturbation. Each time 0.015 mL concentrated bromide was added, resulting 1.0×10^{-5} M bromide after the dilution. Compositions of the reaction solution were $[\text{NaBrO}_3] = 0.05$ M, $[\text{ferroin}] = 1.0 \times 10^{-4}$ M, $[\text{Q}] = 0.03$ M, and $[\text{H}_2\text{SO}_4] = 0.05$ M. To achieve a large number of peaks, nitrogen flow was applied here at a rate of 40 mL/min.

The acid concentration used in this research is 0.05 M, which is much lower than the acid concentration used in existing studies of bromate-based oscillations. Indeed, we are not aware of any report on the bromate-based chemical oscillations under such a low acid concentration. To gain insight into the need of low acid concentration here, Figure 3.5a characterized the influence of benzoquinone on the redox potential of ferriin/ferroin. The cyclic voltammetry spectra in (a) show that the oxidation wave of ferroin shifted to a less positive potential upon the presence of benzoquinone, making the autocatalytic oxidation of ferroin by bromine dioxide radicals easier. This may be the reason that the spontaneous oscillations could still be achieved at such a low acidic condition. During the above measurements it was observed that the addition of benzoquinone into ferriin solution causes the appearance of greenish color, which implicates that benzoquinone might have partially replaced 1,10-phenanthroline. Similar color has also been seen in the ferroin-bromate-CHD reaction, in which benzoquinone is a final product [29-31]. The possible partial complexation of benzoquinone with ferriin might have also played an important role in the ferroin-bromate-CHD system.

Figure 3.5b presents the ^1H NMR spectrum recorded in the CDCl_3 solution obtained from the reaction presented in Figure 3.2a. The solution was extracted after the disappearance of these spontaneous oscillations. The ^1H NMR spectral resonance appearing at $\delta = 7.30$ (d, $J = 3.5$ Hz), 6.93 (d, $J = 10.5$ Hz) and 6.83 (dd, $J = 10.5, 3.5$ Hz) were observed, corresponding to the product 2-bromo-1,4-benzoquinone (BrQ) [32]. The production of BrQ was further confirmed with GC/Ms measurement. The ^1H NMR spectrum obtained from the reaction between 1,4-benzoquinone and bromine is almost

identical to the one presented in Figure 3.5b, suggesting the bromination of benzoquinone by bromine or HOBr.

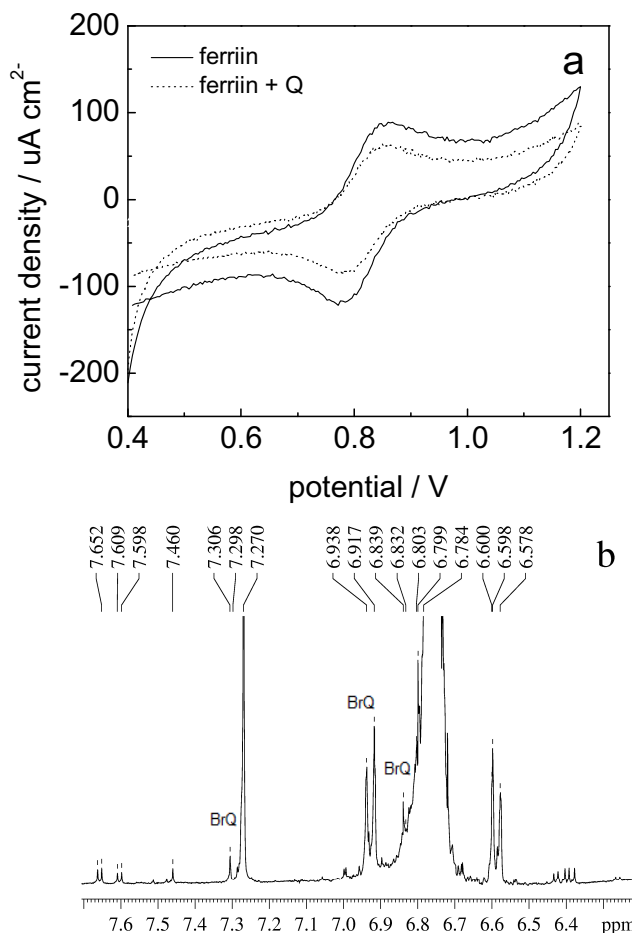
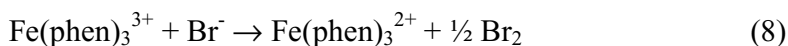
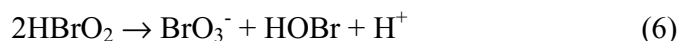
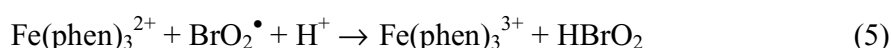
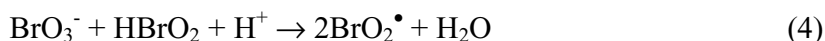
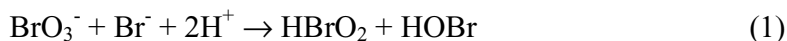


Figure 3.5 (a) Cyclic voltammetry showing the influence of benzoquinone on the redox potential of ferriin/ferroin. The scanning rate is 100 mV/s. The supporting electrolyte is 1 M KNO₃, [ferroin] = 0.0025 M, [Q] = 0.03 M, and [H₂SO₄] = 0.1 M. (b) ¹H NMR (500MHz) spectrum from the reaction carried out in Figure 3.2a 2-bromo-1,4-benzoquinone: δ = 7.30 (d, J = 3.5 Hz), 6.93 (d, J = 10.5 Hz), 6.83 (dd, J = 10.5, 3.5 Hz)

3.4 Conclusions

In this chapter a new type of minimal bromate oscillator is developed, which is capable of generating spontaneous chemical oscillations in a closed system. In comparison to the earlier study of the ferroin-bromate reaction [22], the bromination of benzoquinone by

bromine/HOBr is a function of bromide concentration. The rest reaction mechanism of this ferroin-bromate-benzoquinone system is expected to remain the same as that proposed for the ferroin-bromate reaction [25,26], listed in the following:



Different from the BZ-type oscillators, here the organic substrate benzoquinone does not react with the oxidized metal catalyst ferriin. The regeneration of ferroin must therefore come from other paths, as it is crucial in sustaining the autocatalytic cycles ((4) + (5)). Beck and co-workers have suggested earlier the reduction of ferriin by bromide ions (step (8)). The occurrence of process (8) was confirmed in this study under the conditions employed above.

The success of achieving spontaneous oscillations in the closed ferroin-bromate-benzoquinone system highlights that reaction step (8) can become critical in the bromate-based chemical oscillators. Considering that ferriin, bromate and benzoquinone all exist in the ferroin-bromate-CHD reaction [29-31], the reduction of ferriin by bromide may provide an explanation for the merging of propagating pulses seen in the ferroin-bromate-CHD system [33], in which the tail of the preceding pulse has high concentration of

bromide that may interact with the front of the following pulse that has high concentration of ferriin.

3.5 References

- 1 A. M. Zhabotinsky, *Biofizika*, 1964, 9, 306.
- 2 R. J. Field and M. Burger, Eds. *Oscillations and Traveling Waves in Chemical Systems*, Wiley-Interscience, New York, 1985.
- 3 S. K. Scott, *Oscillations, Waves and Chaos in Chemical Kinetics*, Oxford University Press Inc, New York, 1994.
- 4 Z. Noszticzius and J. Bodiss, *J. Am. Chem. Soc.*, 1979, 101, 3177.
- 5 K. Showalter, R.M. Noyes and K. Bar-Eli, *J. Chem. Phys.*, 1978, 69, 2514.
- 6 M. Orbán and E. Körös, *J. Phys. Chem.*, 1978, 82, 1672.
- 7 Z. Noszticzius, P. Stirling and M. Wittmann, *J. Phys. Chem.*, 1985, 89, 4914.
- 8 M. T. Beck and Z. B. Varadi, *React. Kinet. Catal. Lett.*, 1977, 6, 275.
- 9 L. Adamcikova, D. Misticak and P. Sevcik, *React. Kinet. Catal. Lett.*, 2005, 85, 215.
- 10 V. J. Farage and D. Janjic, *Chem. Phys. Lett.*, 1982, 88, 301.
- 11 E. Körös, M. Orbán and I. Habon, *J. Phys. Chem.*, 1980, 84, 559.
- 12 R. P. Rastogi, P. Chand, M. K. Pandey and M. Das, *J. Phys. Chem. A*, 2005, 109, 4562.
- 13 J. A. Pojman, D. C. Leard and W. West, *J. Am. Chem. Soc.*, 1992, 114, 8298.
- 14 L. Treindl, T. Matsumura-Inoue and P. Ruoff, *J. Phys. Chem. A*, 2002, 106, 5271.
- 15 H. -D. Försterling, S. Murányi and Z. Noszticzius, *J. Phys. Chem.*, 1990, 94, 2915.
- 16 E. J. Heilweil, M. J. Henchman and I. R. Epstein, *J. Am. Chem. Soc.*, 1979, 101, 3698.

- 17 L. F. Salter and J. G. Sheppard, *Int. J. Chem. Kinet.*, 1982, 14, 815.
- 18 P. K. Srivastava, Y. Mori and I. Hanazaki, *J. Phys. Chem.*, 1991, 95, 1636.
- 19 L. Adamčíková, Z. Farbulová and P. Ševčík, *New J. Chem.*, 2001, 25, 487.
- 20 R. J. Field, E. Körös and R. M. Noyes, *J. Am. Chem. Soc.*, 1972, 94, 8649.
- 21 P. Herbine and R. J. Field, *J. Phys. Chem.*, 1980, 84, 1330.
- 22 M. T. Beck, G. Bazsa, K. Hauck and Ber. Bunsenges. *Phys. Chem.*, 1980, 84, 408.
- 23 M. Orban, P. De Kepper and I. R. Epstein, *J. Am. Chem. Soc.*, 1982, 104, 2657.
- 24 W. Geiseler *J. Phys. Chem.*, 1982, 86, 4394.
- 25 V. Gaspar, G. Bazsa and M. T. Beck, *J. Phys. Chem.*, 1985, 89, 5495.
- 26 S. Keki, I. Magyar, M. T. Beck and V. Gaspar, *J. Phys. Chem.*, 1992, 96, 1725.
- 27 B. Zhao and J. Wang, *Chem. Phys. Lett.*, 2006, 430, 41.
- 28 N. Li, J. R. Green and J. Wang, *Chem. Phys. Lett.*, 2007, 447, 241.
- 29 D. S. Huh, H. S. Kim, J. K. Kang, Y. J. Kim, D. H. Kim, S. H. Park, K. Yadav and J. Wang, *Chem. Phys. Lett.*, 2003, 378, 78.
- 30 I. Szalai, K. Kurin-Csörgei, I. R. Epstein and M. Orbán, *J. Phys. Chem. A*, 2003, 107, 10074.
- 31 I. Szalai, K. Kurin-Csörgei and M. Orbán, *Phys. Chem. Chem. Phys.*, 2002, 4, 1271.
- 32 J. Feng, G. R. Green, S. Johnson and J. Wang, *J. Phys. Org. Chem.*, 2011, 24, 507.
- 33 C. T. Hamik, N. Manz, and O. Steinbock, *J. Phys. Chem., A*, 2001, 105, 6144.

Chapter 4: Subtle Photochemical Behavior in the Ferroin-Bromate-Benzoquinone Reaction

4.1 Introduction

As an effort of constructing chemical oscillators with a minimal number of constituents, bromate-bromide-metal catalyst reactions have attracted a great deal of attention, [1-4]. Geislar reported that in a CSTR the bromate-bromide-manganese (II) system could exhibit sustained oscillations and steady state multiplicity [1]. Orban and co-workers obtained a narrow oscillatory region in a flow reactor using cerium or manganous ions to react with bromate and have referred those systems as the minimal bromate oscillators (MBO) [2]. Later, Dutt and co-workers investigated the effect of stirring and mixing modes in the bromate-bromide-cerium (III) reaction [4]. However, for the lack of necessary sources to modulate the regeneration of bromide ions, which took place through the bromination of organic substrates in regular bromate oscillators [5-12], existing minimal bromate oscillators could only function in a CSTR. In chapter 3 we demonstrated the feasibility of introducing an organic substrate into a MBO system to manifest bromide production, but do not reduce the oxidized metal catalyst ferroin [13]. This is the distinction from other ferroin-bromate-substrate oscillators, in which one of the main roles of the substrate is to reduce the oxidized metal catalysts. The newly developed MBO oscillator was able to exhibit spontaneous oscillations in a batch reactor [13].

The unique kinetic role of benzoquinone (Q) and its known photochemical property motivated us to explore the importance of photo perturbation in this batch MBO system. Illuminating benzoquinone solution has been known to potentially induce the photoreduction of benzoquinone, leading to the production of hydroquinone [14], a substance that reacts with bromine dioxide radicals to form an autocatalytic cycle in bromate oscillators [15,16]. As a result, the illuminated batch MBO may become a system consisting of two sub-oscillators and potentially exhibit new complex oscillations [17]. So far, the bromate-benzoquinone oscillations could only be observed under very intense illumination and required very high acid concentrations in comparison to the acid used in the ferriin-bromate-benzoquinone system studied in chapter 3 [18,19].

The study of perturbed nonlinear dynamics has attracted increasing attention in the last two decades due to their ubiquitous existence in nature. Photochemical oscillators provide a convenient way of investigating the interactions between intrinsic dynamics and external forcing of various modes [20-30]. The photosensitivity of bromate-based oscillators seems to always involve the production of bromide ions [31-33]. In this batch MBO system, notably, bromide ions have two conflict dynamic roles: one is to reduce ferriin to support the autocatalytic cycle. The second role is to react with HBrO_2 , which quenches the autocatalytic feedback. As such, light in this batch-MBO system may potentially modulate a variable that has dual functions and thus inserts more intriguing effects. As shown in the following, spontaneous oscillations in the ferriin-bromate-benzoquinone reaction did exhibit subtle response to light, in addition to the extremely high photosensitivity.

4.2 Experimental Procedure

All reactions were run in a thermal-jacketed 50mL glass reactor with the temperature maintained constant at $25.0 \pm 0.1^\circ\text{C}$ by a circulation water bath (ThermoNesLab RTE 7). The reaction was stirred by a magnetic stirrer (Fisher Isotemp) at around 600 rpm for all experiments. A non-transparent Teflon cap was placed on top of the cylindrical reactor to hold electrodes. Volume of the reaction solution was fixed at 30.0 ml. Oscillatory profiles were monitored with a platinum or bromide ion selective electrode coupled with a $\text{Hg} \mid \text{Hg}_2\text{SO}_4 \mid \text{K}_2\text{SO}_4$ reference electrode (Radiometer Analytical, XR200 and M231Pt-9). All measurements were recorded with a personal computer connected to a pH/potential meter (Radiometer PHM220) through a PowerLab/4SP data logger. Except otherwise stated, all reactions were conducted under room lighting and the controlled light perturbation was implemented with a 150 W halogen light source (Fisher Scientific, Model DLS-100HD). Narrow band filters (Melles Griot) with different wavelength range were placed in front of the light source. Light intensity was measured with an optical photometer from Newport (model 1815-C).

Reaction mixtures were prepared from aqueous stock solutions of analytical-grade sodium bromate (NaBrO_3 , Aldrich, 99%), 1.0 M, and sulfuric acid (H_2SO_4 , Aldrich, 95-98%), 6.0 M. Ferroin stock solution (0.01 M) was prepared from a calculated amount of $\text{FeSO}_4 \cdot 7\text{H}_2\text{O}$ (Aldrich, 99+%) and 1,10-phenanthroline (Aldrich, 99+%). Benzoquinone (Sigma-Aldrich, 98%) was directly dissolved in the reaction mixture. Mass spectrometric measurements were performed on a Varian CP-3800/Varian 1200L system, using a 15 m Varian CP-Sil 5CB column. All ^1H -NMR and ^{13}C -NMR studies were performed by Bruker Avance 500MHz spectrometer and with the same sample that was used for mass

spectrometry studies, but dissolved in deuterated chloroform (Cambridge Isotope Laboratories, 99.8%). UV/Vis spectroscopy was obtained with a spectrophotometer from Ocean Optics (USB 2000).

4.3 Results and Discussion

Figure 4.1 presents two time series of the ferroin-bromate-benzoquinone reaction performed (a) in a dark room, and (b) under room light. Before passing through two glass-wall of the reactor and a layer of circulating water the intensity of the room light was measured to be about $20 \mu\text{W}/\text{cm}^2$. Other reaction conditions were $[\text{NaBrO}_3] = 0.05 \text{ M}$, $[\text{ferroin}] = 1.0 \times 10^{-4} \text{ M}$, $[\text{Q}] = 0.035 \text{ M}$, and $[\text{H}_2\text{SO}_4] = 0.05 \text{ M}$. The reactor was sealed with parafilm to prevent the loss of volatile species such as bromine. As shown in (a), in the absence of light spontaneous oscillations appeared after an extremely long induction time ($2.5 \times 10^4 \text{ s}$). There were 6 oscillation peaks in total. The spontaneous oscillation stopped at a high Pt potential, which corresponded to an oxidation steady state with a low bromide concentration and high concentration of ferroin. Under the room light illumination, the oscillatory behaviour in Figure 4.1(b) emerged much earlier, in less than $1.5 \times 10^4 \text{ s}$ from the beginning of the reaction. Notably, the total number of oscillations as well as the oscillation frequency was significantly increased. Since the unilluminated system eventually evolved to an oxidation state where the autocatalytic feedbacks dominate, the observed constructive photo influence was more likely arising from the improved production of inhibitor that suppressed the autocatalytic cycle [34,35].

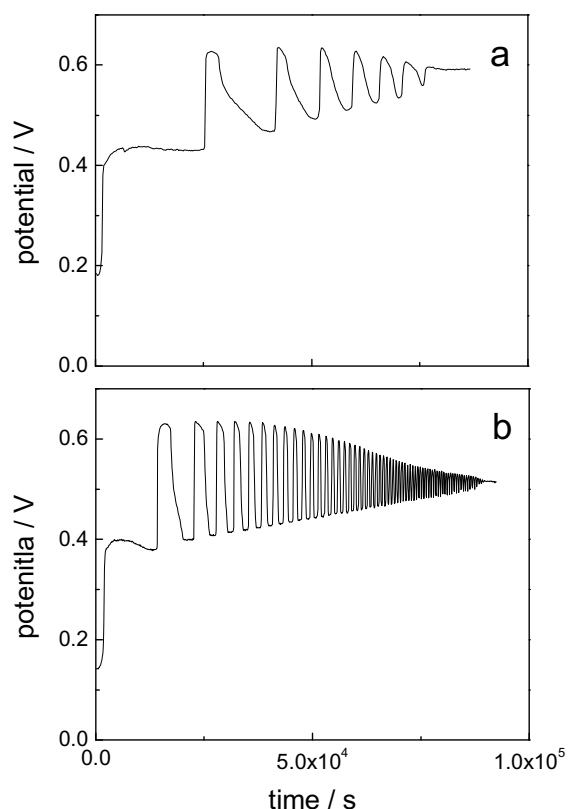


Figure 4.1 Time series of ferroin-bromate-benzoquinone reaction carried out (a) in a dark room, and (b) with the room light on ($I = 20 \mu\text{W}/\text{cm}^2$). Other reaction conditions were $[\text{NaBrO}_3] = 0.05 \text{ M}$, $[\text{ferroin}] = 1.0 \times 10^{-4} \text{ M}$, $[\text{H}_2\text{SO}_4] = 0.05 \text{ M}$, and $[\text{Q}] = 0.035 \text{ M}$.

Figure 4.2a shows a ^1H NMR spectrum recorded in a sample that was obtained from the reaction carried out at $[\text{NaBrO}_3] = 0.05 \text{ M}$, $[\text{ferroin}] = 1.0 \times 10^{-4} \text{ M}$, $[\text{H}_2\text{SO}_4] = 0.05 \text{ M}$ and $[\text{Q}] = 0.035 \text{ M}$. The applied illumination was $15 \mu\text{W}/\text{cm}^2$ within the wavelength between $500 \pm 40 \text{ nm}$. The selection of $500 \pm 40 \text{ nm}$ wavelength range was based on the result listed in Figure 4.3a. The reaction solution was extracted shortly after the disappearance of those spontaneous oscillations. The ^1H -NMR spectral resonance appearing at $\delta = 6.96$ and 7.13 indicates that 2,3-dibromohydroquinone and 2,5-dibromohydroquinone (Br_2HQ) are produced in the illuminated system [36]. The production of dibromohydroquinones was further confirmed by mass spectrometry.

Comparing with the results that monobrominated benzoquinones were the major products in the unilluminated system, spectrum in Figure 4.2a suggests that the bromination of benzoquinone was enhanced by the incident light. Since benzoquinones do not have strong absorption within 500 ± 40 nm, but bromine does, the photochemical process is likely through the reaction of photo-excited bromine with benzoquinone or with monobromobenzoquinone. An important question remained to be resolved is whether the above process was accompanied by bromide production. Perturbation experiments with a pulse-light were compared with bromide perturbation in Figure 4.3.

Figure 4.2b shows two time series of ferriin and bromide reaction measured with UV/Vis spectrophotometer at 510 nm. The reaction 1 was conducted under the illumination of 30 mW/cm^2 white light from a halogen light source, whereas reaction 2 was in the absence of illumination except the light beam from the spectrophotometer. Ferriin was obtained by mixing 3.0×10^{-4} M ferriin with 3.0×10^{-4} M Ce^{4+} in a 0.05 M sulfuric acid solution. After 60 minutes, 0.05 M sodium bromide was added into the cuvette. The two time series illustrate that the reduction of ferriin by bromide was accelerated by light. The increased supply of ferriin, which reacts with bromine dioxide radicals, shall have constructive influence on the autocatalytic cycle. However, if the nonlinear dynamics is already dominated by autocatalytic feedback, such as the case in Figure 4.1a, enhancement of the autocatalytic cycle would insert negative impact on the emergence of spontaneous oscillations.

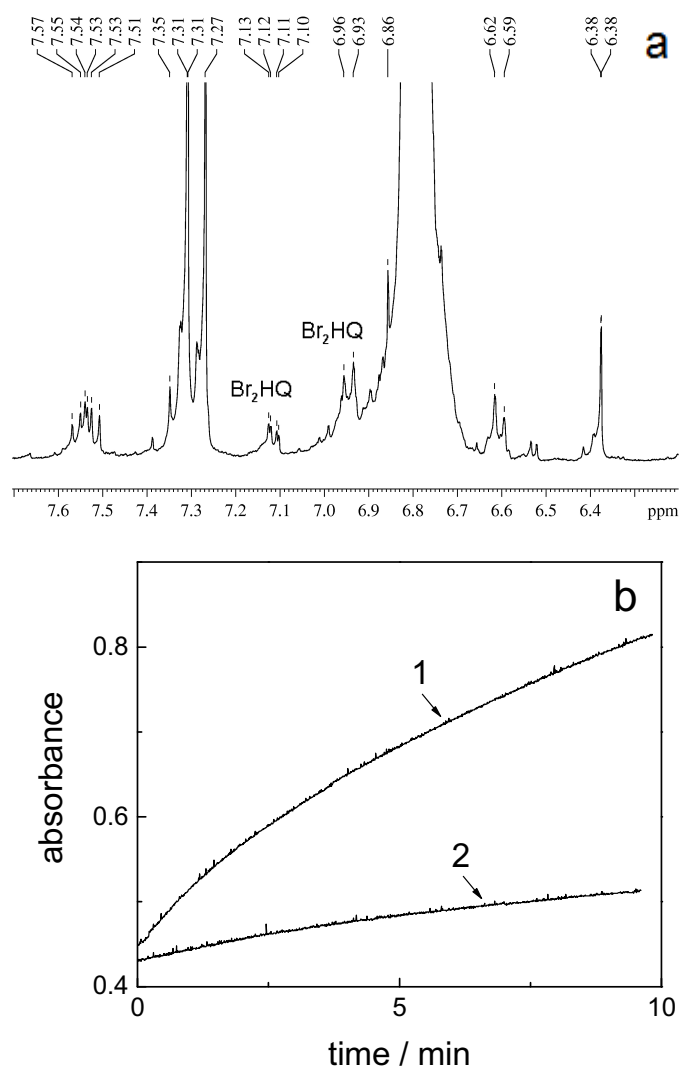


Figure 4.2 (a) ^1H NMR spectrum of an illuminated MBO reaction; (b) Time series of ferriin and bromide reaction collected at 510 nm, where the reaction (1) was illuminated with a $30 \text{ mW}/\text{cm}^2$ white light and reaction (2) was unilluminated.

Figure 4.3a examines the dependence of photosensitivity on the wavelength of incident light. The experiments were performed by placing a narrow band filter between the reactor and a 150 W halogen light source. Each illumination lasted for 5 s. Other reaction

conditions were the same as those used in Figure 4.1b. This result demonstrates that illumination with 700 ± 40 nm light did not cause any change, whereas the strongest response was seen with the incident light of 500 ± 40 nm. A similar trend was seen when the illumination was applied throughout the reaction process, where the oscillatory behavior including the induction time remained the same when the system was illuminated with 700 ± 40 nm light. On the other hand, spontaneous oscillations were quenched when the system was illuminated with light of 500 ± 40 nm or 400 ± 10 nm. No influence was observed either, when a narrow band filter of 260 ± 20 nm was used, which was likely because the halogen light source did not emit much light within such a UV range. The later result suggests that photo-reduction of benzoquinone does not play an important role in the ultra high photosensitivity reported here.

Figure 4.3b presents phase dependence of a bromide perturbation. The reaction was followed by bromide ion selective electrode. Other reaction conditions were the same as those used in Figure 4.1b. The bromide concentration decreased gradually in time, as its concentration reached the bottom of an oscillation peak there was a rapid color change from red to blue. After evolving around the low concentration for a while, bromide concentration underwent a phase of rapid increase, and during such a process the solution color gradually changed from blue to red. A large bromide perturbation at the top of the peak required a very long time to recover and the sharp increase did not occur until bromide concentration has reached the bottom first, which was around $[\text{Br}^-] = 10^{-7}$ M. When the perturbation was applied at a descending phase, after a brief increase due to the addition of bromide, the bromide concentration continued its decrease. When the same magnitude perturbation was applied at the bottom of a peak, the system moved into the

ascending phase right away. Perturbations 3 and 4 in this plot illustrate that the amplitude of the revival peak depends on the amount of bromide added.

Figure 4.3c shows how the spontaneous oscillations responded to a pulse light perturbation ($\lambda = 500 \pm 40$ nm, $\Delta t = 5$ s, intensity = 20 mW/cm²). The Pt potential shifted immediately to a low value when the perturbation was applied at the top, bottom or a declining phase of the Pt potential peak. However, there was barely any change when the same light pulse was applied at the middle of an ascending phase, where the Pt potential continued its increases and then developed into an oscillation of larger amplitude and lower frequency. Detailed examination indicates that there was indeed a tiny drop in the Pt potential when the light perturbation was applied. Characterization with bromide selective electrode indicates that a low Pt potential corresponds to a high bromide concentration. The phenomenon that following a pulse illumination Pt potential always shifts toward a lower value suggests the occurrence of light-induced bromide production. It might take place through reactions $Q + Br_2^* \rightarrow BrQ + Br^-$ or $BrQ + Br_2^* \rightarrow Br_2HQ + Br^-$, where Br_2^* denotes photo-excited bromine molecules, and BrQ represents monobrominated benzoquinones.

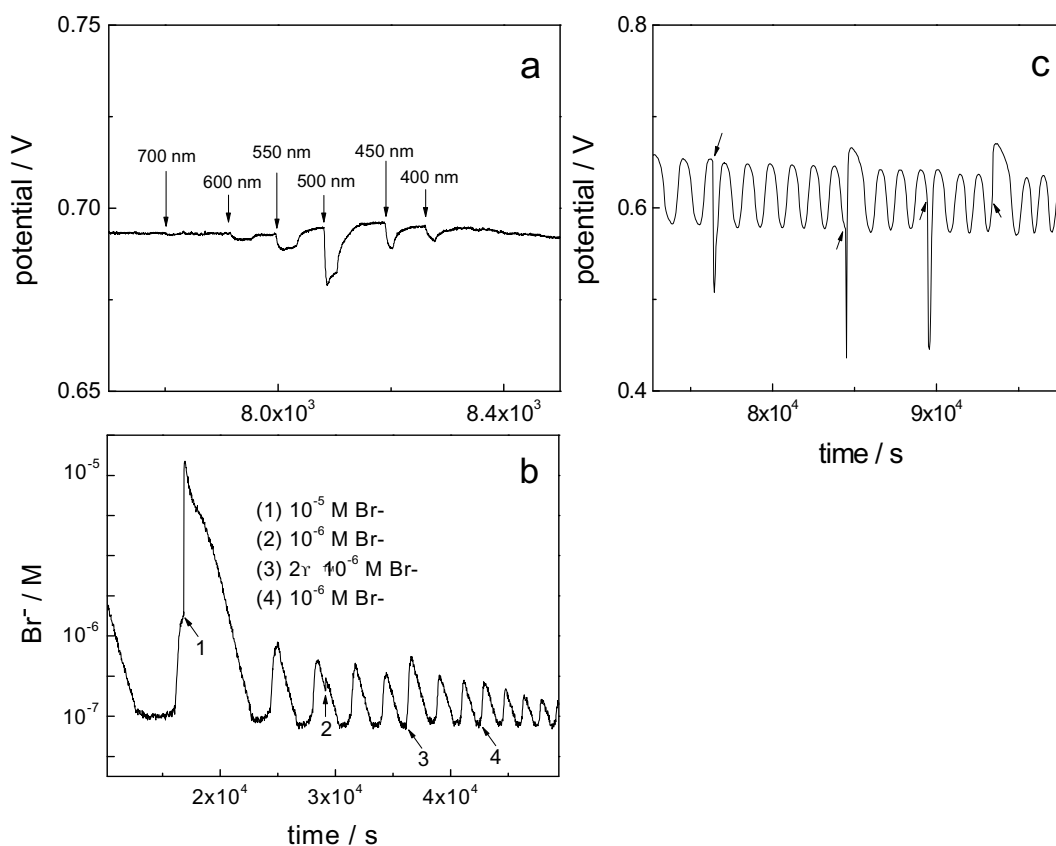


Figure 4.3 Response of ferroin-bromate-benzoquinone reaction to perturbation of (a) 5 s light pulse of different wavelengths, (b) bromide ions, and (c) 5 s light pulse of $\lambda = 500 \pm 40$ nm and $I = 20$ mW/cm². Other reaction conditions were the same as those used in Figure 4.1b.

Figure 4.4 presents three time series of the ferroin-bromate-benzoquinone reaction under the constant illumination of 500 ± 40 nm light: (a) $4 \mu\text{W}/\text{cm}^2$, (b) $15 \mu\text{W}/\text{cm}^2$, and (c) $46 \mu\text{W}/\text{cm}^2$. Other reaction conditions were the same as those used in Figure 4.1a. This series of experiments illustrate that low intensity light, e.g., $4 \mu\text{W}/\text{cm}^2$, shortened the induction time and increased the number of oscillation peak, exhibiting constructive influence on the oscillatory behavior. When the light intensity was increased to $46 \mu\text{W}/\text{cm}^2$, however, spontaneous oscillations were quenched. Note that the attained non-

oscillatory state has a high Pt potential value, which corresponds to a state of low Br^- concentration and high ferriin concentration (i.e., an oxidation steady state), implicating that the autocatalytic feedback overwhelms the production of inhibitor.

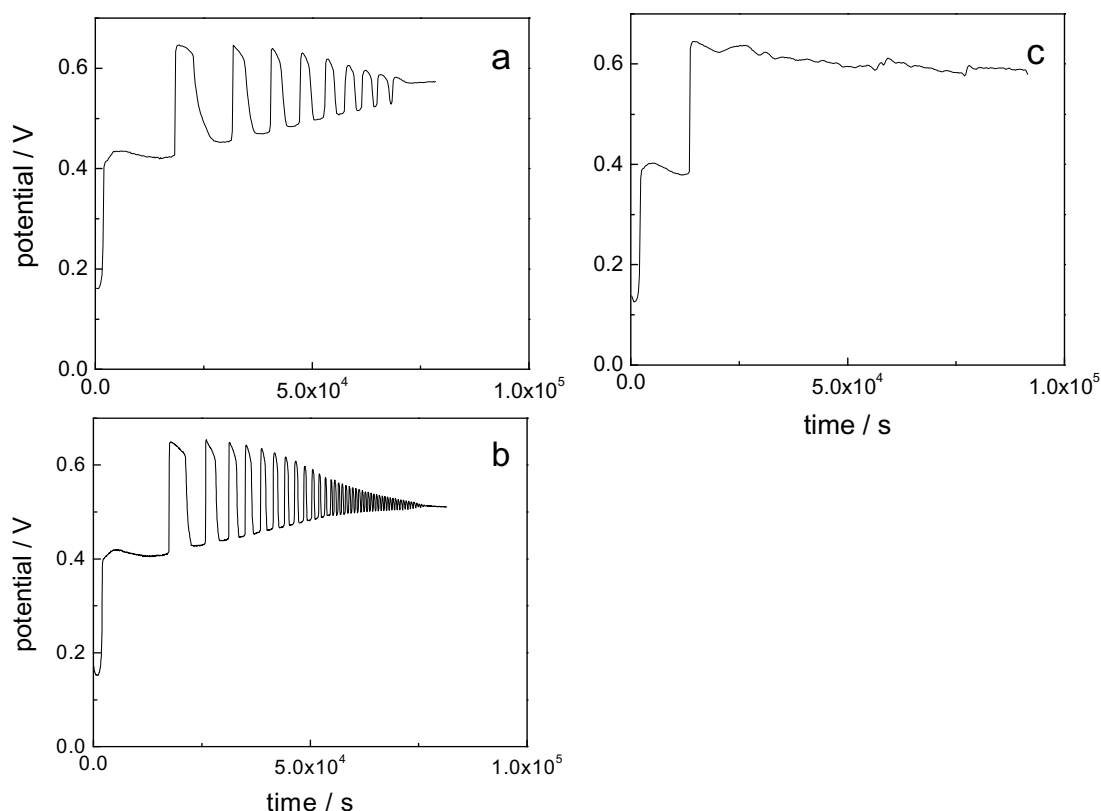
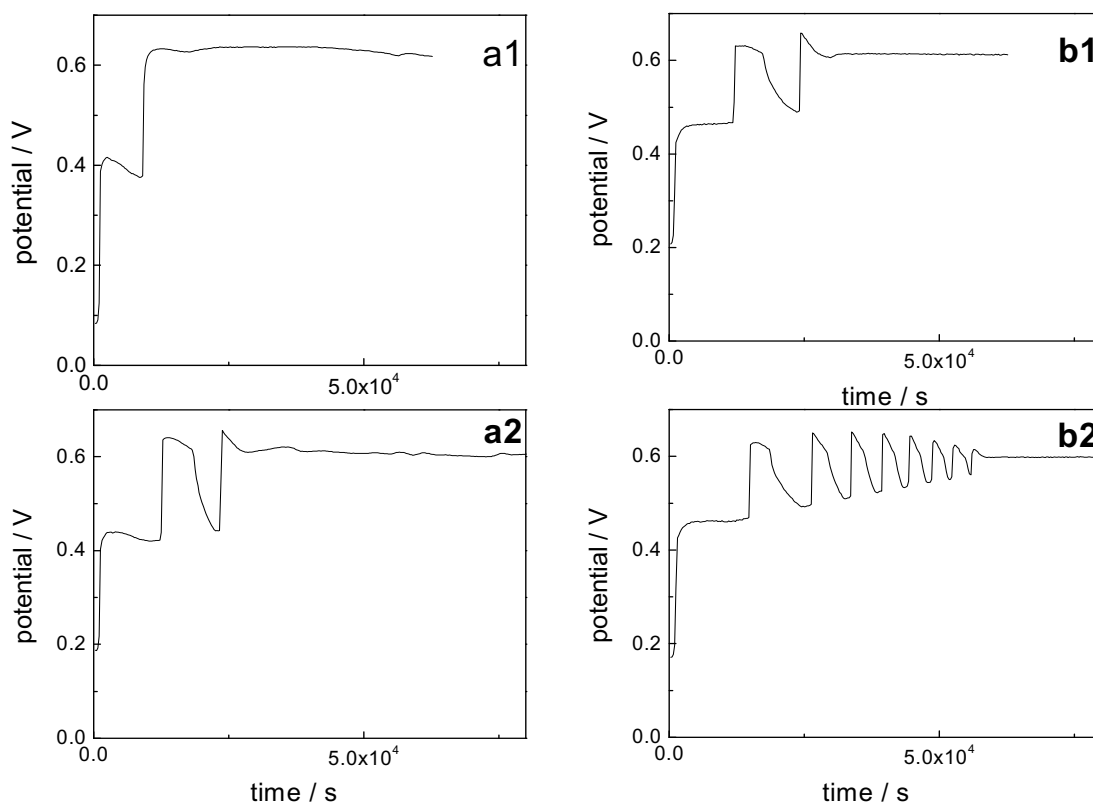


Figure 4.4 Time series of ferriin-bromate-benzoquinone reaction illuminated with light of different intensities: (a) $4 \mu\text{W}/\text{cm}^2$, (b) $15 \mu\text{W}/\text{cm}^2$, and (c) $46 \mu\text{W}/\text{cm}^2$. Other reaction conditions were the same as those used in Figure 4.1a.

Figure 5 presents time series of the ferriin-bromate-benzoquinone reaction at different concentrations of H_2SO_4 : (a1, b1) 0.08 M, (a2, b2) 0.07 M, (a3, b3) 0.05 M, and (a4, b4) 0.03 M. The (a) series of reactions were carried out under the illumination of 500 ± 40 nm light with an intensity of $15 \mu\text{W}/\text{cm}^2$, whereas reactions in the (b) series were unilluminated. These experiments indicate that for the unilluminated system spontaneous

oscillations could only be observed for the H_2SO_4 concentration within 0.03 and 0.09 M. This acid condition is significantly lower than the concentration used commonly in the reported bromate-oscillators and in the bromate-hydroquinone photochemical oscillator [18,19]. Spontaneous oscillations were quenched in (a1), indicating that light has negative impact on the nonlinear behavior. As the acid concentration was decreased, which consequently weakened the autocatalytic feedback via $\text{BrO}_3^- + \text{HBrO}_2 + \text{H}^+ \rightleftharpoons 2\text{BrO}_2 + \text{H}_2\text{O}$ and $\text{ferriin} + \text{BrO}_2 + \text{H}^+ \rightarrow \text{ferriin} + \text{HBrO}_2$, the same light illumination only partially quenched the oscillatory behavior (comparing a2 and b2). As the acid concentration was decreased gradually, the influence of light became negligible. Later, constructive influences took place in (a3) and (a4) as a result of further decreasing H_2SO_4 concentration.



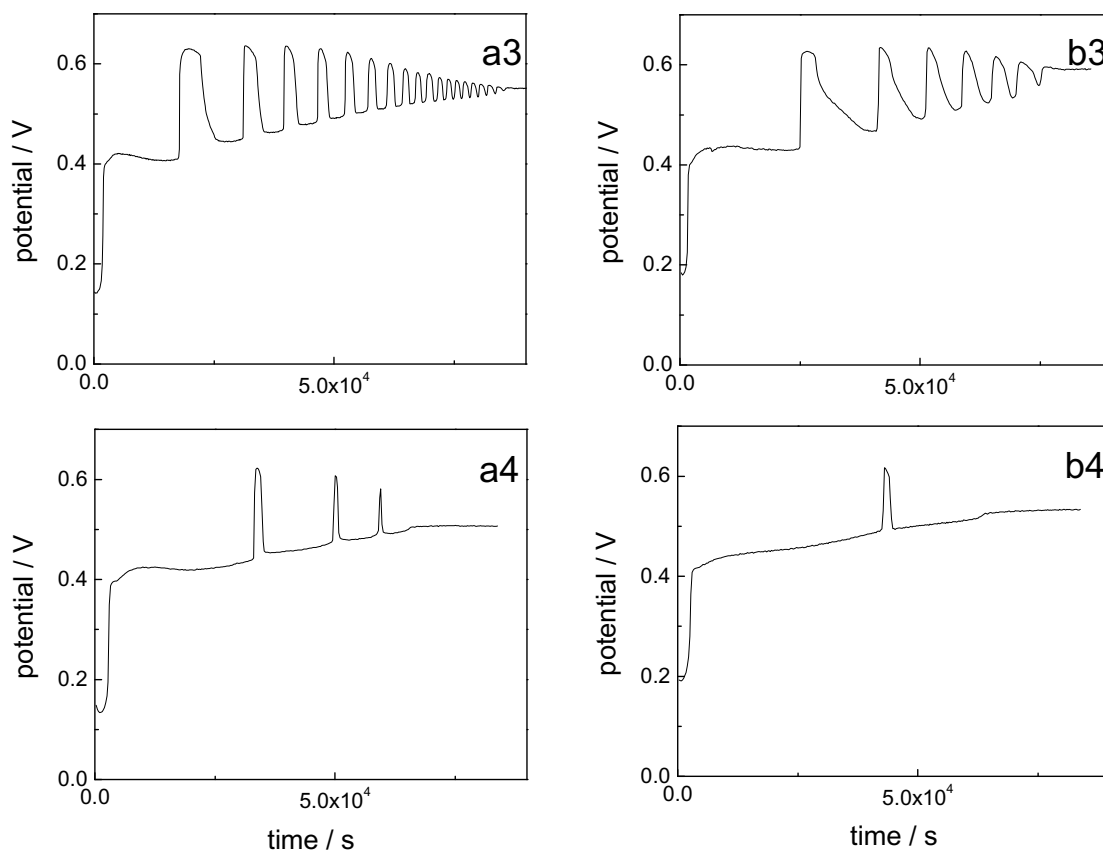


Figure 4.5 Time series of ferriin-bromate-benzoquinone reaction at different sulfuric acid concentrations: (a1, b1) 0.08 M, (a2, b2) 0.07 M, (a3, b3) 0.05 M, and (a4, b4) 0.03 M. Reactions (a1) to (a4) were illuminated with 500 ± 40 nm light of $15 \mu\text{W}/\text{cm}^2$. Reactions (b1) to (b4) were carried out in a dark room. Other conditions were $[\text{NaBrO}_3] = 0.05$ M, $[\text{ferriin}] = 1.0 \times 10^{-4}$ M, and $[\text{Q}] = 0.035$ M.

Theoretical simulations were carried out with a modified FKN model [10], by adding R9, R11, and R12 in Table 4.1. Basic elements of the model are: (R1-R3, R11) the consumption of control intermediate Br^- and (R4-R8) autocatalysis. Reactions R9 and R12 proposed here regulate Br^- variation and their rates are influenced by light. R10 is the initiation of the total reactions. Table 4.2 listed the rate constants used in this study. Most of these were taken from literature [10].

Table 4.1: Model proposed for the ferroin-bromate-Q oscillator

Reactions	
R1	$\text{Br}^- + \text{HOBr} + \text{H}^+ \rightleftharpoons \text{Br}_2 + \text{H}_2\text{O}$
R2	$\text{Br}^- + \text{HBrO}_2 + \text{H}^+ \rightleftharpoons 2\text{HOBr}$
R3	$\text{Br}^- + \text{BrO}_3^- + 2\text{H}^+ \rightleftharpoons \text{HOBr} + \text{HBrO}_2$
R4	$\text{HBrO}_2 + \text{H}^+ \rightleftharpoons \text{H}_2\text{BrO}_2^+$
R5	$\text{HBrO}_2 + \text{H}_2\text{BrO}_2^+ \rightarrow \text{BrO}_3^- + \text{HOBr} + 2\text{H}^+$
R6	$\text{HBrO}_2 + \text{BrO}_3^- + \text{H}^+ \rightleftharpoons \text{Br}_2\text{O}_4 + \text{H}_2\text{O}$
R7	$\text{Br}_2\text{O}_4 \rightleftharpoons 2\text{BrO}_2^\bullet$
R8	$[\text{Fe}(\text{phen})_3]^{2+} + \text{BrO}_2^\bullet + \text{H}^+ \rightleftharpoons [\text{Fe}(\text{phen})_3]^{3+} + \text{HBrO}_2$
R9	$\text{Q} + \text{Br}_2 \rightarrow \text{QBr} + \text{Br}^- + \text{H}^+$
R10	$2[\text{Fe}(\text{phen})_3]^{2+} + \text{BrO}_3^- + 3\text{H}^+ \rightarrow 2[\text{Fe}(\text{phen})_3]^{3+} + \text{HBrO}_2 + \text{H}_2\text{O}$
R11	$[\text{Fe}(\text{phen})_3]^{3+} + \text{Br}^- \rightarrow [\text{Fe}(\text{phen})_3]^{2+} + \frac{1}{2} \text{Br}_2$
R12	$\text{QBr} + \text{H}_2\text{O} \rightarrow \text{QOH} + \text{H}^+ + \text{Br}^-$

Symbols for the organic species: Q = benzoquinone; QBr = 2-bromo-1,4-benzoquinone; QOH = 2-hydroxy-1,4-benzoquinone

Table 4.2: Rate constants used in the modeling of the ferroin-bromate-Q oscillator

	k_{forward}	k_{reverse}	reference
R1	$8 \times 10^7 \text{ M}^{-2} \text{ s}^{-1}$	90 s^{-1}	this work
R2	$2.5 \times 10^6 \text{ M}^{-2} \text{ s}^{-1}$	$2 \times 10^{-5} \text{ M}^{-1} \text{ s}^{-1}$	[10]
R3	$1.2 \text{ M}^{-3} \text{ s}^{-1}$	$3.2 \text{ M}^{-2} \text{ s}^{-1}$	[10]
R4	$2 \times 10^6 \text{ M}^{-1} \text{ s}^{-1}$	$1 \times 10^8 \text{ s}^{-1}$	[10]
R5	$1.7 \times 10^5 \text{ M}^{-1} \text{ s}^{-1}$		[10]
R6	$48 \text{ M}^{-2} \text{ s}^{-1}$	$3.2 \times 10^3 \text{ s}^{-1}$	[10]
R7	$7.5 \times 10^4 \text{ s}^{-1}$	$1.4 \times 10^9 \text{ M}^{-1} \text{ s}^{-1}$	[10]
R8	$1.0 \times 10^7 \text{ M}^{-2} \text{ s}^{-1}$		[10]
R10	$0.02 \text{ mol}^{-3} \text{ dm}^9 \text{ s}^{-1}$		[10]

As shown in Figure 4.6(a), the ferroin-bromate-benzoquinone system generates a series of spontaneous oscillations with a long induction time. When light was applied to the system, which was mimicked via enhancing the bromination of benzoquinone and the reduction of ferroin by bromide ions, oscillations in Figure 4.6(b) have a shorter induction time and higher oscillation frequency. Such a trend is the same as seen in the experiments.

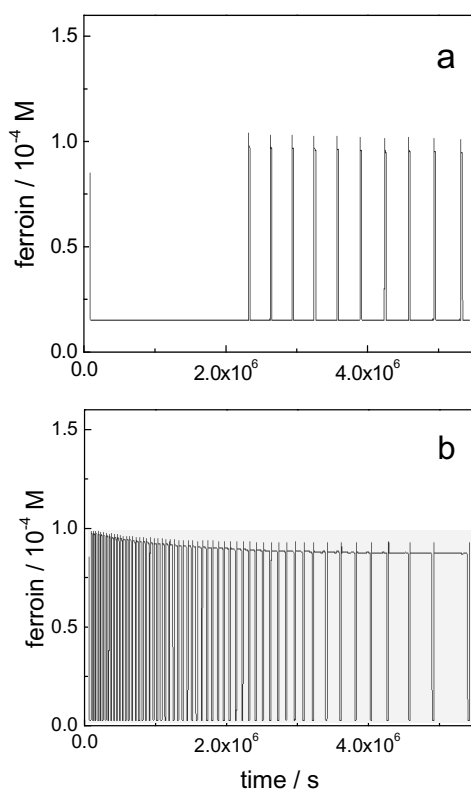


Figure 4.6 (a) Oscillations of the ferroin-bromate-Q reaction in a dark condition. Initial conditions used in the simulation are: $[\text{NaBrO}_3] = 0.05$ M, $[\text{ferroin}] = 1.0 \times 10^{-4}$ M, $[\text{Q}] = 0.035$ M, $[\text{H}^+] = 0.1$ M, $[\text{H}_2\text{O}] = 55$ M and $[\text{Br}^-] = 1 \times 10^{-8}$ M, $k_9 = 1.5 \text{ M}^{-1}\text{s}^{-1}$, $k_{11} = 50 \text{ M}^{-1}\text{s}^{-1}$, $k_{12} = 25 \text{ M}^{-1}\text{s}^{-1}$; (b) time series under the influence of light, implemented by resetting $k_9 = 4 \text{ M}^{-1}\text{s}^{-1}$, $k_{11} = 60 \text{ M}^{-1}\text{s}^{-1}$, $k_{12} = 50 \text{ M}^{-1}\text{s}^{-1}$.

4.4 Conclusions

The ferroin-bromate-benzoquinone reaction was found to have great photo sensitivity, in which light was capable of enhancing or quenching the chemical oscillations. The required light intensity was significantly lower than that reported earlier in a similar chemical system, in which the photo-reduction of benzoquinone was responsible for the overall oscillatory phenomenon [19]. Characterization with NMR and mass spectrometry suggests that light enhanced bromination of benzoquinone, which was accompanied by bromide production. Meanwhile, UV/Vis spectroscopy study indicates that light accelerates the reduction of ferroin by bromide, which consumes bromide ions and supplies ferroin for the autocatalytic process. The preliminary mechanistic study highlights that light could simultaneously implement two opposite effects. Which of the two paths plays a dominant role depends on the conditions of the reaction system. As seen earlier, a transition from constructive to inhibitory took place as merely the acid concentration was adjusted. In addition, as illustrated in Figure 4.4, the influence of light also underwent a transition from constructive to inhibitory when light intensity was increased monotonically. These results clearly demonstrate that illumination is an effective means to implement subtle manipulation of the nonlinear dynamics in the ferroin-bromate-benzoquinone reaction. This low cost, easy to prepare chemical reaction provides a good model system for exploring novel perturbed nonlinear behaviors.

4.5 References

- 1 W. Geiseler, J. Phys. Chem., 1982, 86, 4394.
- 2 M. Orban, P. De Kepper and I. R. Epstein, J. Am. Chem. Soc., 1982, 104, 2657.
- 3 K. Bar-Eli, J. Phys. Chem., 1985, 89, 2855.

- 4 A. K. Dutt and M. Menzinger, *J. Chem. Phys.*, 1999, 110, 7591.
- 5 R. J. Field and P. M. Boyd, *J. Phys. Chem.*, 1985, 89, 3707.
- 6 P. K. Srivastava, Y. Mori and I. Hanazaki, *J. Phys. Chem.*, 1991, 95, 1636.
- 7 K. Pelle, M. Wittmann, Z. Noszticzius, R. Lombardo, C. Sbriziolo and M. L. Turco Liveri, *J. Phys. Chem. A*, 2003, 107, 2039.
- 8 R. P. Rastogi, P. Chand, M. K. Pandey and M. Das, *J. Phys. Chem. A*, 2005, 109, 4562.
- 9 L. Adamčíková, Z. Farbulová and P. Ševčík, *New J. Chem.*, 2001, 25, 487.
- 10 I. Szalai, K. Kurin-Csörgei, I. R. Epstein and M. Orbán, *J. Phys. Chem. A*, 2003, 107, 10074.
- 11 M. Harati and J. Wang, *J. Phys. Chem. A*, 2008, 112, 4241.
- 12 P. I. Kumli, M. Burger, M. J. B. Hauser, S. C. Müller and Zs. Nagy-Ungvárai, *Phys. Chem. Chem. Phys.*, 2003, 5, 5454.
- 13 J. Li and J. Wang, *Chem. Phys. Lett.*, 2011, 508, 320.
- 14 H. Görner, *J. Phys. Chem. A*, 2003, 107, 11587.
- 15 V. J. Farage and D. Janjic, *Chem. Phys. Lett.*, 1982, 88, 301.
- 16 I. Szalai and E. Körös, *J. Phys. Chem. A*, 1998, 102, 6892.
- 17 Y. Chen and J. Wang, *J. Phys. Chem. A*, 2005, 109, 3950.
- 18 B. Zhao and J. Wang, *J. Photochem. Photobiol. A: Chemistry*, 2007, 192, 204.
- 19 N. Li and J. Wang, *J. Phys. Chem. A*, 2009, 113, 6297.
- 20 L. Kuhnert, K. I. Agladze and V. I. Krinsky, *Nature*, 1989, 337, 244.
- 21 O. Steinbock, V. Zykov and S. C. Müller, *Nature*, 1993, 366, 322.
- 22 V. Petrov, Q. Ouyang and H. Swinney, *Nature*, 1997, 388, 655.

- 23 S. Kádár, J. Wang and K. Showalter, *Nature*, 1998, 391, 770.
- 24 J. Wang, S. Kádár, P. Jung and K. Showalter, *Phys. Rev. Lett.*, 1999, 82, 855.
- 25 P. Ruoff, *J. Phys. Chem.*, 1984, 88, 2851.
- 26 A. Kaminaga, Y. Mori and I. Hanazaki, *Chem. Phys. Lett.*, 1997, 279, 339.
- 27 K. Martinez, A. L. Lin, R. Kharrazian, X. Sailer and H. L. Swinney, *Physica D*, 2002, 1, 168.
- 28 I. Cassidy, S. C. Müller, *Phys. Rev. E*, 2006, 74, 026206.
- 29 L. Treindl, D. Knudsen, T. Nakamura, T. Matsumura-Inoue, K. Jørgensen and P. Ruoff, *J. Phys. Chem. A*, 2000, 104, 10783.
- 30 D. S. Huh, Y. J. Kim, H. S. Kim, J. K. Kang and J. Wang, *Phys. Chem. Chem. Phys.*, 2003, 5, 3188.
- 31 P. G. Sorensen, T. Lorenzen and F. Hynne, *J. Phys. Chem.* 1996, 100, 19192.
- 32 A. Kaminaga and I. Hanazaki, *J. Phys. Chem. A*, 1998, 102, 3307.
- 33 S. Kadar, T. Amemiya and K. Showalter, *J. Phys. Chem. A*, 1997, 101, 8200.
- 34 S. K. Scott, *Chemical Chaos*; Oxford University Press: Oxford, U.K., 1991.
- 35 R. J. Field and M. Burger, Eds. *Oscillations and Traveling Waves in Chemical Systems*; Wiley-Interscience: New York, 1985.
- 36 N. Li, J. R. Green and J. Wang, *Chem. Phys. Lett.*, 2007, 447, 241.

Chapter 5: Complex Behavior in the Highly Photosensitive Cerium-Bromate-1,4-Benzoquinone Reaction

5.1 Introduction

Reactions between bromate and organic substrates in an acidic solution with or without the assistance of metal catalysts have been extensively investigated in the context of nonlinear chemical dynamics, in which the overall process can be characterized as the oxidation and bromination of the organic substrate [1-8]. The frequently employed catalysts include ferroin and ruthenium complexes, cerium and manganese ions [1,9]. The oxidation of organic substrate, taking place through its reaction with the oxidized catalyst [10-16], is largely responsible for the regeneration of the reduced metal catalysts for the autocatalytic processes in bromate-based chemical oscillators including the Belousov-Zhabotinsky oscillator. The recycling of the metal catalysts ensures that oscillations can continue. Recent investigations have shown that many aromatic compounds such as hydroquinone and pyrocatechol can be directly oxidized by bromine dioxide radicals to complete the autocatalytic nonlinear feedback, forming uncatalyzed bromate oscillators or forming BZ oscillators with coupled autocatalytic cycles [17-21].

It is useful to point out that, while the reduction of oxidized catalysts (e.g., ferroin, Ce^{4+}) by the organic substrate is a dominant process in the vast majority of bromate-based oscillators, the reduction of Ce^{4+} or ferroin by bromide ions also takes place [22,23]. Kinetic importance of the later process has been largely ignored, presumably because Br^- is better known as an inhibitor in the bromate-based chemical oscillators [1]. In Chapters

3 and 4, it was demonstrated that spontaneous oscillations could be observed in a batch bromate system in which the reduction of ferriin was by Br^- rather than by an organic substrate. Transient oscillations seen in the ferroin-bromate-benzoquinone reaction exhibited both constructive and inhibitory responses to fluorescent ceiling light [24-26]. To understand the photochemistry behind such a great photosensitivity, especially the role of ferroin/ferriin couple, this research investigated the cerium-bromate-Q reaction. The use of cerium does not only enhance the reduction of the inhibitor Br^- (i.e. by the oxidized catalyst), but also provides a slower autocatalytic cycle. Such a kinetic modification therefore simultaneously modulates two key processes in a chemical oscillator and may potentially generate novel nonlinear behavior.

As shown in the following, replacing ferroin with cerium leads to a much longer series of spontaneous oscillations. In addition, complex behaviors such as sequential oscillations are also developed in the cerium-bromate-Q reaction. Same as the ferroin system, however, the cerium-bromate-Q reaction also exhibits great sensitivity to the rather weak fluorescent ceiling light. Investigations on the stability of 2-bromo-1,4-benzoquinone (QBr) provide new insights into the photochemical mechanisms and allow us to construct a model that qualitatively reproduces the experimental observation.

5.2 Experimental Procedure

All reactions were carried out in a thermal-jacketed 50 ml glass reactor with the temperature maintained constant at $25.0 \pm 0.1^\circ\text{C}$ by a circulation water bath (ThermoNesLab RTE 7). The reaction solution was stirred by a magnetic stirrer (Fisher Isotemp) at around 600 rpm. A Teflon cap was placed on top of the cylindrical reactor to hold electrodes and nitrogen/air inflow tube. The air/nitrogen was flowed into the empty

space above the reaction solution in the related experiments. Volume of the reaction solution was fixed at 30.0 ml. Reactions were monitored with a platinum or bromide ion selective electrode coupled to a $\text{Hg} | \text{Hg}_2\text{SO}_4 | \text{K}_2\text{SO}_4$ reference electrode (Radiometer Analytical, XR200 and M231Pt-9). All measurements were recorded with a personal computer connected to a pH/potential meter (Radiometer PHM220) through a PowerLab/4SP data logger. Except otherwise stated, all reactions were conducted in a dark room. The controlled light perturbation was implemented with a 150 W halogen light source (Fisher Scientific, Model DLS-100HD). Narrow band filters (Melles Griot) with different wavelength range were employed to test the wavelength dependence of the photoreaction behavior. Light intensity was measured with an optical photometer from Newport (model 1815-C).

Stock solutions of analytical grade sodium bromate (NaBrO_3 , Aldrich, 99%), 1.0 M, sulfuric acid (H_2SO_4 , Aldrich, 95-98%), 6.0 M and cerium sulphate 0.005M ($\text{Ce}(\text{SO}_4)_2$, Aldrich) were prepared with double distilled water. 1,4-Benzoquinone (Sigma-Aldrich, 98%) was directly dissolved in the reaction mixture. 2-Bromo-1,4-benzoquinone (QBr) was purchased from Tokyo Chemical Industrial Co., Ltd. (Tokyo, Japan). GC/MS measurements were performed on a Varian CP-3800/Varian 1200L system, using a 15 m Varian CP-Sil 5CB column. All ^1H -NMR studies were performed on a Bruker Avance 500MHz spectrometer, using the same sample that was used for GC/MS studies, but dissolved in deuterated chloroform (Cambridge Isotope Laboratories, 99.8%). UV/Vis spectroscopy was obtained with a spectrophotometer from Ocean Optics (USB 2000). Simulations were done with Berkeley Madonna software (Version 8.3.14), by using the Rosenbrock routine for the numerical solution of stiff differential equations [27].

5.3 Results and Discussion

5.3.1 Reaction Behavior in a Dark Room

Figure 5.1 presents time series of the Cerium-bromate-Q reaction under different concentrations of H_2SO_4 : (a) 0.15 M, (b) 0.20 M and (c) 0.25 M. Other reaction compositions are $[\text{NaBrO}_3] = 0.05 \text{ M}$, $[\text{Ce(IV)}] = 1.0 \times 10^{-4} \text{ M}$ and $[\text{Q}] = 0.035 \text{ M}$. Transient spontaneous oscillations were observed for the H_2SO_4 acid concentration between 0.1 and 0.25 M. At 0.15 M a long series of oscillations with an amplitude of more than 60 mV took place. Increasing the acid concentration shortened the induction time slightly, but caused a decrease in the oscillation amplitude.

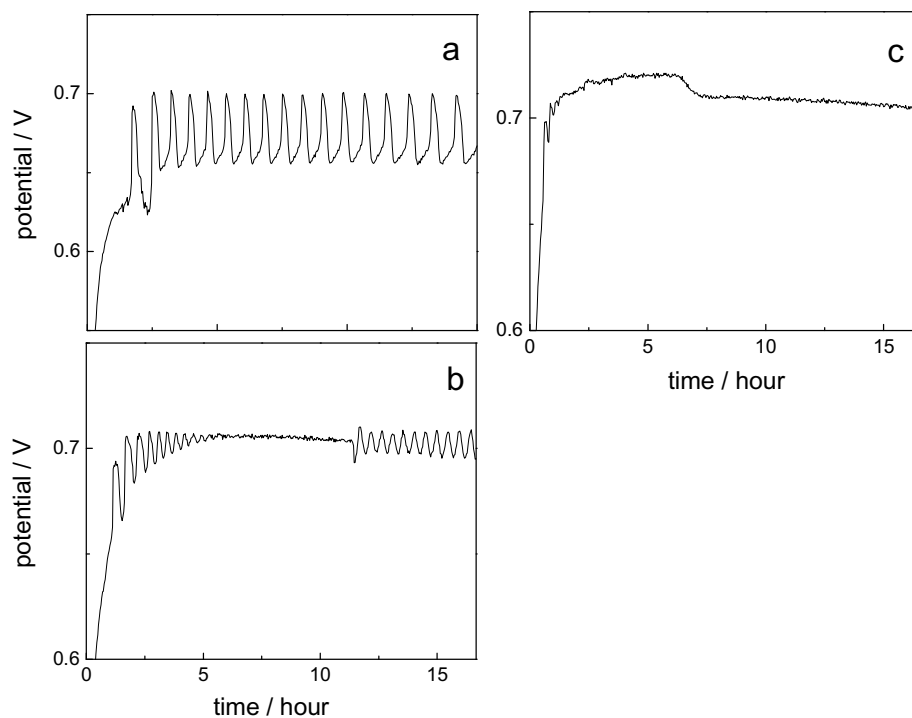


Figure 5.1 Time series of the Ce(IV)-bromate-Q reaction carried out at different sulfuric acid concentrations: (a) 0.15 M, (b) 0.2 M and (c) 0.25 M. Other reaction conditions were $[\text{NaBrO}_3] = 0.05 \text{ M}$, $[\text{Ce(IV)}] = 1.0 \times 10^{-4} \text{ M}$ and $[\text{Q}] = 0.035 \text{ M}$.

Overall, the induction time always stayed longer than 5000 s. A more significant change in the behavior took place at $[\text{H}_2\text{SO}_4] = 0.2 \text{ M}$, where two isolated oscillation windows, referred as sequential oscillations in literature [28], were observed. The system seems to evolve into the quiescent period through a reversed supercritical Hopf-bifurcation [29].

Our earlier study has shown that bromine removal could have significant impact on the behavior of modified BZ reactions [30]. To examine whether the escape of volatile species played a key factor in causing the oscillatory behavior in the above reaction, we have run parallel experiments by flowing nitrogen or air above the reaction solution surface.

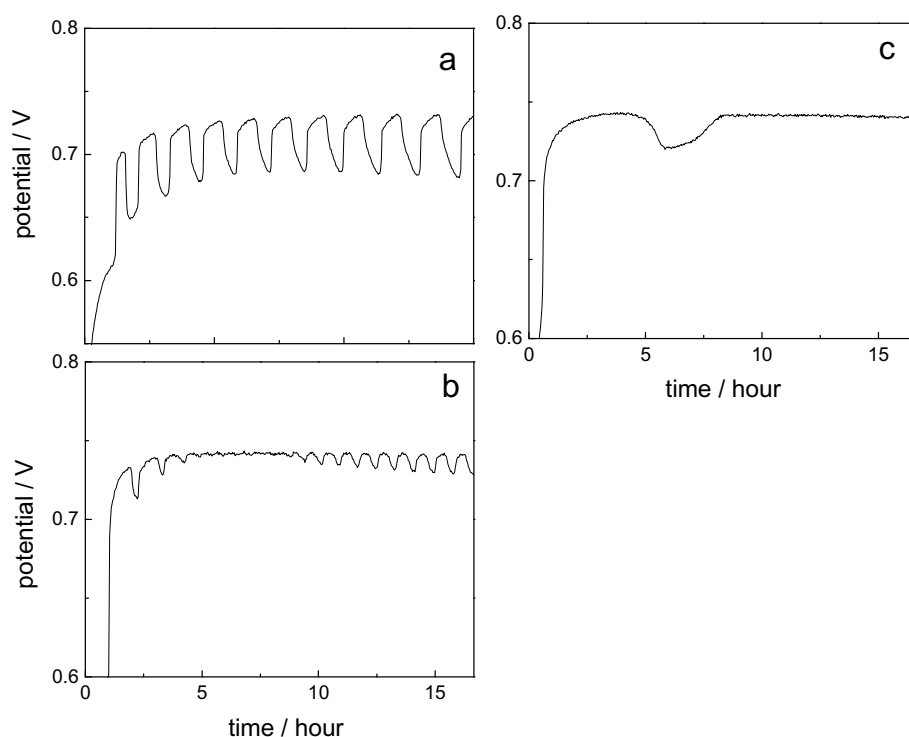


Figure 5.2 Time series obtained at the condition that air was flowing above the reaction solution at a rate of 60 ml/min. Other conditions are the same as the corresponding panel in Figure 5.1.

Figure 5.2 presents the results achieved under the flow of air at 60 ml/min. Comparing the two time series at $[\text{H}_2\text{SO}_4] = 0.15 \text{ M}$, the oscillation wave form changed, in which the system spent a longer time at the oxidized (i.e. high potential) state. It is presumably due to the slow bromide production as a result of bromine removal. Otherwise, the behavior remains qualitatively similar to that seen in Figure 5.1, including the sequential oscillations. The following experiments were conducted under the same configuration as that used in Figure 5.1 (i.e. without flowing air or nitrogen).

Figure 5.3 shows three time series performed at different initial concentrations of Ce(IV): (a) $5.0 \times 10^{-5} \text{ M}$, (b) $1.0 \times 10^{-4} \text{ M}$ and (c) $2.0 \times 10^{-4} \text{ M}$. Other reaction conditions are $[\text{H}_2\text{SO}_4] = 0.2 \text{ M}$, $[\text{NaBrO}_3] = 0.05 \text{ M}$ and $[\text{Q}] = 0.035 \text{ M}$. At the low cerium concentration spontaneous oscillations with an induction time of around 5000 s emerged. Interestingly, as cerium concentration was increased, after the reaction has evolved for some time at the non-oscillatory state, spontaneous oscillations revived at about $4 \times 10^4 \text{ s}$, forming a second oscillation window. At still higher cerium concentration only one group of oscillations with an extremely long induction time ($6 \times 10^4 \text{ s}$) emerged. This long induction time matches the induction time of the second oscillation window seen in Figure 5.3(b), suggesting that the first oscillation window might have been eliminated by increasing cerium concentration. Transient oscillations in Figure 5.3(c) lasted for more than 50 hours. Results in Figure 5.3 demonstrate that the catalyst plays a subtle role in the development of complex behavior. This may be understood based on the fact that Ce(III) is involved in the autocatalytic cycle whereas Ce(IV) reacts with the inhibitor Br^- .

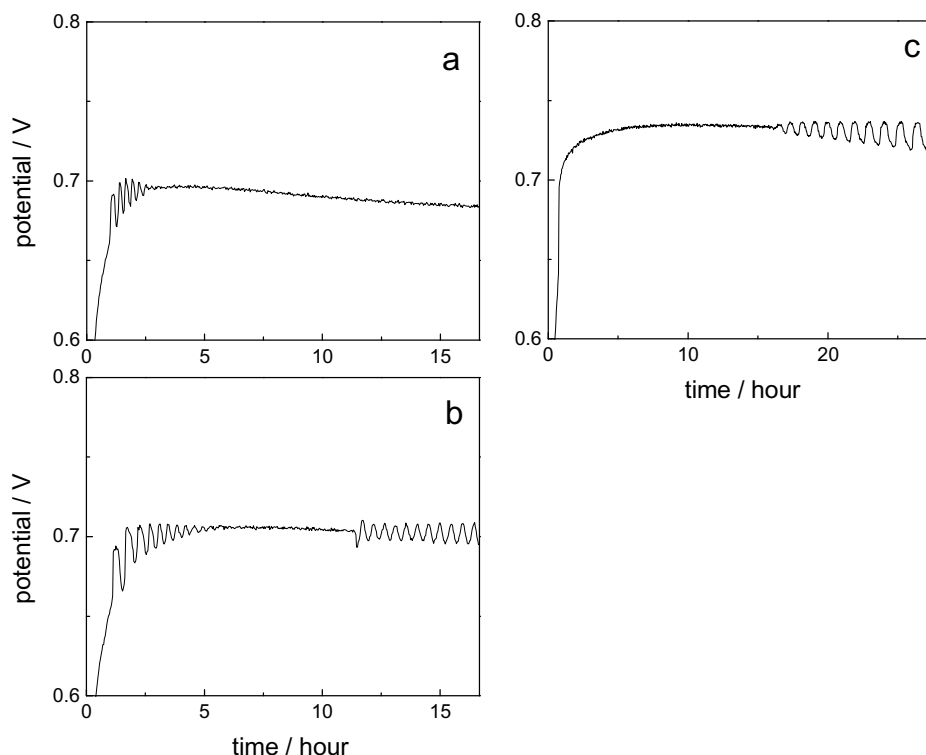


Figure 5.3 Time series of the Cerium-bromate-Q reaction at different concentrations of Ce(IV): (a) 5.0×10^{-5} M, (b) 1.0×10^{-4} M and (c) 2.0×10^{-4} M. Other reaction conditions were the same as those used in Figure 5.1b.

5.3.2 The Influence of Ceiling Light

The fluorescent ceiling light in our lab, which is approximately 2 m above our reactor, has an intensity of around $20 \mu\text{W}/\text{cm}^2$. Note that the reactor has a non-transparent teflon cap, the light can therefore only irradiate into the reactor through its side, penetrating two layers of glasses and a water jacket in between. Figure 5.4 presents time series carried out with different initial concentrations of H_2SO_4 : (a) 0.2 M, (b) 0.15 M, (c) 0.1 M and (d) 0.05 M. The presence of light significantly broadened the concentration range over which spontaneous oscillations could be observed. For example, time series in Figure 5.4(d)

indicates that low frequency oscillations still exist at $[\text{H}_2\text{SO}_4] = 0.05 \text{ M}$, as opposed to the low limit of 0.1 M in a dark room condition. At the high concentration end, it reaches 0.8 M . Reaction in Figure 5.4(a) has the same chemical compositions as that in Figure 5.1(b), but here only one oscillation window is observed. The induction time here is about $3.5 \times 10^4 \text{ s}$, which is on the same order as the induction time of the second oscillation window in Figure 5.1(b). Therefore, light has likely suppressed the first oscillation window. In addition, both the oscillation frequency and amplitude are greatly increased due to the influence of ceiling light (e.g. results at $[\text{H}_2\text{SO}_4] = 0.15$ or 0.20 M).

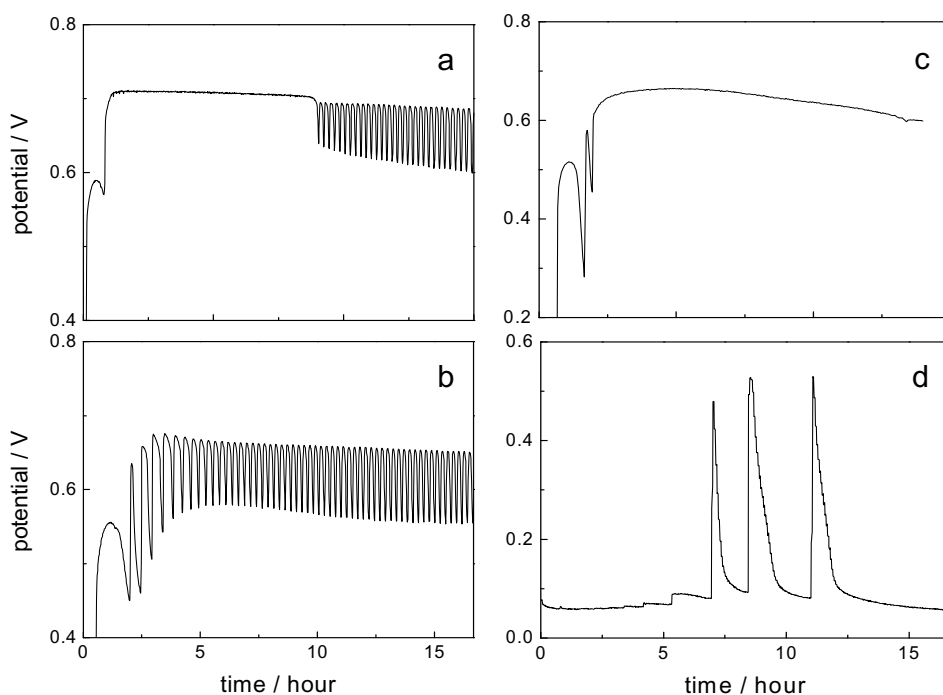


Figure 5.4 Time series of the Ce(IV)-bromate-Q reaction under the irradiation of ceiling light ($20 \mu\text{W}/\text{cm}^2$) with different concentrations of sulfuric acid: (a) 0.2 M , (b) 0.15 M , (c) 0.1 M , and (d) 0.05 M . Other compositions were the same as those used in Figure 5.1.

Figure 5.5 shows time series conducted at different initial concentrations of Ce(IV): (a) $2.5 \times 10^{-5} \text{ M}$, (b) $5.0 \times 10^{-5} \text{ M}$, (c) $2.0 \times 10^{-4} \text{ M}$ and (d) $4.0 \times 10^{-3} \text{ M}$. In addition to the

variations in the oscillation frequency and amplitude, comparison of Figure 5.5 and Figure 5.3 suggests that the ceiling light quenched the first oscillation window. The influence of Cerium concentration on the reaction behavior also changed, where decreasing Ce(IV) from 2.0×10^{-4} M resulted in the disappearance of spontaneous oscillations rather than the emergence of another oscillation window as seen under dark conditions. In Figure 5.5 the induction time became shorter at higher Ce(IV) concentration, as opposed to the increase in induction time at dark conditions. Spontaneous oscillations lasted for longer than a week at the high Ce(IV) concentration, but the oscillation frequency was quite low, for example, 2.7 hours /oscillation in Figure 5.5d.

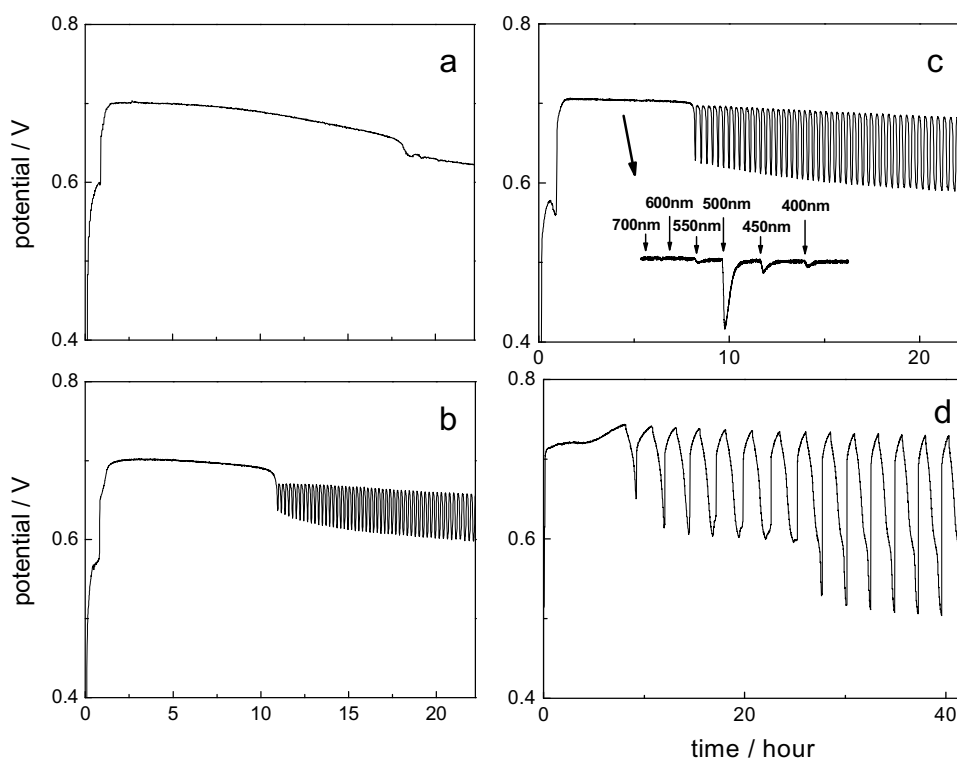


Figure 5.5 Time series of the Ce(IV)-bromate-Q reaction under the irradiation of ceiling light ($20 \mu\text{W}/\text{cm}^2$) with different Ce(IV) concentrations: (a) 2.5×10^{-5} M, (b) 5.0×10^{-5} M, (c) 2.0×10^{-4} M, and (d) 4.0×10^{-3} M. Other reaction conditions were the same as those used in Figure 5.3. The inset in (c) shows responses of the system to light pulse perturbation of different wavelengths.

5.3.3 Wavelength and Intensity Dependence

Photochemical behavior of the Cerium-bromate-Q reaction was also tested with irradiation of specific wavelength. It was implemented by letting white light pass through various narrow band filters. The influence of the pulse-illumination of different wavelengths on the non-oscillatory evolution was presented as an inset in Figure 5.5c. Same as that observed in the ferroin-bromate-Q system [26], the reaction behavior is most sensitive to the incident light of wavelength $\lambda = 500 \pm 40$ nm. Therefore, the extremely strong photosensitivity observed in the cerium or ferroin-bromate-Q system is not due to the catalysts.

Figure 5.6 presents four time series of the Ce(IV)-bromate-Q reaction illuminated with 500 ± 40 nm light of different intensities: (a) $2.5 \mu\text{W}/\text{cm}^2$, (b) $5.0 \mu\text{W}/\text{cm}^2$, (c) $50 \mu\text{W}/\text{cm}^2$ and (d) $500 \mu\text{W}/\text{cm}^2$. Other reaction conditions are the same as those in Figure 5.1b. In Figure 5.6a, both oscillation windows were still there, however the number of oscillation within the first window decreased and oscillations in the second window also stopped earlier (it lasted more than 1.0×10^5 s in Figure 5.1b). The second oscillation window was quenched when the light intensity was increased to $5.0 \mu\text{W}/\text{cm}^2$. Interestingly, further increase of the light intensity revived the second oscillation window (see Figure 5.6c), while causing the disappearance of the first oscillation window. When light intensity was increased to $500 \mu\text{W}/\text{cm}^2$ in Figure 5.6d, spontaneous oscillations were still there, but had a much longer induction time. The oscillation frequency became greatly higher as the light intensity was increased. The above results demonstrate that photochemical reactions have subtle impacts on the oscillatory phenomenon, especially the second oscillation window.

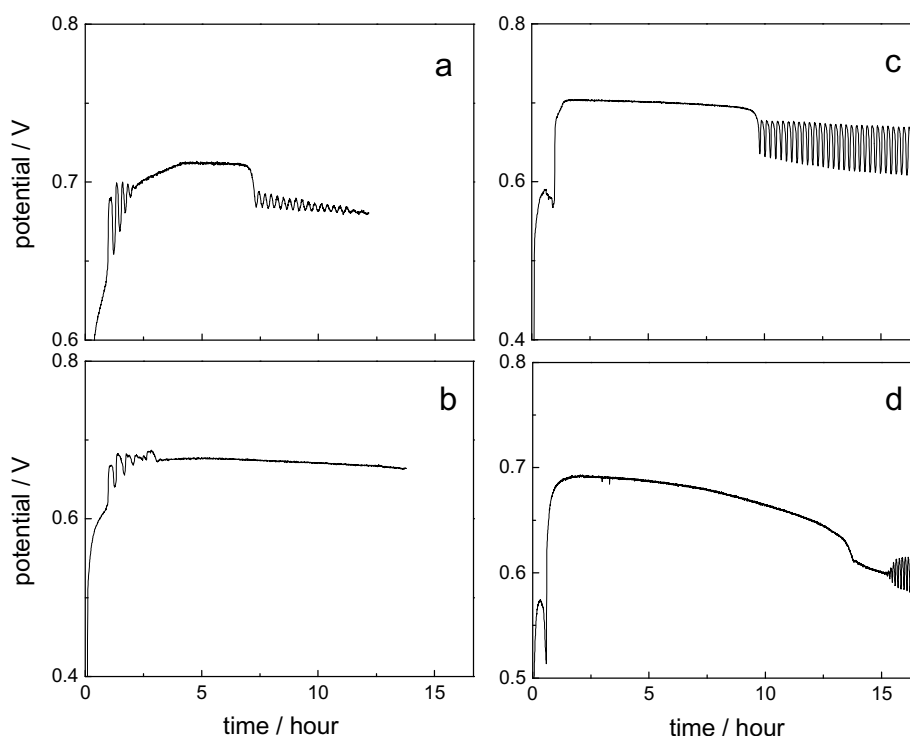


Figure 5.6 Time series of the Ce(IV)-bromate-Q reaction illuminated with 500 ± 40 nm light of different intensities: (a) $2.5 \mu\text{W}/\text{cm}^2$, (b) $5 \mu\text{W}/\text{cm}^2$, (c) $50 \mu\text{W}/\text{cm}^2$, and (d) $500 \mu\text{W}/\text{cm}^2$. Other reaction conditions were the same as Figure 5.1b.

5.3.4 Mechanistic Characterization

A striking feature of the above oscillatory behavior is the long induction time. In Figures 5.7a and 5.7b, influences of photoproducts on the induction time were examined, where at the beginning of each reaction the solution was illuminated with a 150 W halogen light for (a) 150 s and (b) 600 s, respectively. Other conditions were the same as those in Figure 5.4a. The induction time was greatly reduced in Figure 5.7a, in comparison to the time series in Figure 5.4a. This result indicates that products from the photochemical reactions have significant impacts on the induction time. When the illumination time period was increased to 600 s in Figure 5.7b, the induction time was

reduced further, meanwhile the reaction behavior also underwent significant changes, where only a limit number of oscillations were observed, as opposed to the long series in Figure 5.7a.

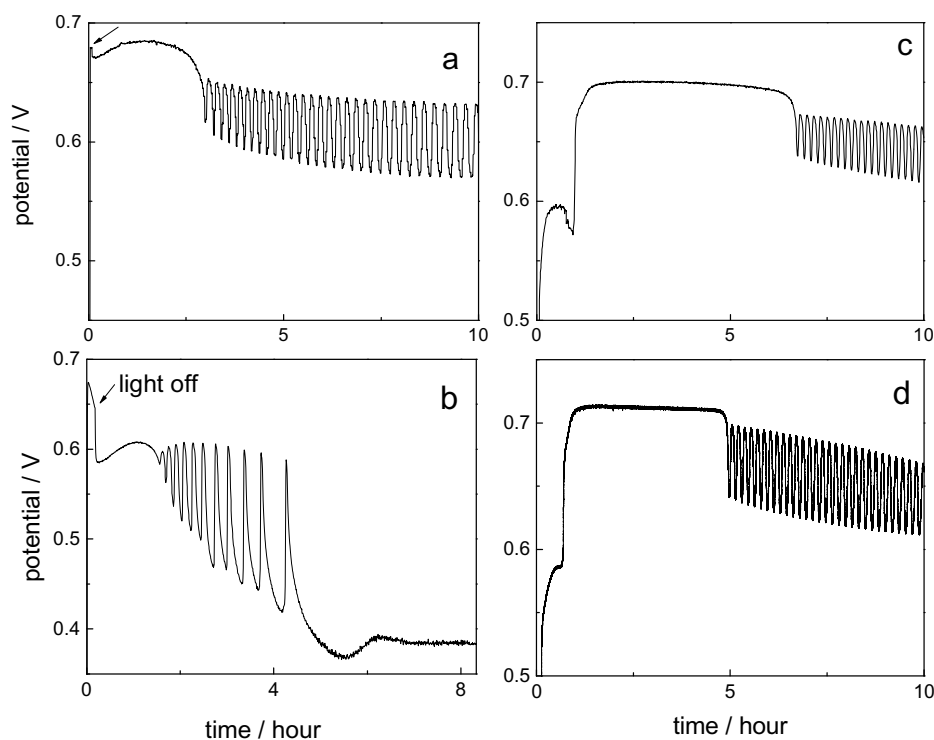


Figure 5.7 Times series carried out with different illumination (150 mW/cm^2) time (a) 150s and (b) 600s. Time series were in the initial presence of 2.0 mM QBr (c) and 4.0 mM QBr (d). Other reaction conditions were the same as those in Figure 5.4a, except $[Q] = 0.033\text{M}$ in (c) and 0.031M in (d).

Our earlier investigation has confirmed the production of bromo-1,4-benzoquinone in the bromate-benzoquinone photoreaction [24,26], although it did not appear as a major product in the spectrum. In Figure 5.7c the reaction performed in Figure 5.4a was repeated with the initial addition of 2.0 mM QBr that was purchased from Tokyo

Chemical Industrial Co., Ltd. To keep the total amounts of substrate constant, the concentration of Q was decreased to 0.033M. The initial presence of QBr reduced the induction time from 3.6×10^4 s to 2.4×10^4 s. Further increase of QBr to 4.0 mM in (d) cut the induction time to 1.75×10^4 s, suggesting that QBr can significantly shorten the induction time. On the other hand, QBr has an adverse effect on the life time of those oscillations, reducing it from 1 week to 12 hours, similar to the transition from (a) to (b) in Figure 5.7.

To examine the stability of QBr, Figure 5.8a measures absorption spectra of 3.0 mM QBr in a 0.1 M H_2SO_4 solution under ceiling light. The spectrum was recorded every 10 minutes. It shows that the absorption peak at 350 nm decreased in time, whereas the peak at 280 nm increased. Bromide ion selective electrode was employed to confirm that bromide ions were produced during the above decomposition of QBr. ^1H -NMR and GC/MS characterization suggest that the product at the absorption of 280 nm is 2-hydroxy-1,4-benzoquinone rather than 1,4-benzoquinone, since there is no chemical shift peak at $\delta = 6.8$. Furthermore, the decomposition of QBr could be enhanced by irradiation, as seen in Figure 5.8b, where two time series of QBr photodecomposition at 20 mW/cm^2 (solid line) and $20 \text{ }\mu\text{W/cm}^2$ light (dash line) were measured with UV/Vis spectrophotometer at 350 nm. Results in Figure 5.8 suggest that the great photosensitivity may take place through photo enhanced decomposition of QBr, in addition to what was suggested earlier that irradiation enhanced QBr production [24,26]. The presence of QOH in the final products of the Cerium-bromate-Q reaction was confirmed by ^1H -NMR and GC/MS spectroscopy.

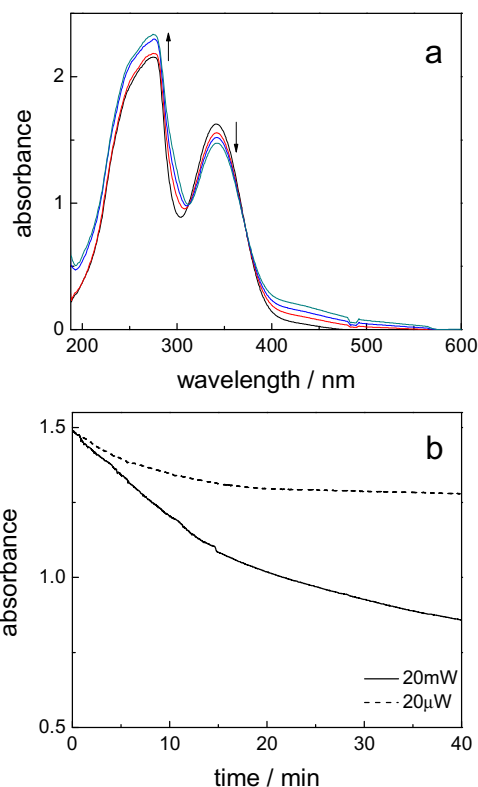


Figure 5.8 (a) Absorption spectra of 0.003M of QBr in 0.1M H_2SO_4 solution, (b) Time series of the same QBr solution collected at 350 nm, where the solution was illuminated with 20 mW/cm² light (solid line) or 20 μW/cm² ceiling light (dash line).

5.3.5 Modeling

Table 5.1 lists the model developed here. It consists of 11 reactions and 14 variables. The core of this model is taken from the FKN mechanism [31], modified to include the production of QBr from bromine and Q and the decomposition of QBr. FKN mechanism has been very successful in reproducing the oscillatory behavior seen in the BZ reaction

as well as in modified BZ reactions [31,32]. Basic elements of the model are: (R1-R3, R10) the consumption of control intermediate Br^- and (R4-R8) autocatalysis. Reactions R9 and R11 proposed here regulate Br^- variation and their rates are influenced by light, as suggested by the mechanistic investigation in this study. Kinetics and mechanisms of the reduction of Ce^{4+} by bromide ions have been investigated earlier and the processes involve the formation of cerium complexes with bromide ions [22,23]. The process is represented by R10 in this research.

Table 5.1: Model proposed for the cerium-bromate-Q oscillator

Reactions	
R1	$\text{Br}^- + \text{HOBr} + \text{H}^+ \rightleftharpoons \text{Br}_2 + \text{H}_2\text{O}$
R2	$\text{Br}^- + \text{HBrO}_2 + \text{H}^+ \rightleftharpoons 2\text{HOBr}$
R3	$\text{Br}^- + \text{BrO}_3^- + 2\text{H}^+ \rightleftharpoons \text{HOBr} + \text{HBrO}_2$
R4	$\text{HBrO}_2 + \text{H}^+ \rightleftharpoons \text{H}_2\text{BrO}_2^+$
R5	$\text{HBrO}_2 + \text{H}_2\text{BrO}_2^+ \rightarrow \text{BrO}_3^- + \text{HOBr} + 2\text{H}^+$
R6	$\text{HBrO}_2 + \text{BrO}_3^- + \text{H}^+ \rightleftharpoons \text{Br}_2\text{O}_4 + \text{H}_2\text{O}$
R7	$\text{Br}_2\text{O}_4 \rightleftharpoons 2\text{BrO}_2^\bullet$
R8	$\text{Ce}^{3+} + \text{BrO}_2^\bullet + \text{H}^+ \rightleftharpoons \text{Ce}^{4+} + \text{HBrO}_2$
R9	$\text{Q} + \text{Br}_2 \rightarrow \text{QBr} + \text{Br}^- + \text{H}^+$
R10	$\text{Ce}^{4+} + \text{Br}^- \rightarrow \text{Ce}^{3+} + \frac{1}{2} \text{Br}_2$
R11	$\text{QBr} + \text{H}_2\text{O} \rightarrow \text{QOH} + \text{H}^+ + \text{Br}^-$

Symbols for the organic species: Q = benzoquinone; QBr = 2-bromo-1,4-benzoquinone; QOH = 2-hydroxy-1,4-benzoquinone

Table 5.2: Rate constants used in the modeling of the cerium-bromate-Q oscillator

	k_{forward}	k_{reverse}	<i>reference</i>
R1	$8 \times 10^7 \text{ M}^{-2} \text{ s}^{-1}$	90 s^{-1}	this work
R2	$2.5 \times 10^6 \text{ M}^{-2} \text{ s}^{-1}$	$2 \times 10^{-5} \text{ M}^{-1} \text{ s}^{-1}$	[33]
R3	$1.2 \text{ M}^{-3} \text{ s}^{-1}$	$3.2 \text{ M}^{-2} \text{ s}^{-1}$	[34]
R4	$2 \times 10^6 \text{ M}^{-1} \text{ s}^{-1}$	$1 \times 10^8 \text{ s}^{-1}$	[35]
R5	$1.7 \times 10^5 \text{ M}^{-1} \text{ s}^{-1}$		[35]
R6	$48 \text{ M}^{-2} \text{ s}^{-1}$	$3.2 \times 10^3 \text{ s}^{-1}$	[34]
R7	$7.5 \times 10^4 \text{ s}^{-1}$	$1.4 \times 10^9 \text{ M}^{-1} \text{ s}^{-1}$	[34]
R8	$6.2 \times 10^4 \text{ M}^{-2} \text{ s}^{-1}$	$1.2 \times 10^4 \text{ M}^{-1} \text{ s}^{-1}$	[34]

Most of the rate constants used in the simulation were taken from literature (see Table 5.2), where they were determined experimentally [33-35]. As shown in Figure 5.9, the proposed model is able to reproduce the oscillatory behavior as well as the influence of light and QBr perturbation. As the light intensity increased in (b), enhanced reactions in R9 and R11 successfully reproduced the constructive influences on oscillation behavior, not only shortening the induction time but also increasing the oscillation frequency. While adding QBr in (a), the induction time was greatly shortened and the oscillation frequency kept the same.

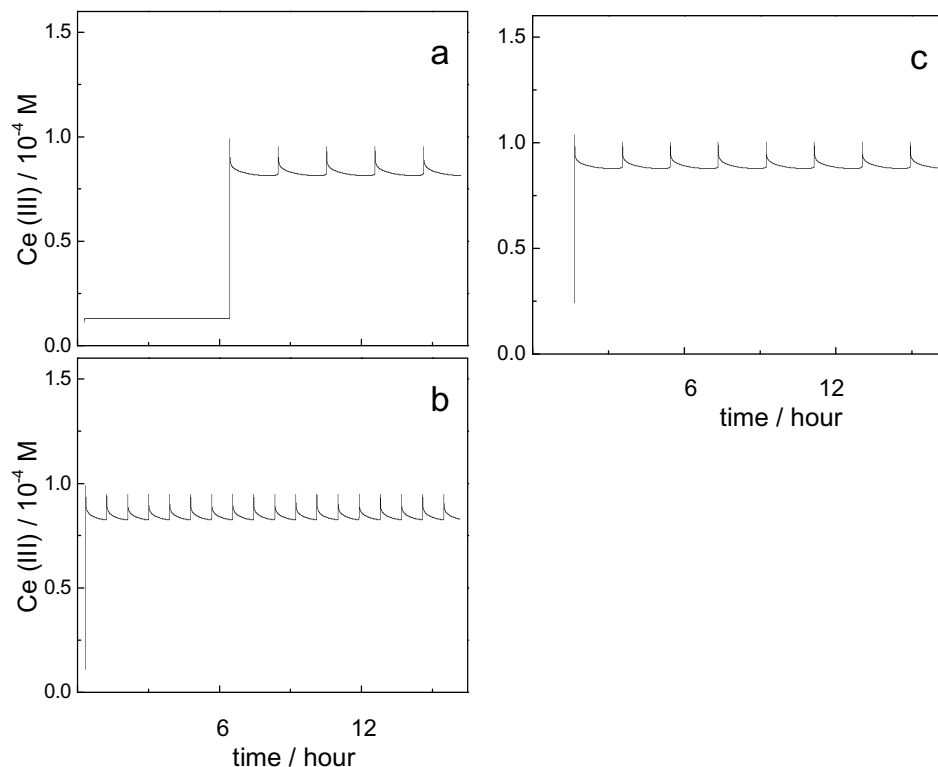


Figure 5.9 (a) Oscillations of the Ce(IV)-bromate-Q reaction in a dark condition. Initial conditions used in the simulation are: $[\text{NaBrO}_3] = 0.05 \text{ M}$, $[\text{Ce(IV)}] = 1.0 \times 10^{-4} \text{ M}$, $[\text{Q}] = 0.035 \text{ M}$, $[\text{H}^+] = 0.4 \text{ M}$, $[\text{H}_2\text{O}] = 55 \text{ M}$, $[\text{Br}^-] = 1 \times 10^{-8} \text{ M}$, $k_9 = 19.9 \text{ M}^{-1}\text{s}^{-1}$, $k_{10} = 1 \times 10^4 \text{ M}^{-1}\text{s}^{-1}$, $k_{11} = 50 \text{ M}^{-1}\text{s}^{-1}$; (b) time series under the influence of light, which was implemented by resetting $k_9 = 40 \text{ M}^{-1}\text{s}^{-1}$, $k_{10} = 1 \times 10^4 \text{ M}^{-1}\text{s}^{-1}$, $k_{11} = 60 \text{ M}^{-1}\text{s}^{-1}$; (c) the initial concentration of QBr was set to $1.0 \times 10^{-6} \text{ M}$, while all other parameters are the same as those in (a).

5.4 Conclusions

Long series of spontaneous oscillations were observed in the closed cerium-bromate-benzoquinone reaction. In comparison to the ferroin-bromate-Q system, here chemical oscillations exist over a broader range of acid concentration, highlighting the importance of the bromide-catalyst reaction. Such a reaction implicates that in a spatially extended

reaction-diffusion medium, it is possible to have a constructive interaction between the front of a propagating pulse and the tail of a preceding pulse, where there are high concentrations of ferriin and Br^- , respectively. Therefore, results reported here shall be useful in understanding the occurrence of merging wave phenomena reported in the ferriin-bromate-cyclohexanedione system [36].

A distinct dynamic property of the Cerium-bromate-Q system is that bromide ions have two contradictory roles: (1) it is an inhibitor to quench the autocatalytic cycle; and (2) it regenerates reduced metal catalyst to maintain the autocatalytic processes. This conflicting role creates the potential of achieving more subtle and complicated nonlinear behaviors. Time series in Figure 5.3 does indicate the presence of sequential oscillations. ^1H -NMR and GC/MS measurements of the cerium-bromate-Q solution show the presence of QBr and hydroxy-benzoquinone. Separated mechanistic analysis illustrates that QBr is unstable and decomposes to produce bromide and hydroxy-benzoquinone. Together with the earlier study [24,26], research conducted in this chapter suggests that the production and decomposition of QBr, rather than the metal catalyst, is the culprit responsible for the observed ultrahigh photosensitivity.

5.5 References

- 1 R. J. Field and M. Burger, Eds. *Oscillations and Traveling Waves in Chemical Systems*, Wiley-Interscience: New York, 1985.
- 2 Z. Noszticzius, P. Stirling and M. Wittmann, *J. Phys. Chem.*, 1985, 89, 4914.
- 3 K. Kurin-Csörgei, I. Szalai and E. Körös, *React. Kinet. Catal. Lett.*, 1995, 54, 217.
- 4 D. S. Huh, Y. J. Kim, H. S. Kim, J. K. Kang and J. Wang, *Phys. Chem. Chem. Phys.*, 2003, 5, 3188.

- 5 L. Treindl, T. Matsumura-Inoue and P. Ruoff, *J. Phys. Chem. A*, 2002, 106, 5271.
- 6 M. Orbán and E. Körös, *J. Phys. Chem.*, 1978, 82, 1672.
- 7 L. Adamcikova, D. Misicak and P. Sevcik, *React. Kinet. Catal. Lett.*, 2005, 85, 215.
- 8 V. J. Farage and D. Janjic, *Chem. Phys. Lett.*, 1982, 88, 301.
- 9 I. R. Epstein and J. A. Pojman, *Introduction to Nonlinear Chemical Dynamics: Oscillations, Waves, Patterns and Chaos*, Oxford University Press, New York, 1998.
- 10 M. K. Ram Reddy, Z. Szlavik, Zs. Nagy-Ungvarai and S. C. Muller, *J. Phys. Chem.*, 1995, 99, 15081.
- 11 K. Showalter, R. M. Noyes and K. Bar-Eli, *J. Chem. Phys.*, 1978, 69, 2514.
- 12 L. Treindl and V. Zvac, *React. Kinet. Catal. Lett.*, 1983, 22, 451.
- 13 R. P. Rastogi, P. Chand, M. K. M. Pandey and M. Das, *J. Phys. Chem. A*, 2005, 109, 4562.
- 14 J. A. Pojman, D. C. Leard and W. West, *J. Am. Chem. Soc.*, 1992, 114, 8298.
- 15 I. Szalai, K. Kurin-Csörgei, I. R. Epstein and M. Orbán, *J. Phys. Chem. A*, 2003, 107, 10074.
- 16 J. Wang, P. G. Sorensen and F. Hynne, *J. Phys. Chem.*, 1994, 98, 725.
- 17 B. Zhao and J. Wang, *Chem. Phys. Lett.*, 2006, 430, 41.
- 18 M. Harati and J. Wang, *Z. Phys. Chem.*, 2008, 222, 997.
- 19 N. Li and J. Wang, *J. Phys. Chem. A*, 2009, 113, 6297.
- 20 I. Szalai, K. Kurin-Csörgei and M. Orbán, *Phys. Chem. Chem. Phys.*, 2002, 4, 1271.
- 21 M. Harati and J. Wang, *J. Phys. Chem. A*, 2008, 112, 4241.
- 22 E. L. King and M. L. Pandow, *J. Am. Chem. Soc.*, 1953, 75, 3063.
- 23 A. Katafias, *Trans. Metal Chem.*, 2006, 31, 907.

- 24 J. Li and J. Wang, Chem. Phys. Lett., 2011, 508, 320.
- 25 K. Kurin-Csörgei, A. M. Zhabotinsky, M. Orbán and I. R. Epstein, J. Phys. Chem., 1996, 100, 5393.
- 26 J. Li and J. Wang, J. Phys. Chem. A, 2012, 116, 386.
- 27 H. H. Rosenbrock, The Computer J., 1963, 5, 329.
- 28 E. J. Heilweil, M. J. Henchman and I. R. Epstein, J. Am. Chem. Soc., 1979, 101, 3698.
- 29 S. K. Scott, Oscillations, Waves and Chaos in Chemical Kinetics, Oxford University Press, 1994.
- 30 J. Li and J. Wang, Phys. Chem. Chem. Phys., 2011, 13, 15539.
- 31 R. J. Field, E. Korös and R. M. Noyes, J. Am. Chem. Soc., 1972, 94, 8649.
- 32 L. Györgyi, S. L. Rempe and R. J. Field, J. Phys. Chem., 1991, 95, 3159.
- 33 H. D. Försterling, S. Murányi and H. Z. Schreiber, Naturforsch, 1989, 44a, 555.
- 34 Y. Gao and H. D. Försterling, J. Phys. Chem., 1995, 99, 8638.
- 35 H. D. Försterling and M. Varga, J. Phys. Chem., 1993, 97, 7932.
- 36 C. T. Hamik, N. Manz and O. Steinbock, J. Phys. Chem. A, 2001, 105, 6144.

Chapter 6: Electrochemically Modified Carbon Electrodes for Simultaneous Determination of Dihydroxybenzene Isomers

6.1 Introduction

Carbon nanotube (CNT) modified electrodes in electroanalysis have attracted a great deal of attention in the last decade, where low detection limits and high resistance to surface fouling have been achieved [1-7]. The fabrication of CNT and carbon nanofibers is unfortunately energy consuming and requires sophisticated chemical control. Recent studies by Compton and co-workers suggested that the significant electrocatalytic activity of CNT is due to the presence of a great number of edge plane sites in their unique microstructure [8,9]. This provides a direction on how to engineer carbon electrodes that are electrocatalytic, but does not require the pre-fabrication of CNT or carbon fibers. In this study, a two-step electrochemical method is developed to alternate the surface microstructure of a solid carbon electrode. When the as-prepared electrode was applied to simultaneously determine 1,4-hydroquinone (H_2Q) and pyrocatechol (CC) in a mixture, a low detection limit was obtained.

1,4-Hydroquinone and pyrocatechol have been applied in various areas such as cosmetic, pesticides and pharmaceutical industry [10,11], as well as in fundamental researches such as the 1,4-cyclohexanedione (CHD)-bromate based oscillators [12] and photo-controlled H_2Q -bromate oscillators [13]. However, the low degradability and toxicity have made H_2Q and CC important environment pollutants. The sensitive determination is important in preventing their buildup to a potentially harmful

concentration. In addition to the techniques involving expensive equipment, including liquid chromatography [14], synchronous fluorescence [15], chemiluminescence [16], gas chromatography/mass spectrometry [17], and pH based-flow injection analysis [18], low cost carbon electrochemical sensors have also been actively pursued [19-24]. The materials investigated include CNT, mesoporous carbon modified glassy carbon electrode, electrospun carbon nanofibers modified electrode and modified carbon paste, etc. In the following commercial solid carbon electrodes were directly modified and the modified electrodes exhibited high sensitivity in the detection of H₂Q and CC mixture. Moreover, the modified electrodes, as a H₂Q selective electrode, can be used for monitoring the concentration change of H₂Q in the strongly interferenced CHD-bromate oscillator that cannot be achieved with common electrodes such as gold or platinum.

6.2 Experimental Procedure

Solid carbon electrodes were purchased from Thermo Fisher Scientific Company. These carbon electrodes were sharpened into a size of 1 mm in diameter and were ultrasonically cleaned in distilled water for 30 min. The above processed carbon electrodes were then polished with a polishing strip from Radiometer Analytical and used as a working electrode to undergo 10 cycles of cyclic voltammetry (CV) in 2.0 M H₂SO₄ solution between 0 and 1.8 V at a rate of 50 mV/s. After rinsing with double distilled water, these electrodes were then placed into a 2.0 M NaOH solution for another 50 cycles of CV between 0 and 1.5 V at a rate of 50 mV/s. After the above treatments, the side of these carbon electrodes is sealed with parafilm so that only the bottom will be in contact with the analyte solution. All the above process took place under room temperature of 22 ± 1 °C.

Sodium hydroxide (NaOH, Merck KGaA, Germany, 97%), Sulfuric acid (H_2SO_4 , Aldrich, 95-98%), 1,4-hydroquinone (H_2Q , Aldrich, >99%) and pyrocatechol (CC, Aldrich, >99%) were all used as received. 1,4-cyclohexanedione-bromate reaction mixtures were prepared from aqueous stock solutions of analytical-grade sodium bromate (NaBrO_3 , Aldrich, 99%), 1.0 M, and sulfuric acid 6.0 M. 1,4-cyclohexanedione (CHD, Aldrich, 98%) was directly dissolved in the reaction mixture. Scanning electron microscopy (SEM) images were taken on a Quanta 200 FEG microscope (FEI, Inc.). Raman spectra of samples were measured using a Renishaw inVia with a 514.5 nm Ar^+ ion laser. All electrochemical experiments were performed at room temperature with a CHI660D electrochemical workstation (CHInstrument, USA). A three-electrode system was employed, using carbon electrodes as the working electrode, a Pt wire as the auxiliary electrode, and a saturated calomel electrode (SCE) as the reference electrode. The scan rate used in CV analysis was 50.0 mV/s. Parameters for differential pulse voltammetry (DPV) were at scan rate of 10 mV/s, 50 mV pulse amplitude and 200 ms pulse width. All potential values given below are referred to the potential of SCE. All kinetic measurements of H_2Q in CHD-bromate reaction were run in a thermal-jacketed 50mL glass reactor with the temperature maintained constant at $25.0 \pm 0.1^\circ\text{C}$ by a circulation water bath (ThermoNesLab RTE 7). Volume of the reaction solution was fixed as 30.0 ml unless otherwise stated. The solution was stirred by a magnetic stirrer (Fisher Isotemp) at around 600 round per minute (rpm). A Teflon cap was placed on top of the cylindrical reactor to hold five electrodes. Oscillatory profiles were monitored with a platinum electrode coupled with a $\text{Hg}|\text{Hg}_2\text{SO}_4|\text{K}_2\text{SO}_4$ reference electrode (Radiometer Analytical, XR200 and M231Pt-9), and recorded with a personal computer

connected to the pH/potential meter (Radiometer PHM220) through a PowerLab/4SP data logger. The other three electrodes were the same as the above DPV electrochemical measurements. During the oscillation, the concentration of H₂Q can be measured on site and on phase.

6.3 Results and Discussion

Figure 6.1 presents SEM images of carbon electrodes: (6.1a) before, (6.1b) after modification in H₂SO₄ solution, and (C) after further modification in NaOH solution. Figure 6.1a shows that the unmodified electrode has a flat surface. Upon the CV treatment in a 2.0 M H₂SO₄ solution, the electrode surface became rough in Figure 6.1b, where a large number of flakes were developed. This structure transformation is related to the formation of oxygen on surface and becomes less prominent if the applied upper potential is low (e.g. lower than 1.3 V). The appearance of carbon flakes does not only increase the surface area, but also creates a large number of edge plane sites. Energy dispersive X-ray spectroscopy (EDX) indicates that oxygen content on the surface decreased to about 0.4% of carbon atoms (atomic ratio), as opposed to 1% on the unmodified electrode. In Figure 6.1c the surface becomes more irregular, where at certain regions columns resemble a stack of carbon flakes can be seen. Another change, as illustrated by EDX in Figure 6.1d, the oxygen content decreased to about 0.1%, suggesting the removal of oxides. Raman scattering is widely used to evaluate the density of edge plane sites by monitoring the ratio I_D/I_G . It is generally accepted that a larger I_D/I_G value represents more disorder and defects and better electrochemical activity [25]. The band locations for both of the unmodified (6.1e) and modified carbon surface (6.1f) are similar, but the I_D/I_G ratios are different (1.25 and 1.61, respectively). The Raman results

imply a higher density of edge plane sites on the modified carbon surface compared to the unmodified.

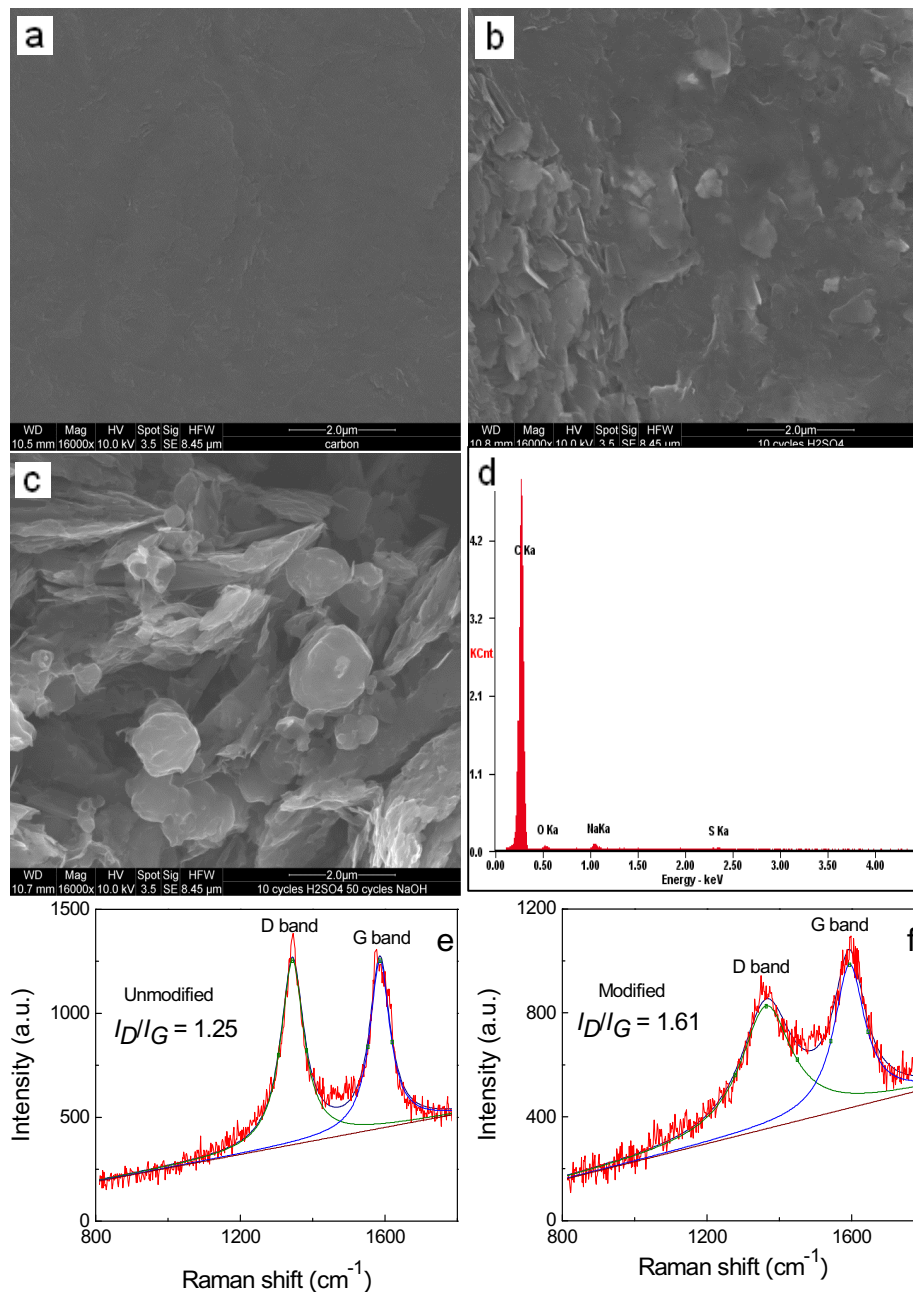


Figure 6.1 SEM images of carbon electrodes: (a) unmodified, (b) modified in H_2SO_4 and (c) modified in H_2SO_4 and NaOH solution. Panel (d) is an EDX spectrum of the electrode shown in (c). Raman spectra of carbon electrodes: (e) unmodified and (f) modified corresponded to a 50% intensity of 514.5 nm exciting laser.

The above results demonstrate that the structure transformation can be readily achieved through CV in acid and then in alkaline solution. We have also examined the protocol of performing structure/chemical modification of the carbon electrode in H_2SO_4 solution only. Although electrodes prepared in such a way did show greatly increased current, they could not produce isolated anodic peaks in a mixture of H_2Q and CC. Note that the unmodified electrode could not produce separated anodic peaks either. When electrodes were only modified in NaOH solution, EDX spectra indicated that there was no decrease in the oxygen content (i.e. no chemical modification). They could produce two well separated anodic peaks in a H_2Q and CC mixture, but will lose their sensitivity after two days.

Figure 6.2a presents the CVs of 0.001 M H_2SO_4 solution at carbon electrodes of (1) unmodified, (2) modified in H_2SO_4 , and (3) modified in H_2SO_4 and NaOH solution shown in Figure 6.1. Notably, there is a significant increase in the background (charging/discharging) current after the electrode was processed in H_2SO_4 solution. This behavior arises from the increase of the total surface area, transforming the electrode into a better capacitor [26]. Interestingly, as shown in curve 3, the background current decreased after the electrode was further treated in NaOH solution. This decrease may result from the combination of two factors: (1) the decrease of total surface area as the structure transformation evolved deeper into this solid electrode, and (2) removal of oxides from the surface. Figure 6.2b presents the CVs of 0.001 M H_2SO_4 solution containing 20.0 μM of H_2Q and CC at (1) unmodified and (2) fully modified electrode. The voltammogram 1 is qualitatively the same as that in Figure 6.2a, suggesting that the untreated electrode is not sensitive to H_2Q and CC. Increasing the concentration of H_2Q

and CC to above $50\text{ }\mu\text{M}$ will lead to one anodic peak in the CV. However, no separated anodic peaks could be obtained, indicating that carbon electrode cannot simultaneously determine H_2Q and CC. With the modification two well separated anodic peaks are seen in the voltammogram 2, where the potential separation between the anodic peaks is slightly above 100 mV . The redox peak separation is about 47 mV for both H_2Q and CC.

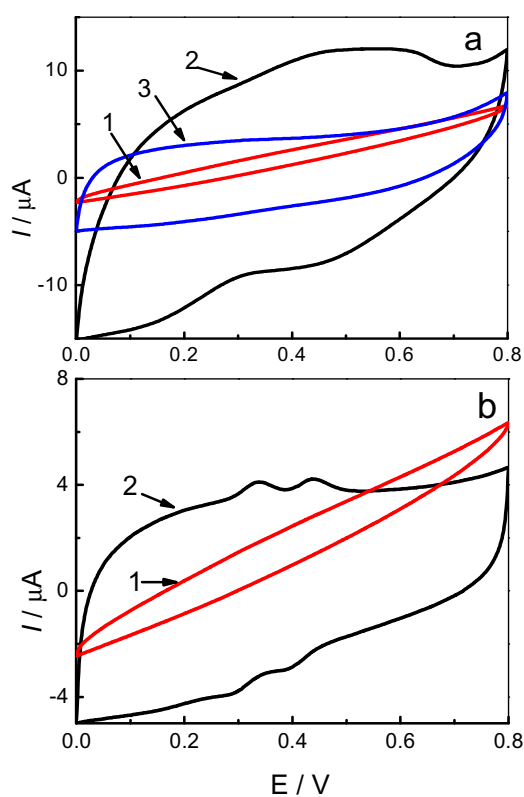


Figure 6.2 (a) CVs at carbon electrodes of unmodified (curve 1), modified in H_2SO_4 (curve 2) and modified in H_2SO_4 and NaOH solution (curve 3) measured in a $0.001\text{ H}_2\text{SO}_4$ solution; (b) CVs of a $0.001\text{ H}_2\text{SO}_4$ solution containing $20.0\text{ }\mu\text{M}$ of H_2Q and CC at carbon electrode (curve 1) and modified carbon electrode (curve 2).

For the simultaneous and quantitative determination of H₂Q and CC DPV spectra at different concentrations of H₂Q were recorded in Figure 6.3a, where CC concentration was kept at 50 μM. When the H₂Q concentration was increased to 3.0 μM, an anodic peak at the potential of 0.3 V became discernible. The inset shows that the peak current varies linearly with H₂Q concentration between 2 and 50.0 μM with $R = 0.996$. Importantly, the anodic peak current of CC is almost uninfluenced by the increase of H₂Q concentration, suggesting that oxidations of CC and H₂Q at the modified electrode are independent of each other. With the DPV technique the detection limit of H₂Q is 2.0 μM in the presence of 50 μM CC interference. Without CC, the low limit is 0.8 μM. This low limit is comparable to that reported recently with CNT and carbon nanofibers [22,23]. There is a detectable current change when H₂Q is decreased from 2.0 to 0.1 μM, implying that the detection limit with an amperometric technique would be much lower. Figure 6.3b presents DPV responses at different concentrations of CC while H₂Q was kept constant at 50.0 μM. Similar to the scenario seen in Figure 6.3A, the anodic peak current of H₂Q stayed almost constant as CC concentration was increased from 0.1 to 100 μM, further confirming that this modified electrode can be employed for simultaneous determination of dihydroxybenzene isomers. The inset in Figure 6.3b illustrates that the peak current increases linearly with CC concentration between 5 and 50 μM with $R = 0.997$. The presence of H₂Q causes that no discernible peak could develop until CC reaches above 5 μM. In the absence of H₂Q, the low limit is 2 μM. From the measurements conducted above the detection sensitivity is calculated to be 66.7 nA/μM for H₂Q and 83.8 nA/μM for CC.

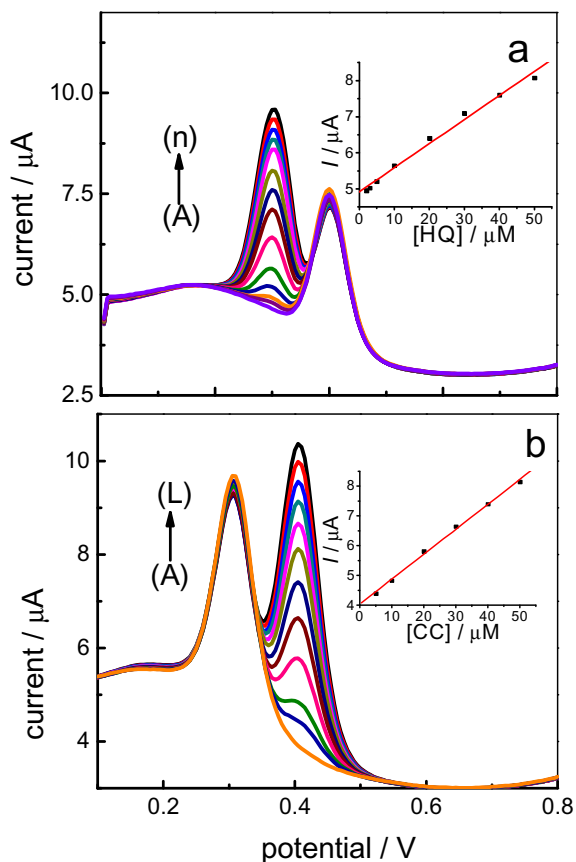


Figure 6.3 DPVs at a modified carbon electrode in (6.2a) 50 μM CC and different concentrations of H_2Q : 0.1, 2.0, 3.0, 5.0, 10.0, 20.0, 30.0, 40.0, 50.0, 60.0, 70.0, 80.0, 90.0, and 100.0 μM (from A to N), and (6.2b) 50 μM H_2Q and different concentrations of CC: 0.1, 5.0, 10.0, 20.0, 30.0, 40.0, 50.0, 60.0, 70.0, 80.0, 90.0 and 100.0 μM (from A to L). The insets show the calibration plots of CC and H_2Q versus peak currents.

In order to test the feasibility of using the above modified carbon electrode to follow the concentration of hydroquinone in a complex environment such as in an oscillatory reaction in which hydroquinone presents as an intermediate. In Figure 6.4 the situ DPV measurements of a bromate-CHD reaction were performed with the modified carbon electrode. Compositions of the reaction solution were $[\text{CHD}] = 0.1 \text{ M}$, $[\text{NaBrO}_3] = 0.1 \text{ M}$,

and $[\text{H}_2\text{SO}_4] = 0.6 \text{ M}$. Under such conditions, the system exhibits spontaneous oscillations with an induction time of 6400 s. Pt redox potential presented in Figure 6.4a illustrates that each oscillation cycle lasts between 3 to 5 minutes.

The in situ DPV tests would allow us to obtain the concentration of H_2Q from their peak current, assuming that there is no other interferent in the reaction system. Based on the parameters used in our study, each DVP spectrum requires about 15 s to complete, therefore we would be able to collect more than 10 spectra within each oscillation period. As shown in Figure 6.4b, these peak currents do oscillate in time, with a frequency the same as that recorded through the redox potential. Further improvement of the measurement (i.e., obtaining more points within each oscillation) relies on shortening the DPV improvement. DPV spectra presented in Figure 6.4c indicate that during the induction time period the concentration of hydroquinone is very low, spontaneous oscillations emerge after the hydroquinone concentration reach a threshold value. The measurements in Figure 6.4b indicate that hydroquinone accumulates in time. Whether such a phenomenon is true needs to be confirmed later, by testing the contribution of other interferents. We would like to note that when gold or Pt electrodes were used to perform the above DPV measurements, no peaks could be observed due to their poor selectivity.

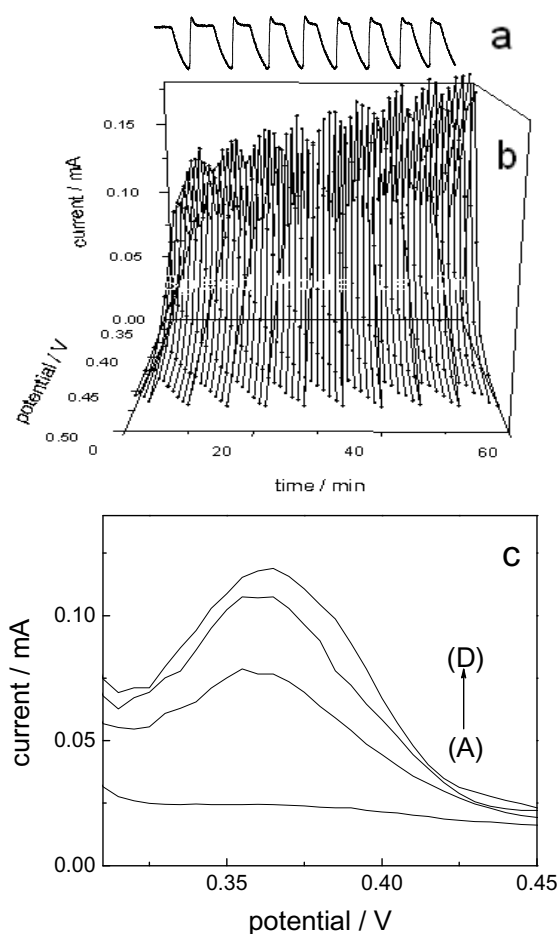


Figure 6.4 Oscillation profiles (a) and corresponding DPV situ tests (b), other reaction conditions were $[\text{CHD}] = 0.1 \text{ M}$, $[\text{NaBrO}_3] = 0.1 \text{ M}$, $[\text{H}_2\text{SO}_4] = 0.6 \text{ M}$. (c) DPV situ measurements during the induction time of CHD-bromate chemical oscillation, (A) right after prepared solution, (B) 2000 s, (C) 4000 s, (D) 6000 s. Oscillation was occurred at around 6400 s.

In Figure 6.5, DPV spectra at different concentrations of H_2Q were conducted in order to establish the standard calibration curve. The two series of experiments illustrate that the peak potential shifted positively as the acid concentration of the electrolyte was increased. In the same solution, however, the peak potential stays constant when hydroquinone concentration was increased. In Figure 6.5a, the acid concentration is the same as that used in Figure 6.4. Comparison of the DVP spectra in Figures 6.4 and 6.5

suggests that H_2Q concentration in the bromate-CHD oscillator is likely at the order of millimolar.

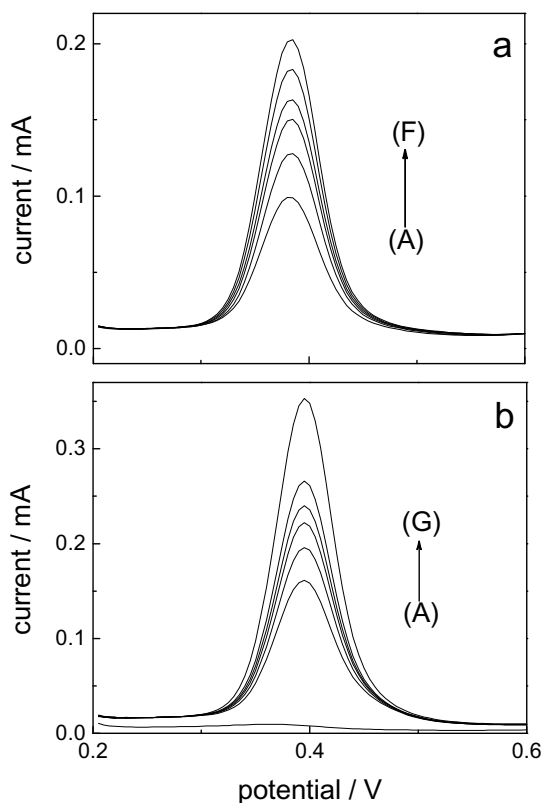


Figure 6.5 DPVs of H_2Q in different H_2SO_4 acid solution (a) 0.6 M and (b) 1.0 M. H_2Q concentrations are 5.0, 6.0, 7.0, 8.0, 9.0, 10.0 mM (from A to F in panel a), and 0, 6.0, 7.0, 8.0, 9.0, 10.0, 15.0 mM (from A to G in panel b).

6.4 Conclusions

A two-step protocol is developed in this study to modify the surface microstructure and chemical compositions of solid carbon electrodes. The modified structure is stable for repeated usage in the electroanalysis of dihydroxybenzene. Using the DPV technique, the modified electrode can simultaneously determine dihydroxybenzene isomers, in which the low detection limit of $2.0 \mu\text{M}$ is as good as that obtained with CNT or carbon

fibers [19-24]. After conducting 30 DPV scans, the calculated relative standard deviation (RSD) is 0.99% for H₂Q and 1.25% for CC, indicating that the modified electrode is robust. We would like to note that, although this behavior has not been reported in CNT or carbon nanofibers based electrodes [19-24], our experiments show that the extended usage of the above modification carbon electrode will lead to the accumulation of dihydroxybenzene on the surface, as evidenced by the occurrence of a small anodic peak in the DPV of 0.001 M H₂SO₄ solution. Immersing the electrode in a 2.0 M NaOH solution for 30 s will remove the residues. On a potential application, such modified carbon electrode can work in a more strongly interferenced environment, such as CHD-bromate reactions. By using situ DPV tests during the CHD-bromate oscillation, we successfully determined the oscillation range of H₂Q concentration, which is significant to understand intermediate dynamics and oscillation mechanism.

6.5 References

- 1 I. M. Musameh, J. Wang, A. Merkoci and Y. Lin, *Electrochem. Commun.*, 2002, 4, 743.
- 2 F. H. Wu, G. C. Zhao and X. W. Wei, *Electrochem. Commun.*, 2002, 4, 690.
- 3 N. S. Lawrence, R. P. Deo and J. Wang, *Anal. Chim. Acta*, 2004, 517, 131.
- 4 J. S. Ye, Y. Wen, W. D. Zhang, L. M. Gan, G. Q. Xu and F. S. Sheu, *Electrochem. Commun.*, 2004, 6, 66.
- 5 A. Salimi, R. Hallaj and G. R. Khayatian, *Electroanalysis*, 2005, 17, 873.
- 6 Y. P. Ding, W. L. Liu, Q. S. Wu and X. G. Wang, *J. Electroanal. Chem.*, 2005, 575, 275.
- 7 F. Jiang, S. Wang, J. J. Lin, H. L. Jin, L. J. Zhang, S. M. Huang and J. Wang, *Electrochem. Commun.*, 2011, 13, 363.

- 8 C. E. Banks, R. R. Moore, T. J. Davies and R. G. Compton, *Chem. Commun.*, 2004, 16, 1804.
- 9 C. E. Banks and R. G. Compton, *Analyst*, 2006, 131, 15.
- 10 A. Asan and I. Isildak, *J. Chromatogr. A*, 2003, 988, 145.
- 11 P. K. Tewari and A. K. Singh *Talanta*, 2001, 53, 823.
- 12 I. Szalai, K. Kurin-Csörgei, I. R. Epstein and M. Orbán, *J. Phys. Chem. A*, 2003, 107, 10074.
- 13 B. Zhao and J. Wang, *Chem. Phys. Lett.*, 2006, 430, 41.
- 14 H. Cui, C. X. He and G. W. Zhao, *J. Chromatogr. A*, 1999, 855, 171.
- 15 M. F. Pistonesi, M. S. Di Nezio, M. E. Centurión, M. E. Palomeque, A. G. Lista and B. S. F. Band, *Talanta*, 2006, 69, 1265.
- 16 S. F. Li, X. Z. Li, J. Xu and X. W. Wei, *Talanta*, 2008, 75, 32.
- 17 S. C. Moldoveanu and M. Kiser, *J. Chromatogr. A*, 2007, 1141, 90.
- 18 J. A. Garcia-Mesa and R. Mateos, *J. Agric. Food Chem.*, 2007, 55, 3863.
- 19 H. L. Qi and C. X. Zhang, *Electroanalysis*, 2005, 17, 832.
- 20 Z. H. Wang, S. J. Li and Q. Z. Lv, *Sens. Actuators B: Chem.*, 2007, 127, 420.
- 21 D. D. Zhang, Y. G. Peng, H. L. Qi, Q. Gao and C. X. Zhang, *Sens. Actuators B*, 2009, 136, 113.
- 22 Q. H. Guo, J. S. Huang, P. Q. Chen, Y. Liu, H. Q. Hou and T. Y. You, *Sens. Actuators B*, 2012, 163, 179.
- 23 Y. P. Ding, W. L. Liu, Q. S. Wu and X. G. Wang, *J. Electroanal. Chem.*, 2005, 575, 275.
- 24 J. Bai, L. P. Guo, J. C. Ndamaniha and B. Qi, *J. Appl. Electrochem.*, 2009, 39,

2497.

25 M. Pumera, T. Sasaki and H. Iwai, Chem. Asian J., 2008, 3, 2046.

26 Y. W. Zhu, S. Murali, M. D. Stoller, K. J. Ganesh, W. W. Cai, P. J. Ferreira, A. Pirkle, R. M. Wallace, K. A. Cychosz, M. Thommes, D. Su, E. A. Stach and R. S. Ruoff, Science, 2011, 332, 1537.

Chapter 7: Conclusions and Perspective

7.1 Conclusions

By employing an organic substrate which reacts with bromine at a moderate rate, this research constructed a chemical oscillator to explore the importance of bromine removal in bromate-based chemical oscillations. In Chapter 2, complex oscillatory behavior was indeed observed in the ferroin-bromate-metol reaction conducted in a batch reactor, where the bromine removal was accomplished via simply flowing air or nitrogen gas above the surface of the reaction solution [1]. In addition, the bromine removal also greatly shortened the induction time of those spontaneous oscillations. The above results highlight the significance of bromine concentration in those bromate-based chemical oscillations. During the oscillatory process periodic color changes between red and green were observed, which allowed us to subsequently investigate the spatiotemporal behavior of the ferroin-bromate-metol oscillator in spatially extended media. Preliminary exploration in a capillary tube led to the observation of pulse merging and propagation failure phenomena at the conditions where the ends of the capillary tube were exposed to air.

Another peculiar behavior observed in the ferroin-bromate-metol system is that the nonlinear behavior strongly also depends on the age of the metol stock solution. Through mass spectroscopy study, our experiments suggest that metol decomposes in air, presumably via reacting with oxygen, to produce hydroquinone and then benzoquinone. The above hypothesis was supported by the kinetics study in which qualitatively the same nonlinear phenomena were achieved by adding certain amounts of 1,4-hydroquinone into

a freshly prepared metol solution. The influence of oxygen on the nonlinear behavior was further confirmed by using air to replace nitrogen stream to remove bromine, where sequential oscillations were observed. Consistent experimental results were obtained showing that increasing the amount of 1,4-hydroquinone in the system causes the transition from simple to sequential oscillations, and increasing oxygen concentration (i.e. enhancing hydroquinone production) also resulted in sequential oscillations. Since complex behavior (i.e., sequential oscillations) emerged after the initial addition of hydroquinone, their appearance is proposed to arise from the competition of two autocatalytic cycles: (1) 1,4-hydroquinone and bromine dioxide radicals reaction, and (2) ferroin and bromine dioxide reaction. Mass spectrometry and NMR measurements illustrate that the major products in the ferroin-bromate-metol systems are 1,4-benzoquinone and bromobenzoquinones. The presence of bromobenzoquinones is particularly inspiring, which motivates us to use 1,4-benzoquinone or closely related reagents to modulate bromine concentration in bromate-based chemical oscillators.

Based on the hypothesis reached in Chapter 2, a new type of minimal bromate oscillator was successfully constructed in Chapter 3, which is ferroin-bromate-benzoquinone reaction [2]. Different from other BZ-type of oscillators, this newly developed bromate oscillator relies on the reaction between ferroin and bromide ions to regenerate ferroin and the organic substrate benzoquinone does not react with ferroin. Beck and co-workers have attempted to utilize the reduction of ferroin by bromide ions to construct a minimal ferroin-bromate oscillator. However, spontaneous oscillations could only be observed in a CSTR [3], where bromide ions were needed in a continuously fed fashion. In this new minimal bromate oscillator, the modulation of bromide ions is

achieved by the bromination of 1,4-benzoquinone with bromine/HOBr, which makes it feasible to achieve transient spontaneous oscillations in a closed system. This research also highlights that the reduction of ferriin by bromide ions can become critical in bromate-based chemical oscillators. For example, in a spatially extended medium, the high concentration of bromide ions in the tail of the preceding pulse may interact with the high concentration of ferriin in the front of the following pulse, generating the phenomena of merging pulses. Indeed, merging behavior has been reported in the ferroin-bromate-CHD medium [4], in which benzoquinone has been detected as one of the final products [5, 6].

The ferroin-bromate-1,4-benzoquinone oscillator developed in chapter 3 exhibited great photosensitivity, especially to light within the wavelength range 500 ± 40 nm. Experiments conducted in chapter 4 illustrate that, depending on the intensity, light could enhance or quench the chemical oscillations [7]. Since the applied light intensity was significantly lower than that used in the earlier studies of bromate-benzoquinone photochemical oscillator [8], the photo-reduction of 1,4-benzoquinone to 1,4-hydroquinone is unlikely to be responsible for the dramatic photosensitivity. Mass spectrometry and NMR measurements indicate light-enhanced bromination of benzoquinone. Meanwhile, UV/Vis spectroscopy suggests that light accelerates the reduction of ferriin by bromide ions, which consumes bromide ions and supplies ferroin for the autocatalytic cycle and therefore could be responsible for the observed constructive influences on the nonlinear behavior. The constructive influences include both increasing the oscillation frequency and the number of oscillation peaks. When light intensity was increased monotonically, the influence of light underwent a transition from

constructive to inhibitory, which may result from the autocatalytic feedback overwhelming the production of inhibitor due to more intense illumination. More systematic investigations are required to confirm the above proposed mechanisms.

To gain further insight into the newly developed minimal bromate oscillator, in the experiments conducted in chapter 5 cerium was used to replace ferroin as the metal catalyst [9]. Cerium has a higher redox potential than ferroin and thus is expected to form a slower autocatalytic cycle, but a faster redox reaction with bromide ions. The cerium-bromate-benzoquinone system exhibited transient complex oscillations (i.e., sequential oscillations). In the presence of a rather weak illumination, those transient chemical oscillations could last for a week! Similar to the ferroin-bromate-benzoquinone system, the cerium system is also most sensitive to the light with the wavelength of 500 ± 40 nm. However, the influences of light on the nonlinear behavior become richer, where as the light intensity was increased gradually, the effect of light goes through constructive, inhibitory and then constructive again. Numerical simulations qualitatively reproduced those spontaneous oscillations in the minimal bromate oscillator.

Besides light-enhanced bromination of benzoquinone and light-accelerated reaction between the metal ions and bromide ions, we also investigated the effect of light on the stability of 2-bromo-1,4-benzoquinone (QBr), a substance detected as the major bromination product of 1,4-benzoquinone. Characterizations with UV/Vis spectroscopy and a selective bromide ion electrode confirmed the occurrence of photodecomposition of QBr. NMR and GC/MS measurements suggest that the photo-decomposition of QBr is accompanied by bromide production, in which QBr photo decomposes to hydroxybenzoquinone. Simulations with a core model of FKN mechanism modified to

incorporate the production of bromobenzoquinone and the decomposition of QBr have successfully reproduced the influence of light on the oscillatory behavior. This low cost and long-lasting chemical oscillator provides a good model system for exploring perturbed nonlinear dynamics that are frequently encountered in nature.

A new kind of modified carbon electrode was developed in chapter 6 for the detection of hydroquinone in bromate-CHD and related chemical oscillators. This low cost, easy to fabricate electrode is stable and can simultaneously detect 1,4-hydroquinone and 1,2-hydroquinone [10], providing an alternative to those carbon nanotube-based electrodes for the sensitive detection of dihydroxybenzene isomers. In this study an easy two-step protocol was developed to electrochemically modify the surface structure in a strong acid solution and chemical compositions of the solid carbon electrode in a strong alkaline solution. By using differential pulse voltammetry (DPV), the modified electrode can simultaneously determine dihydroxybenzene isomers with a low detection limit of 2.0 μM , which is as good as that obtained with carbon nanotubes or carbon nanofibers [11-16]. When being used to monitor the concentration of 1,4-hydroquinone in the CHD-bromate oscillator, the oscillation waveform resembles what was detected with a platinum electrode. It is the first time that a modified carbon electrode can be employed as a situ sensor for detecting hydroquinone.

7.2 Future Work

Understanding the reaction mechanisms of these newly developed bromate-based oscillators will be an important aspect of the future work:

- (1) More detailed elementary reactions need to be identified experimentally and theoretically, which include the light enhanced bromination and photo-

decomposed reactions. How the light wavelength and intensity affect the kinetics of those reactions needs to be further quantified.

- (2) We have attempted to detect radicals during the oscillation with our department electron paramagnetic resonance (EPR) machine, but failed to determine the semiquinone radicals. The reason may be due to the low magnetic field X band or that the life time of the radicals is too short in aqueous solution. If the life time of radicals is too short to be measured by EPR, future work may apply radical trapping methods, in which the reactive radicals react with radical trapping agents, such as DMPO derivatives, to produce a stable radical with a longer life time.
- (3) Many controlling factors which have not been systematically explored during the present experiments, such as temperature influence, different kinds of metal catalysts (manganese, ruthenium, etc) can be carried out in the future.
- (4) The study of pattern formation in the minimal bromate oscillators. The key challenges are the color change and life time of those oscillations. The ferroin-based system has an obvious color change but with a short oscillation window; cerium-based system has a very long oscillation window (> 1 week) in batch conditions but with no visible color change. Future work may focus on the combination of these two metal catalysts in order to get a long-lasting and obvious color changing oscillation.

Another very exciting future project is the application of bromate oscillators in facet-controlled synthesis of nanoparticles. Recently, scientists are becoming more and more aware of the significant role of reaction and diffusion control in nanoparticle synthesis.

One representative example is bimetallic nanoparticles synthesized via directly manipulating the nucleation reaction at varied temperature and growth rate with different injection rates, resulting in new nano-structures [17]. Another way to control the structure of nanoparticles such as gold, palladium, platinum and rhodium is to use halide or pseudo-halide anions [18-21]. The formation of different facets is determined by the concentration of halide ions, which preferentially occupy one facet such as {001} of the Pd. Such a static occupation by halide anions can be replaced by several bromate-based oscillators in which bromide concentration evolves in an oscillatory fashion, such as the CHD-bromate oscillator [22] and 1,4-benzoquinone-bromate photochemical oscillator [8]. As a proof of concept that it is possible to apply these oscillators to modulate the shape and structure of nanoparticles, preliminary work was carried out in the CHD-bromate oscillator.

Reactions were run in a thermal-jacketed 50 mL glass reactor with the temperature maintained constant at $25.0 \pm 0.1^\circ\text{C}$ by a circulation water bath (ThermoNesLab RTE 7). The solution was stirred by a magnetic stirrer (Fisher Isotemp) at around 600 round per minute (rpm). A Teflon cap was placed on top of the cylindrical reactor to hold electrodes. Volume of the reaction solution was fixed as 30.0 mL. Oscillatory profiles were monitored with a platinum electrode coupled with a $\text{Hg}|\text{Hg}_2\text{SO}_4|\text{K}_2\text{SO}_4$ reference electrode (Radiometer Analytical, XR200 and M231Pt-9). All measurements were recorded with a personal computer connected to the pH/potential meter (Radiometer PHM220) through a PowerLab/4SP data logger. Reaction mixtures were prepared from aqueous stock solutions of analytical-grade sodium bromate (NaBrO_3 , Aldrich, 99%), 1.0 M, and sulfuric acid (H_2SO_4 , Aldrich, 95-98%), 6.0 M. 1,4-cyclohexandione (CHD,

Aldrich, 98%) and Palladium oxide hydrate (PdO, Aldrich) were directly dissolved in the reaction mixture. Scanning electron microscopy (SEM) images were taken on a Quanta 200 FEG microscope (FEI, Inc.)

As shown in Figure 7.1, CHD-bromate reaction was carried under different conditions: (a) without adding PdO in the reaction mixture, and (b) adding 20 mg PdO in the reaction mixture at around 3,800 seconds. Compositions of the reaction solution were $[\text{CHD}] = 0.1 \text{ M}$, $[\text{NaBrO}_3] = 0.1 \text{ M}$, $[\text{H}_2\text{SO}_4] = 0.8 \text{ M}$. In (a), spontaneous oscillations took place after about 6,000 seconds. When 20 mg PdO was added in experiment (b), the oscillation behavior was greatly influenced, in which the number of oscillations was largely reduced and the oscillatory frequency was decreased. This result signifies PdO does interact with CHD-bromate reaction, resulting in a slowdown of the autocatalytic cycle.

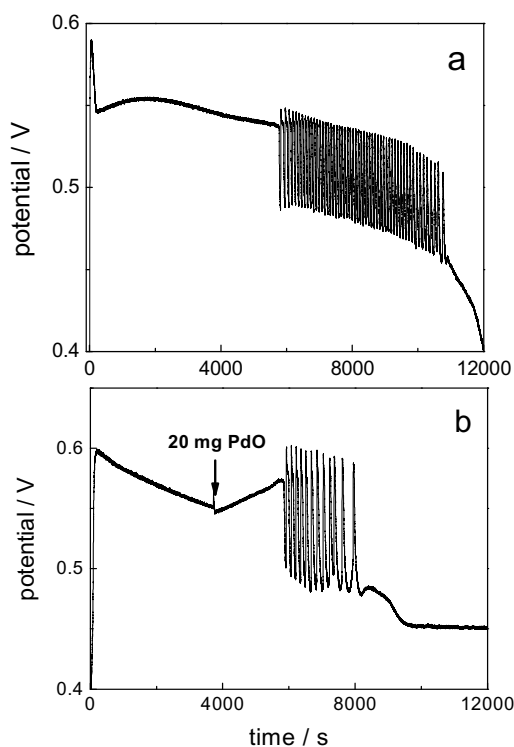


Figure 7.1 Time series of CHD-bromate system without or with PdO, $[\text{CHD}] = 0.1 \text{ M}$, $[\text{NaBrO}_3] = 0.1 \text{ M}$, $[\text{H}_2\text{SO}_4] = 0.8 \text{ M}$, (a) without adding PdO, (b) adding 20 mg PdO at around 3,800 s.

In order to verify the factor of the reaction between CHD-PdO and 1,4-hydroquinone-PdO, Figure 7.2 shows two kinds of elementary reactions, (a) adding 20 mg PdO in the CHD solution at around 3,800 seconds, (b) adding 20 mg PdO in the 1,4-hydroquinone solution at around 3,800 seconds. As shown in (a), after adding PdO, the potential almost remained constant, but in (b), the potential sharply decreased after adding PdO. The results indicate that the reaction between 1,4-hydroquinone and PdO does occur in such conditions.

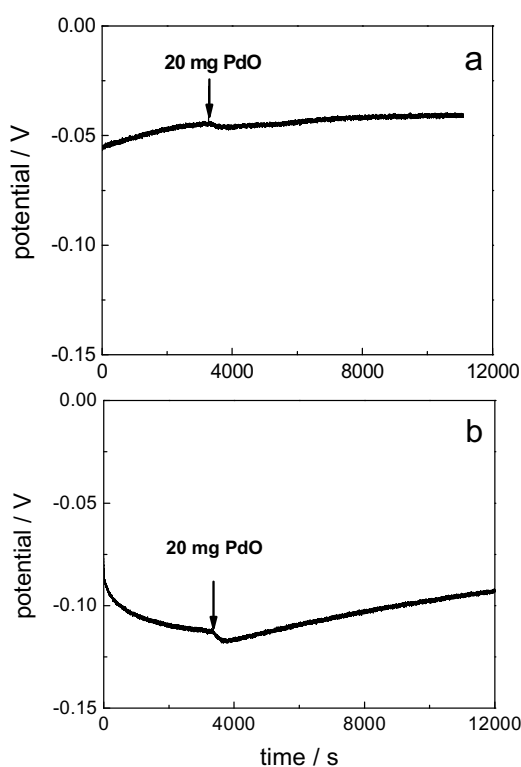


Figure 7.2 Time series of CHD and H₂Q system with PdO, (a) [CHD] = 0.1 M, [H₂SO₄] = 0.8 M, adding 20 mg PdO at around 3800 s, (b) [H₂Q] = 0.1 M, [H₂SO₄] = 0.8 M, adding 20 mg PdO at around 3800 s.

Figure 7.3 presents SEM images of the solid products collected: (a) right after oscillation, (b) one day, (c) two days, (d) four days. All other reaction conditions were the same as in Figure 7.1b. The precipitates were cleaned by diluted water and dried with nitrogen steam. As the reaction time increased, the surface of PdO became brighter and the morphology becomes more porous, EDX data shows the ratio of Pd/O increased from around 1:1 to almost 1.7:1, which means PdO is reduced by 1,4-hydroquinone in the CHD-bromate system.

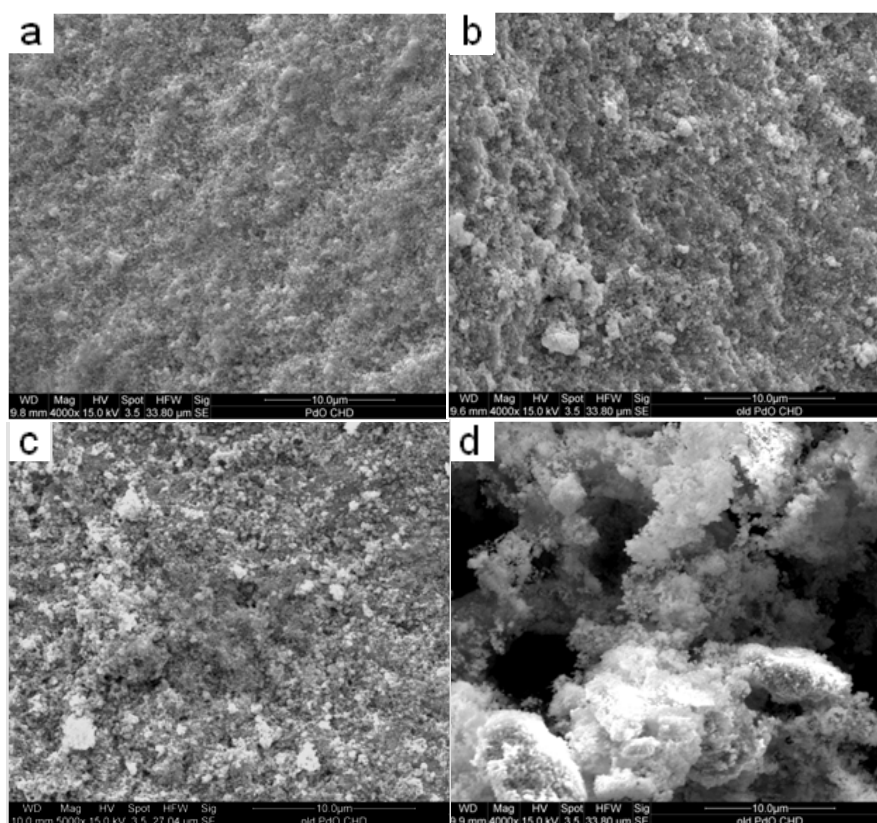


Figure 7.3 SEM images of CHD-Bromate-PdO system with different aging time. (a) right after oscillation, (b) one day, (c) two days, (d) four days. All other reaction conditions were the same as in Figure 7.1b.

The above results lend positive support on the proposed research of fabricating palladium nanoparticles in the CHD-bromate oscillator. However, there still is much work to do regarding the improvement of the chemical oscillator. For example, the oscillation window is too short to affectively influence the shape of Pd nanoparticles, therefore, new types of oscillators need to be designed to meet the requirements, which have long-lasting oscillations with bromide ions and 1,4-hydroquinone as a key intermediate.

7.3 References

- 1 J. Li and J. Wang, Chem. Phys. Lett., 2011, 508, 320.
- 2 J. Li and J. Wang, J. Phys. Chem. A, 2012, 116, 386.
- 3 M. T. Beck, G. Bazsa, K. Hauck and Ber. Bunsenges. Phys. Chem., 1980, 84, 408.
- 4 N. Manz and O. Steinbock, Chaos, 2006, 16, 037112.
- 5 I. Szalai, K. Kurin-Csörgei and M. Orbán, Phys. Chem. Chem. Phys., 2002, 4, 1271.
- 6 I. Szalai, K. Kurin-Csörgei, I. R. Epstein and M. Orbán, J. Phys. Chem. A, 2003, 107, 10074.
- 7 J. Li and J. Wang, J. Phys. Chem. A, 2012, 116, 8130.
- 8 B. Zhao and J. Wang, Chem. Phys. Lett., 2006, 430, 41.
- 9 J. Li and J. Wang, Phys. Chem. Chem. Phys., 2011, 13, 15539.
- 10 X. F. Hu, J. Li and J. Wang, Electrochem. Commun., 2012, 21, 73.
- 11 H. L. Qi and C. X. Zhang, Electroanalysis, 2005, 17, 832.
- 12 Z. H. Wang, S. J. Li and Q. Z. Lv, Sens. Actuators B: Chem., 2007, 127, 420.

- 13 D. D. Zhang, Y. G. Peng, H. L. Qi, Q. Gao and C. X. Zhang, *Sens. Actuators B*, 2009, 136, 113.
- 14 Q. H. Guo, J. S. Huang, P. Q. Chen, Y. Liu, H. Q. Hou and T. Y. You, *Sens. Actuators B*, 2012, 163, 179.
- 15 Y. P. Ding, W. L. Liu, Q. S. Wu and X. G. Wang, *J. Electroanal. Chem.*, 2005, 575, 275.
- 16 J. Bai, L. P. Guo, J. C. Ndamaniha and B. Qi, *J. Appl. Electrochem.*, 2009, 39, 2497.
- 17 K. Lee, M. Kim and H. Kim, *J. Mater. Chem.*, 2010, 20, 3791.
- 18 B. T. Sneed, C. H. Kuo, C. N. Brodsky, and C. K. Tsung, *J. Am. Chem. Soc.*, 2012, 134, 18417.
- 19 W. X. Niu, L. Zhang and G. B. Xu, *ACS Nano*, 2010, 4, 1987.
- 20 W. X. Niu and G. B. Xu, *Nano Today*, 2011, 6, 265.
- 21 J. G. Xu, A. R. Wilson, A. R. Rathmell, J. Howe, M. F. Chi and B. J. Wiley, *ACS Nano*, 2011, 5, 6119.
- 22 B. Zhao and J. Wang, *J. Phys. Chem. A*, 2005, 109, 3647.

Appendix A Code of the Simulation in Chapter 2

```

! solve coupled CHD-BZ reaction model
! with RK4 & euler method and 5-point & 9-point explicit finite difference method
! modified by JunLi
! 2009/10/09
!-----
!-----the simulation_parameters-----
module simulation_parameters
    implicit none
    integer, parameter :: lx=1025,ly=1025 !lx=513,ly=513
    integer, parameter :: nstep=200000
    integer(kind=4) :: no_record=2000
    real(kind=8) :: h=0.00005
    character(len=8) time
end module
!-----
!-----the system_parameters-----
module system_parameters
    implicit none
    real(kind=8) :: e1=0.05
    real(kind=8) :: e2=0.001
    real(kind=8) :: e3=0.8
    real(kind=8) :: q=0.04
    real(kind=8) :: r=0.4
    real(kind=8) :: s=0.4
    real(kind=8) :: f1=1.0
    real(kind=8) :: f2=1.0
    real(kind=8) Du
    parameter(Du=0.000001)
    real(kind=8) Dv
    parameter(Dv=0.00001)
    real(kind=8) Dw
    parameter(Dw=0.00001)
    real(kind=8) Dz
    parameter(Dz=0.00001)
end module
!-----
!-----main program-----
program main
    use simulation_parameters
    use system_parameters
    implicit none

    integer ix,iy,ncount

```

```

real(kind=8):: u(0:lx+1,0:ly+1),unew(lx,ly)
real(kind=8):: v(0:lx+1,0:ly+1),vnew(lx,ly)
real(kind=8):: w(0:lx+1,0:ly+1),wnew(lx,ly)
real(kind=8):: z(0:lx+1,0:ly+1),znew(lx,ly)
real(kind=8):: site1(1:nstep)
real(kind=8):: site2(1:nstep)
real(kind=8):: site3(1:nstep)
real(kind=8):: site4(1:nstep)
real(kind=8):: dr,sldr
real(kind=8):: fu(1:4),fv(1:4),fw(1:4),fz(1:4)

real(kind=8),external :: funcu,funcv,funcw,funcz

dr=0.0002
slidr=h/(dr*dr)

call clock(time)
write(*,"('start time=',A10)") time

call initialize(u,v,w,z)
  do ncount=1,nstep
    call boundary_nonflux(u,v,w,z)

    do ix=1,lx
      do iy=1,ly

fu(1)=funcu(u(ix,iy),v(ix,iy),w(ix,iy),z(ix,iy))
fv(1)=funcv(u(ix,iy),v(ix,iy),w(ix,iy),z(ix,iy))
fw(1)=funcw(u(ix,iy),v(ix,iy),w(ix,iy),z(ix,iy))
fz(1)=funcz(u(ix,iy),v(ix,iy),w(ix,iy),z(ix,iy))

fu(2)=funcu(u(ix,iy)+h/2*fu(1),v(ix,iy)+h/2*fv(1),w(ix,iy)+h/2*fw(1),z(ix,iy)+h/2*fz(1))
fv(2)=funcv(u(ix,iy)+h/2*fu(1),v(ix,iy)+h/2*fv(1),w(ix,iy)+h/2*fw(1),z(ix,iy)+h/2*fz(1))
fw(2)=funcw(u(ix,iy)+h/2*fu(1),v(ix,iy)+h/2*fv(1),w(ix,iy)+h/2*fw(1),z(ix,iy)+h/2*fz(1))
fz(2)=funcz(u(ix,iy)+h/2*fu(1),v(ix,iy)+h/2*fv(1),w(ix,iy)+h/2*fw(1),z(ix,iy)+h/2*fz(1))

fu(3)=funcu(u(ix,iy)+h/2*fu(2),v(ix,iy)+h/2*fv(2),w(ix,iy)+h/2*fw(2),z(ix,iy)+h/2*fz(2))
fv(3)=funcv(u(ix,iy)+h/2*fu(2),v(ix,iy)+h/2*fv(2),w(ix,iy)+h/2*fw(2),z(ix,iy)+h/2*fz(2))
fw(3)=funcw(u(ix,iy)+h/2*fu(2),v(ix,iy)+h/2*fv(2),w(ix,iy)+h/2*fw(2),z(ix,iy)+h/2*fz(2))
fz(3)=funcz(u(ix,iy)+h/2*fu(2),v(ix,iy)+h/2*fv(2),w(ix,iy)+h/2*fw(2),z(ix,iy)+h/2*fz(2))

fu(4)=funcu(u(ix,iy)+h*fu(3),v(ix,iy)+h*fv(3),w(ix,iy)+h*fw(3),z(ix,iy)+h*fz(3))
fv(4)=funcv(u(ix,iy)+h*fu(3),v(ix,iy)+h*fv(3),w(ix,iy)+h*fw(3),z(ix,iy)+h*fz(3))
fw(4)=funcw(u(ix,iy)+h*fu(3),v(ix,iy)+h*fv(3),w(ix,iy)+h*fw(3),z(ix,iy)+h*fz(3))
fz(4)=funcz(u(ix,iy)+h*fu(3),v(ix,iy)+h*fv(3),w(ix,iy)+h*fw(3),z(ix,iy)+h*fz(3))

```

```

unew(ix,iy)=u(ix,iy)+h*(fu(1)+2*fu(2)+2*fu(3)+fu(4))/6+Du*sldr*(u(ix+1,iy-1)+u(ix-1,iy-1)+u(ix+1,iy+1)+u(ix-1,iy+1)+4*u(ix+1,iy)+4*u(ix-1,iy)+4*u(ix,iy+1)+4*u(ix,iy-1)-20*u(ix,iy))
vnew(ix,iy)=v(ix,iy)+h*(fv(1)+2*fv(2)+2*fv(3)+fv(4))/6+Dv*sldr*(v(ix+1,iy-1)+v(ix-1,iy-1)+v(ix+1,iy+1)+v(ix-1,iy+1)+4*v(ix+1,iy)+4*v(ix-1,iy)+4*v(ix,iy+1)+4*v(ix,iy-1)-20*v(ix,iy))

wnew(ix,iy)=w(ix,iy)+h*(fw(1)+2*fw(2)+2*fw(3)+fw(4))/6+Dw*sldr*(w(ix+1,iy-1)+w(ix-1,iy-1)+w(ix+1,iy+1)+w(ix-1,iy+1)+4*w(ix+1,iy)+4*w(ix-1,iy)+4*w(ix,iy+1)+4*w(ix,iy-1)-20*w(ix,iy))
znew(ix,iy)=z(ix,iy)+h*(fz(1)+2*fz(2)+2*fz(3)+fz(4))/6+Dz*sldr*(z(ix+1,iy-1)+z(ix-1,iy-1)+z(ix+1,iy+1)+z(ix-1,iy+1)+4*z(ix+1,iy)+4*z(ix-1,iy)+4*z(ix,iy+1)+4*z(ix,iy-1)-20*z(ix,iy))

!
unew(ix,iy)=u(ix,iy)+h*(funcu(u(ix,iy),v(ix,iy),w(ix,iy),z(ix,iy)))+Du*sldr*(u(ix+1,iy)+u(ix-1,iy)-2*u(ix,iy))+Du*sldr*(u(ix,iy+1)+u(ix,iy-1)-2*u(ix,iy))
!
vnew(ix,iy)=v(ix,iy)+h*(funcv(u(ix,iy),v(ix,iy),w(ix,iy),z(ix,iy)))+Dv*sldr*(v(ix+1,iy)+v(ix-1,iy)-2*v(ix,iy))+Dv*sldr*(v(ix,iy+1)+v(ix,iy-1)-2*v(ix,iy))
!
wnew(ix,iy)=w(ix,iy)+h*(funcw(u(ix,iy),v(ix,iy),w(ix,iy),z(ix,iy)))+Dw*sldr*(w(ix+1,iy)+w(ix-1,iy)-2*w(ix,iy))+Dw*sldr*(w(ix,iy+1)+w(ix,iy-1)-2*w(ix,iy))
!
znew(ix,iy)=z(ix,iy)+h*(funcz(u(ix,iy),v(ix,iy),w(ix,iy),z(ix,iy)))+Dz*sldr*(z(ix+1,iy)+z(ix-1,iy)-2*z(ix,iy))+Dz*sldr*(z(ix,iy+1)+z(ix,iy-1)-2*z(ix,iy))
    enddo
    enddo

do ix=1,lx
    do iy=1,ly
        u(ix,iy)=unew(ix,iy)
        v(ix,iy)=vnew(ix,iy)
        w(ix,iy)=wnew(ix,iy)
        z(ix,iy)=znew(ix,iy)
    enddo
enddo

site1(ncount)=u(300,300)
site2(ncount)=v(300,300)
site3(ncount)=w(300,300)
site4(ncount)=z(300,300)
!site1(ncount)=u(500,500)
!site2(ncount)=v(500,500)
!site3(ncount)=w(500,500)
!site4(ncount)=z(500,500)

```

```

    call writfile(u,v,w,z,ncount)
  enddo

!enddo
  open(unit=60,file="C:\Documents and Settings\User\Desktop\Jun
Li\breathing\results\site1.dat")
    write(60,"(E20.8E4)") site1
    close(60)
  open(unit=60,file="C:\Documents and Settings\User\Desktop\Jun
Li\breathing\results\site2.dat")
    write(60,"(E20.8E4)") site2
    close(60)
  open(unit=60,file="C:\Documents and Settings\User\Desktop\Jun
Li\breathing\results\site3.dat")
    write(60,"(E20.8E4)") site3
    close(60)
  open(unit=60,file="C:\Documents and Settings\User\Desktop\Jun
Li\breathing\results\site4.dat")
    write(60,"(E20.8E4)") site4
    close(60)
!enddo
  call clock(time)
  write(*,"('end time=',A10)") time

end program main

subroutine boundary_nonflux(u,v,w,z)
  use simulation_parameters
  implicit none
  integer ix,iy
  real (kind=8) :: u(0:lx+1,0:ly+1),v(0:lx+1,0:ly+1),w(0:lx+1,0:ly+1),z(0:lx+1,0:ly+1)

  (1) set boudary conditions: nonflux
  do iy=1,ly
    u(0,iy)=u(1,iy)
    u(lx+1,iy)=u(lx,iy)
  enddo
  do ix=0,lx+1
    u(ix,0)=u(ix,1)
    u(ix,ly+1)=u(ix,ly)
  enddo
  do iy=1,ly
    v(0,iy)=v(1,iy)
    v(lx+1,iy)=v(lx,iy)
  enddo
  do ix=0,lx+1

```

```

v(ix,0)=v(ix,1)
v(ix,ly+1)=v(ix,ly)
enddo
do iy=1,ly
w(0,iy)=w(1,iy)
w(lx+1,iy)=w(lx,iy)
end do
do ix=0,lx+1
w(ix,0)=w(ix,1)
w(ix,ly+1)=w(ix,ly)
end do
do iy=1,ly
z(0,iy)=z(1,iy)
z(lx+1,iy)=z(lx,iy)
end do
do ix=0,lx+1
z(ix,0)=z(ix,1)
z(ix,ly+1)=z(ix,ly)
end do
!setting over
end

```

```

(2) u = HBrO3
real(kind=8) function funcu(x,y,m,n)
use system_parameters
implicit none
real(kind=8) :: x,y,m,n

```

```

funcu=(1/e1)*(q*y-x*y+x-x*x+n*x)
end function

```

```

(3) v = Br-
real(kind=8) function funcv(x,y,m,n)
use system_parameters
implicit none
real(kind=8) :: x,y,m,n

```

```

funcv=(1/e2)*(-q*y-x*y+f1*m+r*f2*n)
end function

```

```

(4) w = Ce (IV)
real(kind=8) function funcw(x,y,m,n)
use system_parameters
implicit none
real(kind=8) :: x,y,m,n

```

```
funcw=x-m-s*m
end function
```

```
(5) z = H2Q
real(kind=8) function funcz(x,y,m,n)
use system_parameters
implicit none
real(kind=8) :: x,y,m,n !m=w, n=z
```

```
funcz=(1/e3)*(2*s*m-x*n-r*n)
end function
```

```
(6) subroutine initialize(u,v,w,z)
use simulation_parameters
use system_parameters
implicit none
real(kind=8) :: u(0:lx+1,0:ly+1),v(0:lx+1,0:ly+1),w(0:lx+1,0:ly+1),z(0:lx+1,0:ly+1)
real(kind=8) uss,vss,wss,zss
integer ix,iy
```

```
uss=0.49011
vss=0.89780
wss=0.35008
zss=0.31464
```

```
do ix=1,lx
  do iy=1,ly

    u(ix,iy)=uss*real(ix-513)/real(1025)+uss
    v(ix,iy)=vss
    w(ix,iy)=wss*real(iy-513)/real(1025)+wss
    z(ix,iy)=zss
```

```
  end do
end do
```

```
end subroutine
```

```
(7) subroutine writfile(u,v,w,z,ncount)
use simulation_parameters
implicit none
real(kind=8) ::
u(0:lx+1,0:ly+1),v(0:lx+1,0:ly+1),w(0:lx+1,0:ly+1),z(0:lx+1,0:ly+1)
integer :: ix,iy,ncount
real(kind=8) :: counter
```

```

character:: name1,name2,name3,name4,c1,c2,c3
integer :: no,n1,n2,n3

counter=mod(ncount,no_record) !è?1??ü??3y,?ðcounter==0
if (counter==0) then
    no=int(ncount/no_record)
    n1=int(no/100)
    no=no-100*n1
    n2=int(no/10)
    n3=no-n2*10
    name1="u"
    name2="v"
    name3="w"
    name4="z"
    n1=n1+48
    n2=n2+48
    n3=n3+48
    c1=char(n1)
    c2=char(n2)
    c3=char(n3)

    open (unit=90,file="C:\Documents and Settings\User\Desktop\Jun
Li\breathing\results\\"//name1//c1//c2//c3//".dat")
        write(90,"(1025E20.8E4)")((u(ix,iy),ix=1,lx),iy=1,ly)
        close(90)
    open (unit=90,file="C:\Documents and Settings\User\Desktop\Jun
Li\breathing\results\\"//name2//c1//c2//c3//".dat")
        write(90,"(1025E20.8E4)")((v(ix,iy),ix=1,lx),iy=1,ly)
        close(90)
    open (unit=90,file="C:\Documents and Settings\User\Desktop\Jun
Li\breathing\results\\"//name3//c1//c2//c3//".dat")
        write(90,"(1025E20.8E4)")((w(ix,iy),ix=1,lx),iy=1,ly)
        close(90)
    open (unit=90,file="C:\Documents and Settings\User\Desktop\Jun
Li\breathing\results\\"//name4//c1//c2//c3//".dat")
        write(90,"(1025E20.8E4)")((z(ix,iy),ix=1,lx),iy=1,ly)
        close(90)

endif
end

```

Appendix B A Code of the Simulation in Table 4.1

METHOD STIFF

STARTTIME = 0

STOPTIME=10

DT = 0.02

{ 1: Br+HBr+H <--> Br2+H2O }

RXN1 = K1f*Br*HBr*H - K1r*Br2*H2O

K1f = 8e+007

K1r = 90

INIT Br = 1e-008

INIT Br2 = 0

INIT H = 0.2

INIT H2O = 55

INIT HBr = 0

d/dt(Br) = -RXN1-RXN2-RXN3+RXN10-RXN12+RXN13

d/dt(Br2) = +RXN1-RXN10+RXN12

d/dt(H) = -RXN1-RXN2-2*RXN3-RXN4+2*RXN5-RXN6-RXN8+RXN10-2*RXN11-RXN13

d/dt(H2O) = +RXN1+RXN6+RXN9+RXN11

d/dt(HBr) = -RXN1+2*RXN2+RXN3+RXN5-RXN9

{ 2: Br+HBrO2+H <--> 2HBr }

RXN2 = K2f*Br*HBrO2*H - K2r*HBr^2

K2f = 2.5e+006

K2r = 2e-005

INIT HBrO2 = 0

d/dt(HBrO2) = -RXN2+RXN3-RXN4-RXN5-RXN6+RXN8+RXN11

{ 3: Br+BrO3+2H <--> HBr+HBrO2 }

RXN3 = K3f*Br*BrO3*H^2 - K3r*HBr*HBrO2

K3f = 1.2

K3r = 3.2

INIT BrO3 = 0.05

d/dt(BrO3) = -RXN3+RXN5-RXN6-RXN11

{ 4: HBrO2+H <--> H2BrO2 }

RXN4 = K4f*HBrO2*H - K4r*H2BrO2

K4f = 2e+006

K4r = 1e+008

INIT H2BrO2 = 0

d/dt(H2BrO2) = +RXN4-RXN5

{ 5: HBrO2+H2BrO2 <--> BrO3+HBr+2H }

RXN5 = K5f*HBrO2*H2BrO2 - K5r*BrO3*HBr*H^2

K5f = 170000

K5r = 0

{ 6: HBrO2+BrO3+H <--> Br2O4+H2O }

RXN6 = K6f*HBrO2*BrO3*H - K6r*Br2O4*H2O

K6f = 48

```

K6r = 3200
INIT Br2O4 = 0
d/dt(Br2O4) = +RXN6-RXN7

{ 7: Br2O4 <--> 2BrO2 }
RXN7 = K7f*Br2O4 - K7r*BrO2^2
K7f = 75000
K7r = 1.4e+009
INIT BrO2 = 0
d/dt(BrO2) = +2*RXN7-RXN8

{ 8: Fe2+BrO2+H <--> Fe3+HBrO2 }
RXN8 = K8f*Fe2*BrO2*H - K8r*Fe3*HBrO2
K8f = 1e+007
K8r = 0
INIT Fe2 = 0.0001
INIT Fe3 = 0
d/dt(Fe2) = -RXN8-2*RXN11+RXN12+RXN13
d/dt(Fe3) = +RXN8+2*RXN11-RXN12-RXN13

{ 9: Q+HBr <--> QBr+H2O }
RXN9 = K9f*Q*HBr - K9r*QBr*H2O
K9f = 0
K9r = 0
INIT Q = 0.035
INIT QBr = 0
d/dt(Q) = -RXN9-RXN10+RXN13
d/dt(QBr) = +RXN9+RXN10-RXN13

{ 10: Q+Br2 <--> QBr+Br+H }
RXN10 = K10f*Q*Br2 - K10r*QBr*Br*H
K10f = 1.5
K10r = 0

{ 11: 2Fe2+BrO3+3H <--> 2Fe3+HBrO2+H2O }
RXN11 = K11f*Fe2^2*BrO3*H^2 - K11r*Fe3^2*HBrO2*H2O
K11f = 0.02
K11r = 0

{ 12: Fe3+Br <--> Fe2+1/2Br2 }
RXN12 = K12f*Fe3*Br - K12r*Fe2*Br2^0.5
K12f = 50
K12r = 0

{ 13: QBr + H2O<-->QOH+H+Br }
RXN13 = K13f*QBr - K13r*Q*Br
K13f = 25
K13r = 0

```

Appendix C A Code of the Simulation in Table 5.1

METHOD STIFF

STARTTIME = 0

STOPTIME=10

DT = 0.02

```
{ 1: Br+HBr+H <--> Br2+H2O }
  RXN1 = K1f*Br*HBr*H - K1r*Br2*H2O
  K1f = 8e+007
  K1r = 90
  INIT Br = 1e-008
  INIT Br2 = 0
  INIT H = 0.2
  INIT H2O = 55
  INIT HBr = 0
  d/dt(Br) = -RXN1-RXN2-RXN3+RXN10-RXN12+RXN13
  d/dt(Br2) = +RXN1-RXN10+RXN12
  d/dt(H) = -RXN1-RXN2-2*RXN3-RXN4+2*RXN5-RXN6-RXN8+RXN10-2*RXN11-RXN13
  d/dt(H2O) = +RXN1+RXN6+RXN9+RXN11
  d/dt(HBr) = -RXN1+2*RXN2+RXN3+RXN5-RXN9

{ 2: Br+HBrO2+H <--> 2HBr }
  RXN2 = K2f*Br*HBrO2*H - K2r*HBr^2
  K2f = 2.5e+006
  K2r = 2e-005
  INIT HBrO2 = 0
  d/dt(HBrO2) = -RXN2+RXN3-RXN4-RXN5-RXN6+RXN8+RXN11

{ 3: Br+BrO3+2H <--> HBr+HBrO2 }
  RXN3 = K3f*Br*BrO3*H^2 - K3r*HBr*HBrO2
  K3f = 1.2
  K3r = 3.2
  INIT BrO3 = 0.05
  d/dt(BrO3) = -RXN3+RXN5-RXN6-RXN11

{ 4: HBrO2+H <--> H2BrO2 }
  RXN4 = K4f*HBrO2*H - K4r*H2BrO2
  K4f = 2e+006
  K4r = 1e+008
  INIT H2BrO2 = 0
  d/dt(H2BrO2) = +RXN4-RXN5

{ 5: HBrO2+H2BrO2 <--> BrO3+HBr+2H }
  RXN5 = K5f*HBrO2*H2BrO2 - K5r*BrO3*HBr*H^2
  K5f = 170000
  K5r = 0

{ 6: HBrO2+BrO3+H <--> Br2O4+H2O }
  RXN6 = K6f*HBrO2*BrO3*H - K6r*Br2O4*H2O
  K6f = 48
  K6r = 3200
```

```

INIT Br2O4 = 0
d/dt(Br2O4) = +RXN6-RXN7

{ 7: Br2O4 <--> 2BrO2 }
RXN7 = K7f*Br2O4 - K7r*BrO2^2
K7f = 75000
K7r = 1.4e+009
INIT BrO2 = 0
d/dt(BrO2) = +2*RXN7-RXN8

{ 8: Ce3+BrO2+H <--> Ce4+HBrO2 }
RXN8 = K8f*Ce3*BrO2*H - K8r*Ce4*HBrO2
K8f = 6.2e+004
K8r = 1.2e+004
INIT Ce3 = 0.0001
INIT Ce4 = 0
d/dt(Ce3) = -RXN8-2*RXN11+RXN12+RXN13
d/dt(Ce4) = +RXN8+2*RXN11-RXN12-RXN13

{ 9: Q+HBr <--> QBr+H2O }
RXN9 = K9f*Q*HBr - K9r*QBr*H2O
K9f = 0
K9r = 0
INIT Q = 0.035
INIT QBr = 0
d/dt(Q) = -RXN9-RXN10+RXN13
d/dt(QBr) = +RXN9+RXN10-RXN13

{ 10: Q+Br2 <--> QBr+Br+H }
RXN10 = K10f*Q*Br2 - K10r*QBr*Br*H
K10f = 40
K10r = 0

{ 11: 2Ce3+BrO3+3H <--> 2Ce4+HBrO2+H2O }
RXN11 = K11f*Ce3^2*BrO3*H^2 - K11r*Ce4^2*HBrO2*H2O
K11f = 0
K11r = 0

{ 12: Ce4+Br <--> Ce3+1/2Br2 }
RXN12 = K12f*Ce4*Br - K12r*Ce3*Br2^0.5
K12f = 10000
K12r = 0

{ 13: QBr + H2O<-->QOH+H+Br }
RXN13 = K13f*QBr - K13r*Q*Br
K13f = 60
K13r = 0

```

Appredix D Copyright Releases Chem. Phys. Lett.**ELSEVIER LICENSE
TERMS AND CONDITIONS**

Feb 08, 2013

This is a License Agreement between Jun Li ("You") and Elsevier ("Elsevier") provided by Copyright Clearance Center ("CCC"). The license consists of your order details, the terms and conditions provided by Elsevier, and the payment terms and conditions.

All payments must be made in full to CCC. For payment instructions, please see information listed at the bottom of this form.

Supplier	Elsevier Limited The Boulevard, Langford Lane Kidlington, Oxford, OX5 1GB, UK
Registered Company Number	1982084
Customer name	Jun Li
Customer address	
License number	3084270510082
License date	Feb 08, 2013
Licensed content publisher	Elsevier
Licensed content publication	Chemical Physics Letters
Licensed content title	Design of batch minimal bromate oscillator
Licensed content author	Jun Li, Jichang Wang
Licensed content date	27 May 2011
Licensed content volume number	508
Licensed content issue number	4–6
Number of pages	4
Start Page	320

End Page	323
Type of Use	reuse in a thesis/dissertation
Portion	full article
Format	both print and electronic
Are you the author of this Elsevier article?	Yes
Will you be translating?	No
Order reference number	
Title of your thesis/dissertation	Designing and Manipulating Bromate-Based Oscillators
Expected completion date	Apr 2013
Estimated size (number of pages)	180
Elsevier VAT number	GB 494 6272 12
Permissions price	0.00 USD
VAT/Local Sales Tax	0.0 USD / 0.0 GBP
Total	0.00 USD
Terms and Conditions	

INTRODUCTION

1. The publisher for this copyrighted material is Elsevier. By clicking "accept" in connection with completing this licensing transaction, you agree that the following terms and conditions apply to this transaction (along with the Billing and Payment terms and conditions established by Copyright Clearance Center, Inc. ("CCC"), at the time that you opened your Rightslink account and that are available at any time at <http://myaccount.copyright.com>).

GENERAL TERMS

2. Elsevier hereby grants you permission to reproduce the aforementioned material subject to the terms and conditions indicated.

3. Acknowledgement: If any part of the material to be used (for example, figures) has appeared in our publication with credit or acknowledgement to another source, permission must also be sought from that source. If such permission is not obtained then that material may not be included in your publication/copies. Suitable acknowledgement to the source must be made, either as a footnote or in a reference list at the end of your publication, as follows:

“Reprinted from Publication title, Vol /edition number, Author(s), Title of article / title of chapter, Pages No., Copyright (Year), with permission from Elsevier [OR APPLICABLE SOCIETY COPYRIGHT OWNER].” Also Lancet special credit - “Reprinted from The Lancet, Vol. number, Author(s), Title of article, Pages No., Copyright (Year), with permission from Elsevier.”

4. Reproduction of this material is confined to the purpose and/or media for which permission is hereby given.

5. Altering/Modifying Material: Not Permitted. However figures and illustrations may be altered/adapted minimally to serve your work. Any other abbreviations, additions, deletions and/or any other alterations shall be made only with prior written authorization of Elsevier Ltd. (Please contact Elsevier at permissions@elsevier.com)

6. If the permission fee for the requested use of our material is waived in this instance, please be advised that your future requests for Elsevier materials may attract a fee.

7. Reservation of Rights: Publisher reserves all rights not specifically granted in the combination of (i) the license details provided by you and accepted in the course of this licensing transaction, (ii) these terms and conditions and (iii) CCC's Billing and Payment terms and conditions.

8. License Contingent Upon Payment: While you may exercise the rights licensed immediately upon issuance of the license at the end of the licensing process for the transaction, provided that you have disclosed complete and accurate details of your proposed use, no license is finally effective unless and until full payment is received from you (either by publisher or by CCC) as provided in CCC's Billing and Payment terms and conditions. If full payment is not received on a timely basis, then any license preliminarily granted shall be deemed automatically revoked and shall be void as if never granted. Further, in the event that you breach any of these terms and conditions or any of CCC's Billing and Payment terms and conditions, the license is automatically revoked and shall be void as if never granted. Use of materials as described in a revoked license, as well as any use of the materials beyond the scope of an unrevoked license, may constitute copyright infringement and publisher reserves the right to take any and all action to protect its copyright in the materials.

9. Warranties: Publisher makes no representations or warranties with respect to the licensed material.

10. **Indemnity:** You hereby indemnify and agree to hold harmless publisher and CCC, and their respective officers, directors, employees and agents, from and against any and all claims arising out of your use of the licensed material other than as specifically authorized pursuant to this license.

11. **No Transfer of License:** This license is personal to you and may not be sublicensed, assigned, or transferred by you to any other person without publisher's written permission.

12. **No Amendment Except in Writing:** This license may not be amended except in a writing signed by both parties (or, in the case of publisher, by CCC on publisher's behalf).

13. **Objection to Contrary Terms:** Publisher hereby objects to any terms contained in any purchase order, acknowledgment, check endorsement or other writing prepared by you, which terms are inconsistent with these terms and conditions or CCC's Billing and Payment terms and conditions. These terms and conditions, together with CCC's Billing and Payment terms and conditions (which are incorporated herein), comprise the entire agreement between you and publisher (and CCC) concerning this licensing transaction. In the event of any conflict between your obligations established by these terms and conditions and those established by CCC's Billing and Payment terms and conditions, these terms and conditions shall control.

14. **Revocation:** Elsevier or Copyright Clearance Center may deny the permissions described in this License at their sole discretion, for any reason or no reason, with a full refund payable to you. Notice of such denial will be made using the contact information provided by you. Failure to receive such notice will not alter or invalidate the denial. In no event will Elsevier or Copyright Clearance Center be responsible or liable for any costs, expenses or damage incurred by you as a result of a denial of your permission request, other than a refund of the amount(s) paid by you to Elsevier and/or Copyright Clearance Center for denied permissions.

LIMITED LICENSE

The following terms and conditions apply only to specific license types:

15. **Translation:** This permission is granted for non-exclusive world **English** rights only unless your license was granted for translation rights. If you licensed translation rights you may only translate this content into the languages you requested. A professional translator must perform all translations and reproduce the content word for word preserving the integrity of the article. If this license is to re-use 1 or 2 figures then permission is granted for non-exclusive world rights in all languages.

16. **Website:** The following terms and conditions apply to electronic reserve and author

websites:

Electronic reserve: If licensed material is to be posted to website, the web site is to be password-protected and made available only to bona fide students registered on a relevant course if:

This license was made in connection with a course,

This permission is granted for 1 year only. You may obtain a license for future website posting,

All content posted to the web site must maintain the copyright information line on the bottom of each image,

A hyper-text must be included to the Homepage of the journal from which you are licensing at <http://www.sciencedirect.com/science/journal/xxxxx> or the Elsevier homepage for books at <http://www.elsevier.com> , and

Central Storage: This license does not include permission for a scanned version of the material to be stored in a central repository such as that provided by Heron/XanEdu.

17. Author website for journals with the following additional clauses:

All content posted to the web site must maintain the copyright information line on the bottom of each image, and the permission granted is limited to the personal version of your paper. You are not allowed to download and post the published electronic version of your article (whether PDF or HTML, proof or final version), nor may you scan the printed edition to create an electronic version. A hyper-text must be included to the Homepage of the journal from which you are licensing

at <http://www.sciencedirect.com/science/journal/xxxxx> . As part of our normal production process, you will receive an e-mail notice when your article appears on Elsevier's online service ScienceDirect (www.sciencedirect.com). That e-mail will include the article's Digital Object Identifier (DOI). This number provides the electronic link to the published article and should be included in the posting of your personal version. We ask that you wait until you receive this e-mail and have the DOI to do any posting.

Central Storage: This license does not include permission for a scanned version of the material to be stored in a central repository such as that provided by Heron/XanEdu.

18. Author website for books with the following additional clauses:

Authors are permitted to place a brief summary of their work online only.

A hyper-text must be included to the Elsevier homepage at <http://www.elsevier.com> . All content posted to the web site must maintain the copyright information line on the bottom of each image. You are not allowed to download and post the published electronic version of your chapter, nor may you scan the printed edition to create an electronic version.

Central Storage: This license does not include permission for a scanned version of the material to be stored in a central repository such as that provided by Heron/XanEdu.

19. Website (regular and for author): A hyper-text must be included to the Homepage of the journal from which you are licensing

at <http://www.sciencedirect.com/science/journal/xxxxx>. or for books to the Elsevier

homepage at <http://www.elsevier.com>

20. Thesis/Dissertation: If your license is for use in a thesis/dissertation your thesis may be submitted to your institution in either print or electronic form. Should your thesis be published commercially, please reapply for permission. These requirements include permission for the Library and Archives of Canada to supply single copies, on demand, of the complete thesis and include permission for UMI to supply single copies, on demand, of the complete thesis. Should your thesis be published commercially, please reapply for permission.

21. Other Conditions:

v1.6

If you would like to pay for this license now, please remit this license along with your payment made payable to "COPYRIGHT CLEARANCE CENTER" otherwise you will be invoiced within 48 hours of the license date. Payment should be in the form of a check or money order referencing your account number and this invoice number RLNK500952965.

Once you receive your invoice for this order, you may pay your invoice by credit card. Please follow instructions provided at that time.

**Make Payment To:
Copyright Clearance Center
Dept 001
P.O. Box 843006
Boston, MA 02284-3006**

For suggestions or comments regarding this order, contact RightsLink Customer Support: customercare@copyright.com or +1-877-622-5543 (toll free in the US) or +1-978-646-2777.

Gratis licenses (referencing \$0 in the Total field) are free. Please retain this printable license for your reference. No payment is required.

Appredix E Copyright Releases J. Phys. Chem. A

American Chemical Society's Policy on Theses and Dissertations

If your university requires you to obtain permission, you must use the RightsLink permission system.
See RightsLink instructions at <http://pubs.acs.org/page/copyright/permissions.html>.

This is regarding request for permission to include your paper(s) or portions of text from your paper(s) in your thesis. Permission is now automatically granted; please pay special attention to the **implications** paragraph below. The Copyright Subcommittee of the Joint Board/Council Committees on Publications approved the following:

Copyright permission for published and submitted material from theses and dissertations

ACS extends blanket permission to students to include in their theses and dissertations their own articles, or portions thereof, that have been published in ACS journals or submitted to ACS journals for publication, provided that the ACS copyright credit line is noted on the appropriate page(s).

Publishing implications of electronic publication of theses and dissertation material

Students and their mentors should be aware that posting of theses and dissertation material on the Web prior to submission of material from that thesis or dissertation to an ACS journal may affect publication in that journal. Whether Web posting is considered prior publication may be evaluated on a case-by-case basis by the journal's editor. If an ACS journal editor considers Web posting to be "prior publication", the paper will not be accepted for publication in that journal. If you intend to submit your unpublished paper to ACS for publication, check with the appropriate editor prior to posting your manuscript electronically.

Reuse/Republishing of the Entire Work in Theses or Collections: Authors may reuse all or part of the Submitted, Accepted or Published Work in a thesis or dissertation that the author writes and is required to submit to satisfy the criteria of degree-granting institutions. Such reuse is permitted subject to the ACS' "Ethical Guidelines to Publication of Chemical Research" (<http://pubs.acs.org/page/policy/ethics/index.html>); the author should secure written confirmation (via letter or email) from the respective ACS journal editor(s) to avoid potential conflicts with journal prior publication*/embargo policies. Appropriate citation of the Published Work must be made. If the thesis or dissertation to be published is in electronic format, a direct link to the Published Work must also be included using the ACS Articles on Request author-directed link – see <http://pubs.acs.org/page/policy/articlesonrequest/index.html>

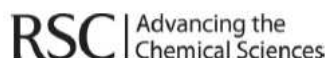
* Prior publication policies of ACS journals are posted on the ACS website at <http://pubs.acs.org/page/policy/prior/index.html>

If your paper has not yet been published by ACS, please print the following credit line on the first page of your article: "Reproduced (or 'Reproduced in part') with permission from [JOURNAL NAME], in press (or 'submitted for publication'). Unpublished work copyright [CURRENT YEAR] American Chemical Society." Include appropriate information.

If your paper has already been published by ACS and you want to include the text or portions of the text in your thesis/dissertation, please print the ACS copyright credit line on the first page of your article: "Reproduced (or 'Reproduced in part') with permission from [FULL REFERENCE CITATION.] Copyright [YEAR] American Chemical Society." Include appropriate information.

Submission to a Dissertation Distributor: If you plan to submit your thesis to UMI or to another dissertation distributor, you should not include the unpublished ACS paper in your thesis if the thesis will be disseminated electronically, until ACS has published your paper. After publication of the paper by ACS, you may release the entire thesis (not the individual ACS article by itself) for electronic dissemination through the distributor; ACS's copyright credit line should be printed on the first page of the ACS paper.

Appredix F Copyright Releases Phys. Chem. Chem. Phys.



Royal Society of Chemistry
Thomas Graham House
Science Park
Milton Road
Cambridge
CB4 0WF

Tel: +44 (0)1223 420 066
Fax: +44 (0)1223 423 623
Email: contracts-copyright@rsc.org

www.rsc.org

Acknowledgements to be used by RSC authors

Authors of RSC books and journal articles can reproduce material (for example a figure) from the RSC publication in a non-RSC publication, including theses, without formally requesting permission providing that the correct acknowledgement is given to the RSC publication. This permission extends to reproduction of large portions of text or the whole article or book chapter when being reproduced in a thesis.

The acknowledgement to be used depends on the RSC publication in which the material was published and the form of the acknowledgements is as follows:

- For material being reproduced from an article in *New Journal of Chemistry* the acknowledgement should be in the form:
 - [Original citation] - Reproduced by permission of The Royal Society of Chemistry (RSC) on behalf of the Centre National de la Recherche Scientifique (CNRS) and the RSC
- For material being reproduced from an article *Photochemical & Photobiological Sciences* the acknowledgement should be in the form:
 - [Original citation] - Reproduced by permission of The Royal Society of Chemistry (RSC) on behalf of the European Society for Photobiology, the European Photochemistry Association, and RSC
- For material being reproduced from an article in *Physical Chemistry Chemical Physics* the acknowledgement should be in the form:
 - [Original citation] - Reproduced by permission of the PCCP Owner Societies
- For material reproduced from books and any other journal the acknowledgement should be in the form:
 - [Original citation] - Reproduced by permission of The Royal Society of Chemistry

The acknowledgement should also include a hyperlink to the article on the RSC website.

The form of the acknowledgement is also specified in the RSC agreement/licence signed by the corresponding author.

Except in cases of republication in a thesis, this express permission does not cover the reproduction of large portions of text from the RSC publication or reproduction of the whole article or book chapter.

A publisher of a non-RSC publication can use this document as proof that permission is granted to use the material in the non-RSC publication.

Appredix G Copyright Releases Electrochem. Commun.**ELSEVIER LICENSE
TERMS AND CONDITIONS**

Feb 08, 2013

This is a License Agreement between Jun Li ("You") and Elsevier ("Elsevier") provided by Copyright Clearance Center ("CCC"). The license consists of your order details, the terms and conditions provided by Elsevier, and the payment terms and conditions.

All payments must be made in full to CCC. For payment instructions, please see information listed at the bottom of this form.

Supplier	Elsevier Limited The Boulevard, Langford Lane Kidlington, Oxford, OX5 1GB, UK
Registered Company Number	1982084
Customer name	Jun Li
Customer address	
License number	3084300025905
License date	Feb 08, 2013
Licensed content publisher	Elsevier
Licensed content publication	Electrochemistry Communications
Licensed content title	Structural transformation of carbon electrodes for simultaneous determination of dihydroxybenzene isomers
Licensed content author	Xuefeng Hu, Jun Li, Jichang Wang
Licensed content date	July 2012
Licensed content volume number	21
Licensed content issue number	
Number of pages	4
Start Page	73

End Page	76
Type of Use	reuse in a thesis/dissertation
Intended publisher of new work	other
Portion	full article
Format	both print and electronic
Are you the author of this Elsevier article?	Yes
Will you be translating?	No
Order reference number	
Title of your thesis/dissertation	Designing and Manipulating Bromate-Based Oscillators
Expected completion date	Apr 2013
Estimated size (number of pages)	180
Elsevier VAT number	GB 494 6272 12
Permissions price	0.00 USD
VAT/Local Sales Tax	0.0 USD / 0.0 GBP
Total	0.00 USD
Terms and Conditions	

INTRODUCTION

1. The publisher for this copyrighted material is Elsevier. By clicking "accept" in connection with completing this licensing transaction, you agree that the following terms and conditions apply to this transaction (along with the Billing and Payment terms and conditions established by Copyright Clearance Center, Inc. ("CCC"), at the time that you opened your Rightslink account and that are available at any time at <http://myaccount.copyright.com>).

GENERAL TERMS

2. Elsevier hereby grants you permission to reproduce the aforementioned material subject

to the terms and conditions indicated.

3. Acknowledgement: If any part of the material to be used (for example, figures) has appeared in our publication with credit or acknowledgement to another source, permission must also be sought from that source. If such permission is not obtained then that material may not be included in your publication/copies. Suitable acknowledgement to the source must be made, either as a footnote or in a reference list at the end of your publication, as follows:

“Reprinted from Publication title, Vol /edition number, Author(s), Title of article / title of chapter, Pages No., Copyright (Year), with permission from Elsevier [OR APPLICABLE SOCIETY COPYRIGHT OWNER].” Also Lancet special credit - “Reprinted from The Lancet, Vol. number, Author(s), Title of article, Pages No., Copyright (Year), with permission from Elsevier.”

4. Reproduction of this material is confined to the purpose and/or media for which permission is hereby given.

5. Altering/Modifying Material: Not Permitted. However figures and illustrations may be altered/adapted minimally to serve your work. Any other abbreviations, additions, deletions and/or any other alterations shall be made only with prior written authorization of Elsevier Ltd. (Please contact Elsevier at permissions@elsevier.com)

6. If the permission fee for the requested use of our material is waived in this instance, please be advised that your future requests for Elsevier materials may attract a fee.

7. Reservation of Rights: Publisher reserves all rights not specifically granted in the combination of (i) the license details provided by you and accepted in the course of this licensing transaction, (ii) these terms and conditions and (iii) CCC's Billing and Payment terms and conditions.

8. License Contingent Upon Payment: While you may exercise the rights licensed immediately upon issuance of the license at the end of the licensing process for the transaction, provided that you have disclosed complete and accurate details of your proposed use, no license is finally effective unless and until full payment is received from you (either by publisher or by CCC) as provided in CCC's Billing and Payment terms and conditions. If full payment is not received on a timely basis, then any license preliminarily granted shall be deemed automatically revoked and shall be void as if never granted. Further, in the event that you breach any of these terms and conditions or any of CCC's Billing and Payment terms and conditions, the license is automatically revoked and shall be void as if never granted. Use of materials as described in a revoked license, as well as any use of the materials beyond the scope of an unrevoked license, may constitute copyright infringement and publisher reserves the right to take any and all action to protect its copyright in the materials.

9. Warranties: Publisher makes no representations or warranties with respect to the

licensed material.

10. **Indemnity:** You hereby indemnify and agree to hold harmless publisher and CCC, and their respective officers, directors, employees and agents, from and against any and all claims arising out of your use of the licensed material other than as specifically authorized pursuant to this license.

11. **No Transfer of License:** This license is personal to you and may not be sublicensed, assigned, or transferred by you to any other person without publisher's written permission.

12. **No Amendment Except in Writing:** This license may not be amended except in a writing signed by both parties (or, in the case of publisher, by CCC on publisher's behalf).

13. **Objection to Contrary Terms:** Publisher hereby objects to any terms contained in any purchase order, acknowledgment, check endorsement or other writing prepared by you, which terms are inconsistent with these terms and conditions or CCC's Billing and Payment terms and conditions. These terms and conditions, together with CCC's Billing and Payment terms and conditions (which are incorporated herein), comprise the entire agreement between you and publisher (and CCC) concerning this licensing transaction. In the event of any conflict between your obligations established by these terms and conditions and those established by CCC's Billing and Payment terms and conditions, these terms and conditions shall control.

14. **Revocation:** Elsevier or Copyright Clearance Center may deny the permissions described in this License at their sole discretion, for any reason or no reason, with a full refund payable to you. Notice of such denial will be made using the contact information provided by you. Failure to receive such notice will not alter or invalidate the denial. In no event will Elsevier or Copyright Clearance Center be responsible or liable for any costs, expenses or damage incurred by you as a result of a denial of your permission request, other than a refund of the amount(s) paid by you to Elsevier and/or Copyright Clearance Center for denied permissions.

LIMITED LICENSE

The following terms and conditions apply only to specific license types:

15. **Translation:** This permission is granted for non-exclusive world **English** rights only unless your license was granted for translation rights. If you licensed translation rights you may only translate this content into the languages you requested. A professional translator must perform all translations and reproduce the content word for word preserving the integrity of the article. If this license is to re-use 1 or 2 figures then

permission is granted for non-exclusive world rights in all languages.

16. Website: The following terms and conditions apply to electronic reserve and author websites:

Electronic reserve: If licensed material is to be posted to website, the web site is to be password-protected and made available only to bona fide students registered on a relevant course if:

This license was made in connection with a course,

This permission is granted for 1 year only. You may obtain a license for future website posting,

All content posted to the web site must maintain the copyright information line on the bottom of each image,

A hyper-text must be included to the Homepage of the journal from which you are licensing at <http://www.sciencedirect.com/science/journal/xxxxx> or the Elsevier homepage for books at <http://www.elsevier.com> , and

Central Storage: This license does not include permission for a scanned version of the material to be stored in a central repository such as that provided by Heron/XanEdu.

17. Author website for journals with the following additional clauses:

All content posted to the web site must maintain the copyright information line on the bottom of each image, and the permission granted is limited to the personal version of your paper. You are not allowed to download and post the published electronic version of your article (whether PDF or HTML, proof or final version), nor may you scan the printed edition to create an electronic version. A hyper-text must be included to the Homepage of the journal from which you are licensing

at <http://www.sciencedirect.com/science/journal/xxxxx> . As part of our normal production process, you will receive an e-mail notice when your article appears on Elsevier's online service ScienceDirect (www.sciencedirect.com). That e-mail will include the article's Digital Object Identifier (DOI). This number provides the electronic link to the published article and should be included in the posting of your personal version. We ask that you wait until you receive this e-mail and have the DOI to do any posting.

Central Storage: This license does not include permission for a scanned version of the material to be stored in a central repository such as that provided by Heron/XanEdu.

18. Author website for books with the following additional clauses:

Authors are permitted to place a brief summary of their work online only.

A hyper-text must be included to the Elsevier homepage at <http://www.elsevier.com> . All content posted to the web site must maintain the copyright information line on the bottom of each image. You are not allowed to download and post the published electronic version of your chapter, nor may you scan the printed edition to create an electronic version.

Central Storage: This license does not include permission for a scanned version of the material to be stored in a central repository such as that provided by Heron/XanEdu.

19. **Website** (regular and for author): A hyper-text must be included to the Homepage of the journal from which you are licensing at <http://www.sciencedirect.com/science/journal/xxxxx>. or for books to the Elsevier homepage at <http://www.elsevier.com>

20. **Thesis/Dissertation:** If your license is for use in a thesis/dissertation your thesis may be submitted to your institution in either print or electronic form. Should your thesis be published commercially, please reapply for permission. These requirements include permission for the Library and Archives of Canada to supply single copies, on demand, of the complete thesis and include permission for UMI to supply single copies, on demand, of the complete thesis. Should your thesis be published commercially, please reapply for permission.

21. **Other Conditions:**

v1.6

If you would like to pay for this license now, please remit this license along with your payment made payable to "COPYRIGHT CLEARANCE CENTER" otherwise you will be invoiced within 48 hours of the license date. Payment should be in the form of a check or money order referencing your account number and this invoice number RLNK500953022.

Once you receive your invoice for this order, you may pay your invoice by credit card. Please follow instructions provided at that time.

Make Payment To:
Copyright Clearance Center
Dept 001
P.O. Box 843006
Boston, MA 02284-3006

For suggestions or comments regarding this order, contact RightsLink Customer Support: customercare@copyright.com or +1-877-622-5543 (toll free in the US) or +1-978-646-2777.

Gratis licenses (referencing \$0 in the Total field) are free. Please retain this printable license for your reference. No payment is required.

VITA AUCTORIS

NAME	Jun Li
YEARS OF BIRTH	1983
PLACE OF BIRTH	Changzhi, China P. R.
EDUCATION	<p>Chinese University of Mining and Technology, China P. R. B.Sc. 2002-2006</p> <p>Chinese University of Mining and Technology, China P. R. M.Sc. 2006-2009</p> <p>University of Windsor, Ontario, Canada 2009-2013</p>